# Characterization of Weathering Products on Duluth Complex Rocks and Implications for Metal Mobility, Mesaba Deposit, Minnesota, USA

A THESIS

SUBMITTED TO THE FACULTY OF

UNIVERSITY OF MINNESOTA

BY

Paul Michael Fix

IN PARTIAL FULFILLMENT OF THE REQUIREMENTS

FOR THE DEGREE OF

MASTER OF SCIENCE

Advisors: Tamara Diedrich, James Miller

December, 2015

**Acknowledgements**

First and foremost, I would like to thank my advisor, Dr. Tamara Diedrich, for the generous amount of timely guidance and feedback she gave during this project. All of her efforts toward this thesis went beyond the duties of a consulting geochemist. She motivated me throughout every step of the project, was an excellent advisor, and surely helped lay a strong foundation for my future.

I would like to thank Dr. Jim Miller for sharing his passion for geology, constructing and maintaining the Precambrian Research Center (PRC) as a tool to facilitate support for students, and providing so many opportunities for everyone to learn geology, most importantly, outside of the classroom. Jim has taught me so much about geology through PRC field camp, Institute on Lake Superior Geology activities, and countless field trips and social events. In addition, he introduced me to many other inspirational geologists, many who are now friends.

Dr. Bryan Bandli, former SEM lab manager at UMD, provided excellent guidance on SEM and XRD sample preparation and analysis methods. Synchrotron-based analyses were conducted with the help of Dr. Andrea Foster. She was directly responsible for writing a successful beam time proposal and advising data collection, reduction, and interpretation. The time working and learning with Andrea and Bryan was invaluable.

The geology department at University of Minnesota-Duluth (UMD) and many of the employees at Barr Engineering Company (Barr) deserve acknowledgement for the support (and necessary distractions) they provided. There was always someone around willing to give advice or share a story - the times will be remembered fondly.

This project was entirely funded by support from Teck American (Teck) through PRC and Barr. Specifically, I recognize the support of Dave Godlewski and Andrew Thrift of Teck. Also, thank you to Barr for providing an opportunity for me to gain professional experience and, with PRC and Teck, making this product of collaborative work possible.

Prior to attending UMD, the education and mentorship I received at University of Wisconsin- Stevens Point, especially by Dr. Kevin Hefferan, prepared me for this project in many ways.

Last, but definitely not least, I would like to thank my parents for backing my decisions and financially supporting my education.

Acknowledgement of SSRL: *Use of the Stanford Synchrotron Radiation Lightsource, SLAC National Accelerator Laboratory, is supported by the U.S. Department of Energy, Office of Science, Office of Basic Energy Sciences under Contract No. DE-AC02-76SF00515.*

**Abstract**

The Mesaba deposit is a copper-nickel-platinum group element (Cu-Ni-PGE) prospect hosted by the Duluth Complex and located in northeastern Minnesota near the town of Babbitt. If mined, sulfide-bearing waste rock will be generated. During the environmental review process, predictions of the quality of mine-impacted waters associated with various mine features (e.g. waste rock piles, pit lakes) will be used to inform waste and water management strategies during and following mining.

The quality of mine-impacted water at a future mine will reflect the combined effect of kinetically controlled release of constituents by mineral oxidation and dissolution reactions and attenuation of constituents through precipitation and related weathering product formation reactions. This study characterizes weathering products that formed on exposures of sulfide-bearing rock that occurs on the Mesaba Project site. The results from material characterization were used to inform a conceptual model that incorporates weathering products as controls on the concentrations of metals and metalloids in waters draining Duluth Complex systems.

Weathered samples from the site were characterized using bulk chemical techniques, transmitted and reflected light microscopy, powder X-ray diffraction (XRD), scanning electron microscopy with energy dispersive spectroscopy (SEM-EDS), and synchrotron based micro-analysis including X-ray fluorescence (μXRF) and X-ray absorption spectroscopy (μXAS). Weathering product characterization showed copper can be attenuated in iron-oxide rich weathering products that show compositional banding. The banded coatings contain alternating silicon and iron rich layers and can contain up to

several weight percent copper (as determined by semi-quantitative EDS measurements). In addition, the secondary copper mineral malachite was identified as a surface precipitate. Arsenic was also found to be contained in the previously mentioned coatings in the form of both As (III) and As (V). Weathering products containing other contaminants of interest (i.e. Ni, Co, Zn) were not positively identified, possibly due to the detection limits of the methods used.

Following solid phase characterization, screening-level geochemical modeling using the program Geochemist's Workbench was conducted to compare the theoretical control exerted by weathering products to actual water quality observations from weathering experiments conducted by the Minnesota Department of Natural Resources and as part of the project development. Based on composition trends, solubility controls may include malachite for copper, $Ni(OH)_2$ for nickel, $CoCO_3$ for cobalt, and smithsonite for zinc. In general, the theoretical controls are not definite, and the water chemistry data are highly variable.

The results of this study are relevant to predicting the fate of metals released from Duluth Complex rock exposed to oxidizing atmospheric conditions such as would be found in mine features (including waste rock piles, pit lake high walls) and experimental systems (including humidity cell tests, column tests, field-based weathering experiments).

**Table of Contents**

**List of Tables**

**List of Figures**

# 1 Introduction

The chemistry of mine-impacted water is dependent on a suite of geochemical reactions that result in either the release or attenuation of chemical constituents. Examples of these reactions include: oxidation or dissolution of primary minerals release constituents; while precipitation of secondary minerals, sorption onto primary or secondary minerals, and coprecipitation attenuate chemical constituents. For the purpose of this thesis, two types of phases, *weathering products* and *primary minerals*, have been defined to avoid ambiguity. Because amorphous phases are not "minerals" by definition (i.e. naturally occurring crystalline materials with a definite composition) the more general term "weathering products" will be used in this thesis except in cases where the crystalline nature of the weathering product is known, by X-ray diffraction. Weathering products are defined as solids that formed as a result of surficial weathering processes. The components contained in weathering products can include elements formerly contained in primary minerals (prior to exposure), atmospheric components (e.g. carbon and water), and from fluids that have reacted with the primary mineral under subaerial conditions. Primary minerals formed prior to exposure on earth's surface by magmatic and/or metamorphic processes (e.g. olivine, chlorite). In some cases, there is uncertainty as to the origin (primary or secondary) of a given phase. For a recent discussion on the definition of *mineral* in the field of environmental minerology, see Caraballo et al., 2015.

As indicated above, weathering products are of particular interest in these systems because they act to control the transport of contaminants to the surrounding environments as mine wastes are transformed through weathering (Blowes et al., 1994; Cornell & Schwertmann, 2006; Jamieson, 2011). A robust geochemical prediction of the quality of mine-impacted water requires characterization of both release and attenuation reactions and the factors that influence each. This knowledge can lead to more accurate mine-water quality predictions, less expensive mitigation, quicker project approvals, and an overall decrease environmental risks (Nordstrom and Alpers, 1999; INAP, 2009; Price, 2009; Nordstrom, 2011; Jamieson et al., 2015)

Copper-Ni-PGE magmatic sulfide deposits have been known in the Duluth Complex for decades, but to-date, none have been mined in Minnesota. This thesis focuses on characterization of weathering products formed after subaerial weathering of mineralized Duluth Complex rock in order to augment the basis for understanding metal mobility in this environment. It uses rock exposed at a current exploration property as a proxy for waste that could be generated at a future mine.

The results have been incorporated into a conceptual model that describes chemical processes responsible for paragenesis under subaerial conditions. The conceptual model specifically focuses on metal attenuation, and builds on an extensive body of previous mine waste research on Duluth Complex rock.

## 1.1 Duluth Complex Cu-Ni-PGE deposits

Currently, several companies are evaluating the potential of Cu-Ni-PGE prospects and deposits in the Duluth Complex as viable future mines. The Duluth Complex is a large composite mafic intrusion emplaced approximately 1.1 billion years ago during the Mid-continent rift. Along the western edge of the Complex, in Minnesota, portions of the Partridge River Intrusion (PRI), South Kawishiwi Intrusion (SKI), and Bathtub Intrusion (BTI) are enriched in Cu-Ni-PGE magmatic sulfides (Miller et al., 2002; Severson and Hauck, 2008). As a whole, the Duluth Complex has been estimated to contain *well over* 4.4 billion metric tons of material averaging 0.66% copper, 0.20% nickel (Listerud and Meineke, 1977; Peterson, 2010; Miller and Nicholson, 2013). Precious metals (Pd+Pt+Au) add significant value to the resource as a co-product (e.g. Peterson, 2010).

Magmatic Cu-Ni-PGE sulfide deposits form as the result of the segregation and concentration of droplets of liquid sulfide from mafic or ultramafic magma and the partitioning of chalcophile elements into these droplets from the silicate magma (Naldrett, 1999; Naldrett, 2004). Sulfide saturation (i.e. the formation of sulfide droplets in a magma) is a critical step in the formation of a magmatic sulfide deposit. The simplest way of promoting sulfide saturation is to increase the concentration of sulfur in the magma by addition from an external source (Robb, 2005). This is the favored model for

Duluth Complex deposits, in which external sulfur is sourced from the underlying Paleoproterozoic Virginia Formation metasedimentary rocks. The sulfur incorporation mechanisms, timing of sulfide saturation, and the location of sulfur sources and ore zones are currently being researched and debated for Duluth Complex deposits (e.g. Steiner, 2014; Queffurus and Barnes, 2014)

Basal Duluth Complex mineralization is hosted mostly by troctolitic rocks (plagioclase + olivine +/- pyroxene). Sulfide mineralization consists of mostly pyrrhotite, chalcopyrite, cubanite and minor pentlandite, generally occurring as disseminated grains among silicate phases in the troctolite, but also as veinlets, inclusions in silicates, intergrowths with hydrous minerals, and as rare massive sulfide segregations (Miller et al., 2002 and references therein).

The extent of Duluth Complex deposits is defined by lease boundaries (past and present) and the knowledge that has evolved from decades of exploration programs of various magnitudes (Figure 1-1). Thus, individual deposits that appear to have distinct boundaries on a map, are actually very similar in terms of geological attributes. For example, the similarities with respect to mineralization and rock type have allowed Severson and Hauck (2008) to correlate lithological units across individual deposits.

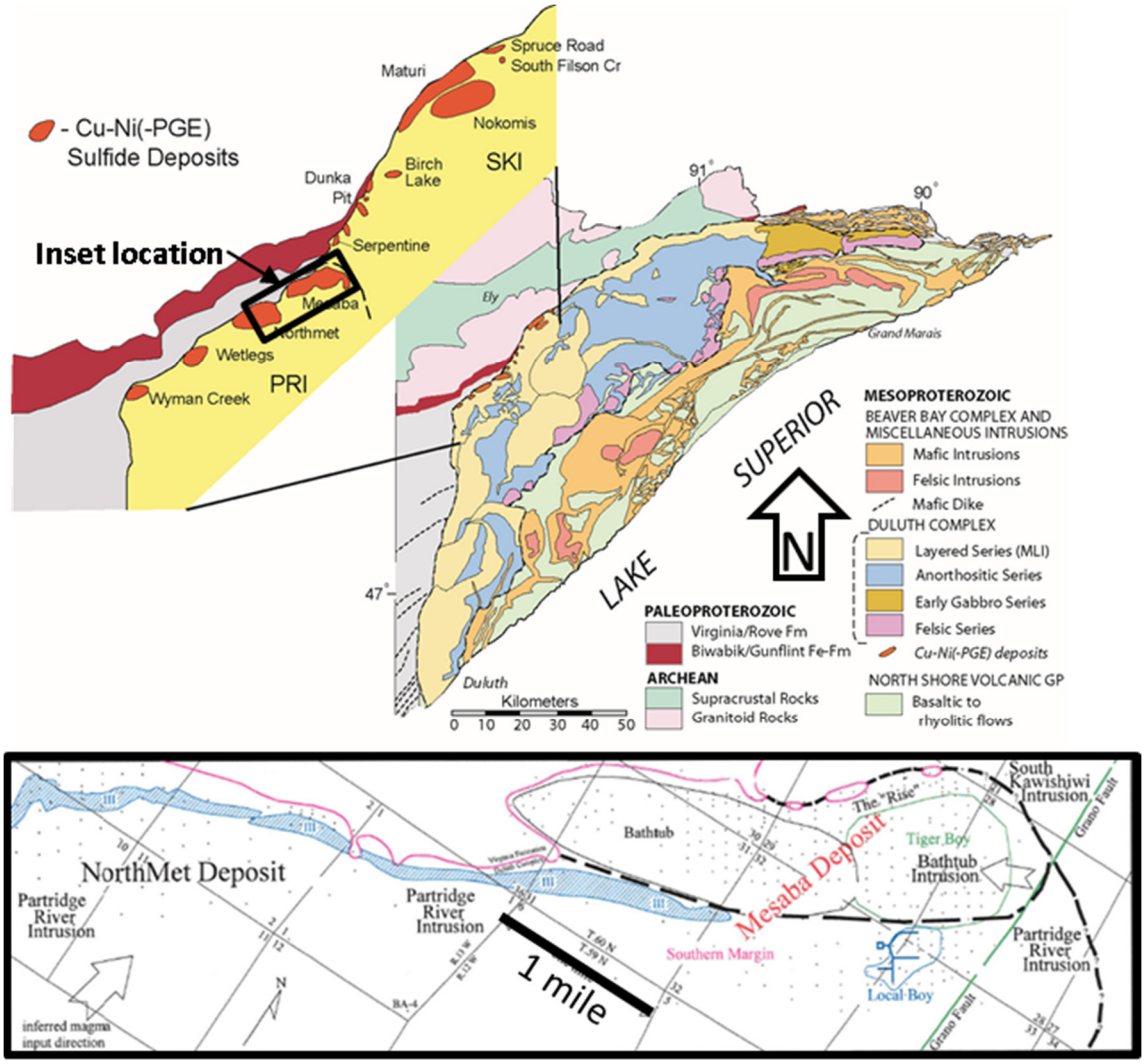


Figure 1-1. Map showing the locations of delineated Cu-Ni-PGE deposits and bedrock geology in northeastern Minnesota. Inset (lower map) shows the Mesaba deposit in greater detail (Modified from Miller and Nicholson, 2013 and Severson and Hauck, 2008).

### 1.1.1 Rock types

Igneous units have been defined based on modal silicate mineral abundance. Most rock types found in Duluth Complex deposits can be classified using the Mafic Group plot in Miller et al., 2002 (Figure 1-2). Using this classification scheme, most rocks are variations of troctolite- a cumulate rock containing dominantly plagioclase and olivine

and lesser amounts of pyroxene (high Ca pyroxene> low Ca pyroxene). Locally, ultramafic rocks such as picrite and peridotite occur in addition to xenoliths of hornfels Virginia Formation, iron formation, and Mid-continent rift basalts. Minor phases include ilmenite, titano-magnetite, and biotite in addition to magmatic alteration minerals such as chlorite, serpentine, epidote, prehnite, and calcite.

### 1.1.2 Sulfide mineralogy and distribution

Disseminated sulfide mineralization includes pyrrhotite ($Fe_{(1-x)}S$), chalcopyrite ($CuFeS_2$), cubanite ($CuFe_2S_3$), and pentlandite ($(Fe,Ni)_9S_8$) as well as other sulfides and minerals containing Co, Zn, As and platinum group elements (PGEs). Chaotic mineralization with respect to the sulfide mineral assemblage and abundance is common to Duluth Complex deposits. Tenors have been observed to generally increase away from the footwall contact as chalcopyrite becomes dominant over pyrrhotite + cubanite although the highest grade material occurs close to the footwall (e.g. Ripley and Alawi, 1986; Teck, 2010).

### 1.1.3 Mesaba Deposit

The Mesaba deposit, formerly named the Babbitt Deposit, is hosted in portions of the Partridge River intrusion and newly defined Bathtub intrusion (Severson and Hauck, 2008) in northeastern MN. The deposit has been evaluated as a Cu-Ni resource by several companies over the last 50+ years starting with Bear Creek Mining from 1958-1971. In 1973, AMAX acquired the property and conducted a significant diamond drill program in addition to developing a 512 m shaft and 1,160 m of underground drifts. This development work triggered the Minnesota Cu-Ni environmental study and the creation of the AMAX experimental waste rock piles (described in section 1.6) (Minnesota Environmental Quality Board, 1979). In 1981, AMAX abandoned the property due to low metal prices and complex metallurgy. In 2000, Teck acquired the property and has been conducting mineral exploration and environmental activities to-date (Teck

American, 2010). The geology of the Mesaba deposit is generally characteristic of the mineralized basal Duluth Complex described above.

This study focuses on weathered material which is not widespread on the surface of the property because of extensive glacial cover (Miller and Severson, 2005), see Figure 1-3. Drilling has shown that the deposit has not been extensively oxidized below the glacial cover, so weathered material would not be a large source of waste rock if the deposit was mined (Severson, 2014 personal communication). Rock sampled for this thesis came from a few of the sparse exposures on-site.

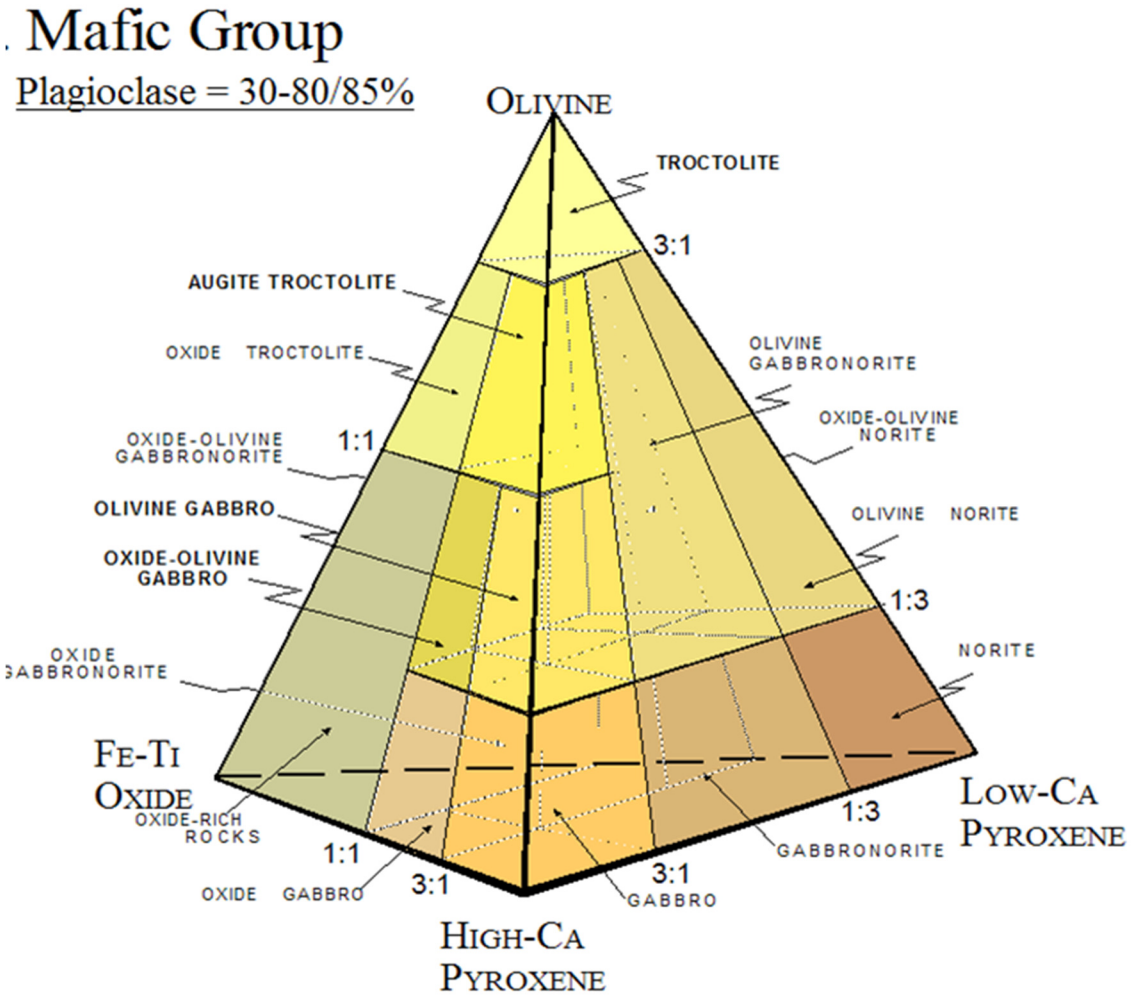


Figure 1-2. Rock classification scheme used to delineate rock types based on visual estimation of the modal abundance of minerals (from Miller et al., 2002).

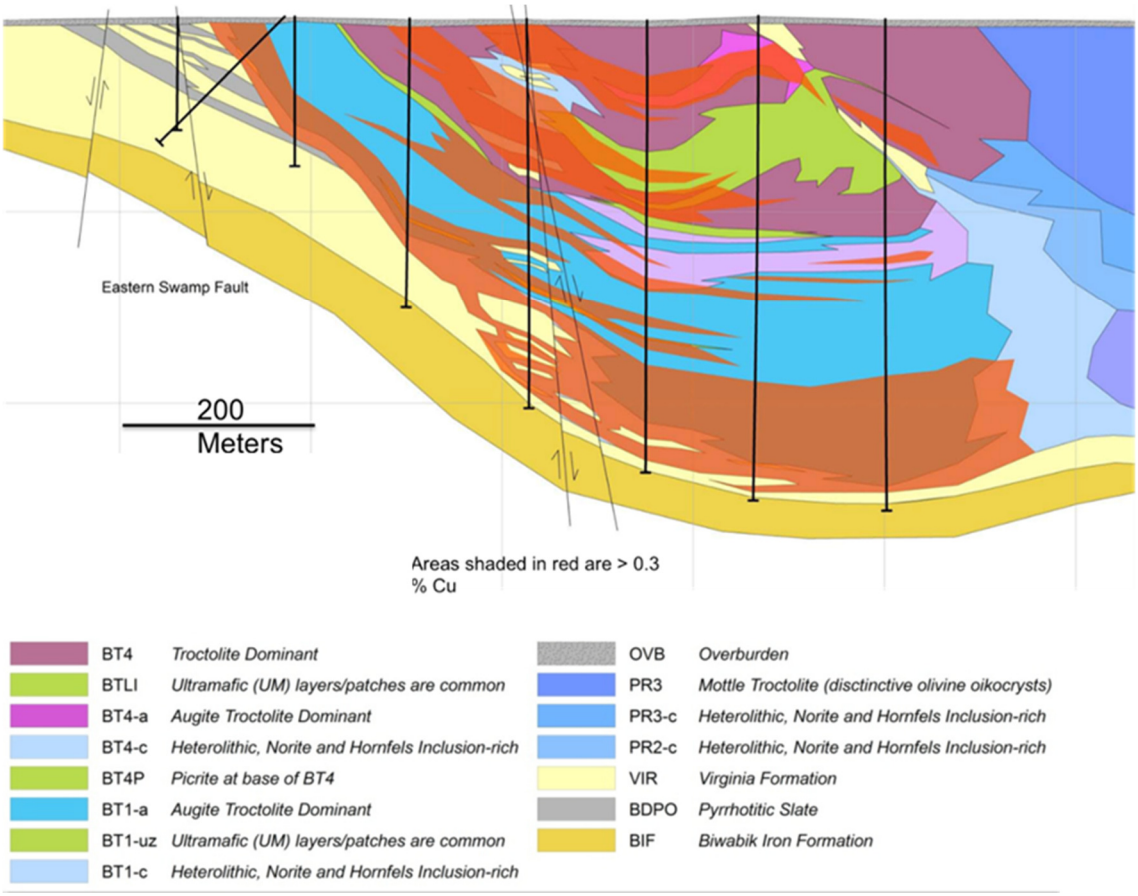


Figure 1-3. Cross section through the Mesaba deposit shown to illustrate the dominance of troctolitic rock types throughout, and the general distribution of ore-grade material (red denotes > 0.3 wt. % copper). Note thin, extensive overburden unit. (Modified from Teck American, 2010)

## 1.2 Mine waste geochemistry

The geochemical evolution of mine-waste systems is site specific and dependent on a number of factors. Major factors include the composition of the primary mineral assemblage, temperature, pH, and redox potential as well as hydrologic conditions, and the mass and surface area of the rock. Geochemical modeling can be used to predict the chemistry of water draining specific types of mine wastes for example, tailings, acid generating waste rock and non-acid generating waste rock (INAP, 2009). Effective segregation of various mined materials, along with implementation of appropriate rock

management strategies for each waste type, can help minimize environmental impacts of mining- especially acid mine drainage (AMD) (Blowes, et al., 1994; Kuipers et al., 2006). Even with successful mitigation of AMD, circumneutral-pH drainage may also be an environmental concern as it can contain concentrations of certain components that exceed water quality standards (Price, 2009; Plante et al., 2014). As a part of mine planning and environmental impact assessment, predictions of mine water quality are being developed and refined for Duluth Complex projects.

The oxidation of iron-bearing sulfide minerals can release acidity, sulfate, iron, and trace metals (e.g. Reaction 1-3) while other minerals (e.g. carbonates and silicates) can supply alkalinity (e.g. Reaction 1-5) and other environmental contaminants. Lastly, newly formed weathering products further influence the system as solid-phase controls on aqueous-species concentrations. Acid production/ acid neutralization reactions and precipitation reactions important to understanding the pH of water draining Duluth Complex waste systems are presented below.

### 1.2.1 Sulfide oxidation

Sulfide mineral oxidation (e.g. Reaction 1-1, Reaction 1-2) is thermodynamically favored and kinetically fast in oxidizing, water-bearing systems (Pugh et al., 1984; Plumlee et al., 1999). All of the major sulfide minerals in Duluth complex rocks contain ferrous iron, thus these minerals are considered acid producing (Reaction 1-4). A review of pyrrhotite oxidation is presented by Belzile et al. (2004) and is summarized below. Reactions for other sulfide minerals are similar, except, in addition to S and Fe, other metals (e.g. Cu, Ni) are released.

Pyrrhotite shows a non-stoichiometric composition as $Fe_{1-x}S$ where $x$ varies from 0 (FeS, troilite) to 0.125 ($Fe_7S_8$). The non-stoichiometry is due to a system of ordered vacancies within the Fe lattice. Oxygen and ferric iron are the two most important oxidants for pyrrhotite. When $O_2$ is the primary oxidant, as is the case for pH>4, the reaction can proceed as follows:

Reaction 1-1

$$Fe_{(1-x)}S_{(s)} + (2-(1/2)x)\ O_2 + xH_2O \rightarrow (1-x)Fe^{2+} + SO_4^{2-}{}_{(aq)} + 2xH^+{}_{(aq)}$$

Under acidic conditions, where ferric iron is soluble, it acts as the oxidant and the reaction proceeds as:

Reaction 1-2

$$Fe_{(1-x)}S_{(s)} + (8-(2)x)\ Fe^{3+} + 4H_2O \rightarrow (9-3x)Fe^{2+} + SO_4^{2-}{}_{(aq)} + 8H^+{}_{(aq)}$$

Ferrous iron ($Fe^{++}$) is insoluble (~pH >4.5) and is oxidized to ferric iron ($Fe^{+++}$) (Reaction 1-3) it can then precipitate as a solid poorly crystalline iron oxide (Reaction 1-4):

Reaction 1-3

$$Fe^{2+} + ¼\ O_{2(aq)} + 2H^+ \rightarrow Fe^{3+} + ½\ H_2O$$

Reaction 1-4

$$Fe^{3+} + 3H_2O \rightarrow Fe(OH)_{3(s)} + 3H^+$$

It is possible to balance the pyrrhotite oxidation reaction where proton generation is much less than pyrite on a mole sulfur basis, but this is not consistent with field observations that suggest similar acid generation rates (Jambor, 2003). The formula $Fe_5^{2+}Fe_2^{3+}S_8$ may approximate complex ferrous-ferric interactions in pyrrhotite, thus the oxidizable Fe component is $Fe_5S_8$ or $Fe_{1.25}S_2$, close to the mole ratio of pyrite (Jambor, 2003).

It has been suggested that the crystal structure of pyrrhotite can affect its oxidation rate because increased vacancies may facilitate diffusion of Fe to the oxidation surface. While this explanation is consistent with observations of pyrrhotite reacting 20-100 times faster than pyrite, consensus in the literature has not been reached as to the

relative reaction rates of pyrrhotite grains of different crystal structures (for example Langman et al., 2015).

As oxidation progresses, sulfur is completely removed through progressive oxidation reactions ending with sulfate ($SO_4^{2-}$). The iron component of pyrrhotite can be mobilized as an aqueous species or can form ferric iron minerals such as goethite, lepidocrocite, and ferrihydrite (Jambor and Dutrizac, 1998).

### 1.2.2 Silicate dissolution

Intermediate composition plagioclase and olivine (+ pyroxene) are the dominant silicate minerals that form Duluth Complex deposit rocks (Section 1.1.1) (Miller, et al. 2002). These minerals are considered fast weathering silicates and can provide significant acid neutralization potential (Jambor and Blowes, 1998; Jambor, 2003; Brantley, 2008). Plagioclase and olivine dissolution reactions (Reaction 1-5, Reaction 1-6) in the presence of water acidified by carbonic acid are presented below.

Reaction 1-5:

$$CaAl_2Si_2O_8 + H_2O + 2\ H_2CO_3 \rightarrow Ca^{2+}_{(aq)} + Al_2\ Si_2O_5(OH)_{4(s)} + 2\ HCO_3^-$$

$$2NaAlSi_3O_4 + H_2O + 2\ H_2CO_3 \rightarrow 2Na^{2+}_{(aq)} + Al_2\ Si_2O_5(OH)_{4(s)} + 4SiO_{2(s)} + 2HCO_3^-$$

Reaction 1-6:

$$MgFeSiO_{4\ (Fo50)} + 4\ H_2CO_3 + 2H_2O \rightarrow Mg^{2+} + Fe^{2+} + H_4SiO_2 + 4HCO_3^- + 2H_2O$$

Both the anorthite and albite components of plagioclase produce alkalinity during dissolution, however plagioclase with higher anorthite content typically reacts faster (e.g. Schott et al., 2009). Dissolution of the forsterite (Mg) component of olivine contributes to the production of alkalinity. The fayalite component however, does not contribute alkalinity or acidity, because oxidation of $Fe^{2+}$ is an acid generating process regardless of the Fe source (Reaction 1-4) (Jambor, 2003). Nickel will also be released by olivine

dissolution- Ni concentrations in Mesaba deposit olivine grains range from 400-2000 mg/kg (Al-Alawi, 1985)

Dissolution mechanisms, rate limiting steps, and final products of silicate dissolution has been well studied (e.g. Lasaga and Kirkpatrick, 1981; Schott et al., 2009 and references therein). Generally, dissolution has been observed to be a step-wise process. In the case of plagioclase, first, the exchange of $Na^+$ and $Ca^{2+}$ for $H^+$ results in an increase in solution pH. Second, $Al^{3+}$ is released into solution due to the breaking of Si–O–Al bonds. The final step is breaking Si-O-Si bonds, releasing dissolved Si. Reaction rates are dependent on solution pH, surface area, and the saturation index for the mineral of interest. Dissolution rates increase with greater surface area, far from equilibrium conditions (i.e. low concentrations of aqueous Ca, Na, Si, Al) and in acidic water. Like sulfide minerals, reported dissolution rates in the literature vary by several orders of magnitude for individual mineral species (Schott et al., 2009). Eary and Williamson (2006) have shown, using only published reaction rate data for silicate and sulfide minerals and numerical modeling, that the dissolution of silicates can produce neutral-pH conditions in the presence of low sulfide mineral abundance. This has also been observed for sulfide-bearing waste rock piles at mine sites (Plante, et al., 2010). As a side note, materials in waste rock piles are not typically reacting under water-saturated conditions. As such, 'moist air' is probably the dominant reactant. In light of this, incorporation of experimental data conducted under water-saturated conditions to predictive evaluations of waste rock pile water chemistry can be problematic (Jerz and Rimstidt, 2004).

### 1.2.3 Weathering product formation as a metal attenuation mechanism

Precipitation of discrete trace-metal secondary minerals (e.g. malachite) and sorption/coprecipitation on poorly crystalline iron oxides (e.g. ferrihydrite) are commonly inferred (e.g. Eary, 1999; SRK, 2007) and observed (e.g. Valente and Gomes, 2009; Smith et al., 2013) as solubility controls for metal concentrations in mine waters. A schematic of the complex geochemistry occurring at the grain scale is provided in Figure 1-4.

Metal attenuation by weathering products in natural and mine impacted systems has been investigated though direct observation (microscopy, spectroscopy) and geochemical modeling (e.g. Plumlee et al. 1999; Petrunic, 2009; Smith et al. 2013). High-resolution analytical tools are often required to investigate secondary minerals because of their small size, poor crystallinity, and low concentrations. A combination of methods is required to adequately characterize weathering products and the co-existing water (Nicholas, et al. 2007a; Jamieson et al., 2015).

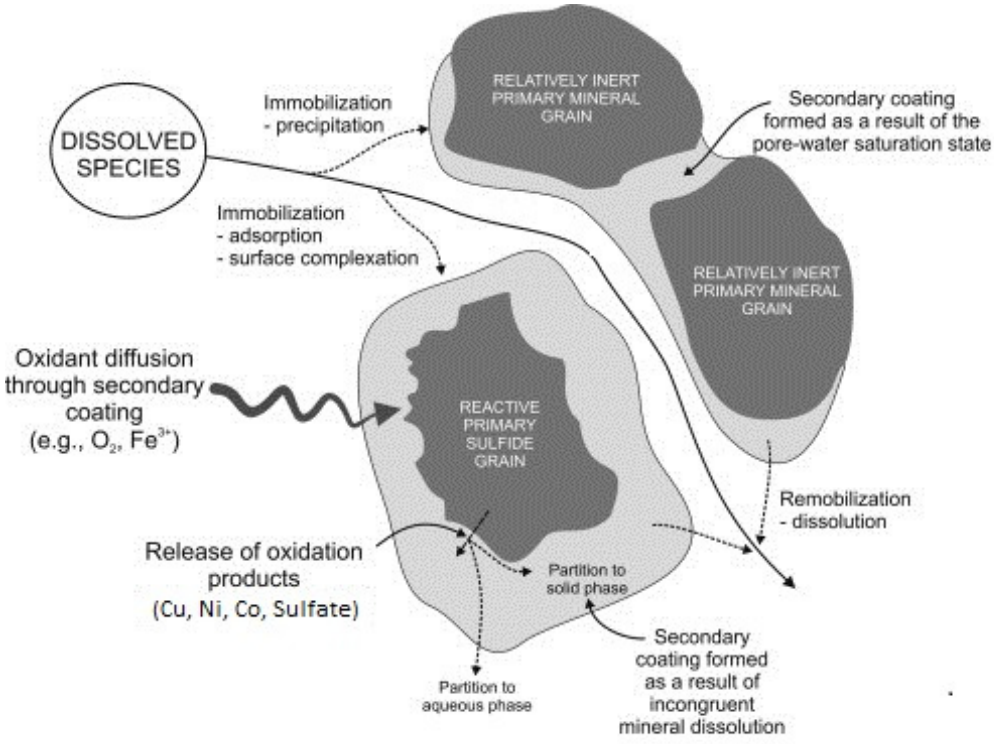


Figure 1-4. Schematic diagram showing some of the geochemical processes in sulfide-bearing mine waste systems that may lead to diverse weathering products and aqueous species concentrations. Modified from Petrunic et al., 2009.

## 1.3 Previous studies on Duluth Complex rock as future mine waste

There is a large body of existing work that demonstrates primary mineral sources of acidity, sulfate, metals, and acid neutralization for Duluth Complex rock in addition to some studies on weathering products. The Minnesota Department of Natural Resources (MDNR) and others have been researching mine waste drainage associated with Duluth Complex rock since the mid-1970s using a variety of methods (see Lapakko and Antonson, 2012 for a complete summary and references to other works). There has also been extensive characterization of rock conducted as a part of environmental review for NorthMet, a proposed Duluth Complex project (SRK, 2007). A review of mine waste characterization methods and results from Duluth Complex studies is presented below.

## 1.4 Laboratory kinetic tests

Laboratory kinetic tests are conducted on small masses of well characterized material to evaluate drainage chemistry though time under controlled conditions (Price, 2009). Pre-test characterization can include mineralogy and petrology, particle sizing, and chemical composition (bulk and grain-scale). Following the initial material characterization an artificial weathering environment is created where reaction rates are determined though the measurement of chemical constituents contained in an aqueous leachate.

One commonly employed kinetic test method that has been used to characterize Duluth Complex rock is the humidity cell test (HCT). The ASTM standard method uses a plastic column filled with 1 kg of crushed rock, exposed to alternating dry and humid air, and rinsed weakly with distilled water (ASTM D5744-2013). MDNR kinetic tests (using ASTM- type humidity cells and similar apparatuses) have yielded an especially valuable public dataset. The findings from small-scale kinetic tests are summarized below.

1. Oxidation of sulfide minerals (including but not limited to: pyrrhotite ($Fe_{(1-x)}S$), chalcopyrite ($CuFeS_2$), cubanite ($CuFe_2S_3$), and pentlandite ($(Fe,Ni)_9S_8$)) are the main source of acidity, sulfate, iron, and trace metals in the drainage (Lapakko, 1980).
2. Rock containing less than 0.22 weight percent S consistently generates drainage pH above 6 over long time periods (18+ years in some long-term tests) and, therefore, is not acid generating. Generally, sulfur content of the rock controls trends in pH as well as sulfate and trace metal release (Lapakko et al., 2004a).
3. The main acid-neutralizing mineral is anorthite-rich plagioclase. Olivine and pyroxene can also contribute to acid neutralization in addition to accessory silicates including biotite, chlorite and amphibole (Lapakko et al., 2004a).
4. Comparisons of leachate chemistry between acidic and neutral pH kinetic test cells indicate metals are strongly attenuated in the neutral pH test apparatuses (SRK, 2007).
5. Materials from a laboratory kinetic test have been analysed by scanning electron microscopy (SEM). Iron rich secondary phases associated with oxidized regions of sulfide grains commonly contain significant amounts of silicon and aluminium (Nicholas et al., 2007b).

## 1.5 Field test barrels

In June 2013, plastic barrels were filled with crushed (-1 in.) low sulfur Mesaba deposit rock (Table 1-1) and placed on site, open to the atmosphere, as a part of environmental geochemistry test work (Figure 1-5). Precipitation contacts the material and is collected below, where it is periodically analyzed for pH and conductivity in the field, and then sampled (bottled) and sent to a lab for complete chemical analysis. Leachate chemistry from July, 2013 to October, 2014 was available for use in this thesis. The leachate is typically more concentrated (higher total dissolved solids) than HTC

leachate, but it is still well below gypsum saturation (i.e. $SO_4$ and Ca typically around 100 mg/L each).


Figure 1-5. Photo of barrel tests constructed on site at Mesaba in June, 2013. Small lower buckets are used to collect water (atmospheric precipitation) that drains through the crushed rock contained in the barrels.

Table 1-1. Summary of Mesaba barrel experiment rock characteristics.

| Barrel | Mass (kg) | Sulfur Content (wt. %) |
|---|---|---|
| B1 - Troctolite | 300 | 0.01 |
| B2 - Troctolite | 300 | 0.01 |
| B3 - Troctolite | 300 | 0.10 |
| B4 - Troctolite | 100 | 0.10 |
| B5 - Troctolite | 300 | 0.30 |
| B6 - Ultramafic | 300 | 0.03 |
| B7 - Virginia Fm. | 300 | 0.30 |
| B8 - Blank | - | - |

## 1.6 Field test piles

Large-scale experimental waste rock piles have provided additional information on Duluth Complex weathering. The following review was summarized from Lapakko, 1993b and Lapakko et al., 2004.

In the early 1970s, MDNR and AMAX (an exploration company planning mine development at Mesaba) constructed six test piles (AMAX piles) containing 820-1300 tons of deposit material each (Figure 1-6). Natural precipitation drained through the piled rock and was collected from containment structures below. Leachate characteristics were monitored from 1977 to 1994 when the piles were decommissioned (encapsulated in concrete). The material used represents rock that, by today's standards, would likely be considered 'ore grade'.

All AMAX piles eventually produced acid rock drainage (ARD) characterized by low pH and high metals concentrations. However, before 'going acidic' several piles produced circum-neutral pH water for a significant time. The geochemical response of the AMAX piles and small scale kinetic tests containing the same material was similar. This suggests small scale tests can be used for their intended purpose: to predict certain aspects of the geochemical response of larger systems. The results from the tests both showed decreasing pH, increasing sulfate, fairly constant calcium release, and increased magnesium release over time. Quantitatively, constituent release rates (flux) for the large-scale tests were 11-36 percent of lab-based rates (per unit mass). This is likely a combination of differences with respect to secondary mineral formation, reactive surface area, temperature, preferential flow paths, oxygen diffusion gradients and other factors that differ between the two test environments (Lapakko et al., 2004b). The AMAX pile data are particularly valuable due the scale of the experiment (leading to the creation of highly concentrated waters, e.g. ~ gypsum saturation), the level of material characterization pre- and post-experiment, and the long duration of leachate monitoring. Limitations include the high-sulfur content of the rock and the limited list of analytes. For example, arsenic was not measured in the drainage.

Figure 1-6. Photograph showing the construction of large-scale AMAX test piles (from Lapakko et al., 2004).

### 1.6.1 Field test pile secondary minerals

There has been some previous characterization of attenuation mechanisms and weathering products in Duluth Complex rock. Work to-date has mostly focused on AMAX pile material using sequential chemical extractions, mineral characterization, and numerical modeling (Lapakko, 1993b; Kelsey, 1996; Lapakko et al., 2004). In addition, limited SEM analysis of decommissioned small-scale kinetic test material has also been completed (Nicholas et al., 2007).

Kelsey (1996) worked with material from AMAX pile FL 1 (see Lapakko et al., 2004 for a complete summary of pile characteristics) to evaluate the degree of metal attenuation provided by secondary iron oxides. The study documented metal attenuation using a sequential chemical extraction procedure that specifically targeted iron-rich weathering products and also employed geochemical modeling. To model metal sorption as an attenuation mechanism, inverse modeling using a MINTEQAK triple layer sorption code and site density/ surface complexation constants for hydrous ferric oxide (HFO)

reported in Dzombak and Morel (1990) were employed in the study. In addition, X-ray diffraction (XRD) of the material was used to investigate the mineral identity of the iron-rich weathering products.

Results from the sequential chemical extraction showed limited trace metal attenuation in the studied AMAX system. This was attributed to the low pH of the effluent and competition for adsorption sites by other ions in solution. Although low in concentration, Cu was contained in poorly crystalline secondary iron phases at the highest concentration followed by Ni, Zn, and Co. No crystalline secondary iron oxide/ hydroxide minerals were definitely identified using XRD. The modeled water chemistry generally reflected the actual observed concentrations of $H^+$ and major/ trace ions. The modeled sorption onto HFO generally followed actual observations from the sequential extraction.

During deconstruction of the test piles in 1994, MDNR submitted weathering products for characterization by XRD and scanning electron microscopy. Minerals identified included montmorillonite group clays, native copper and sulfur, malachite, secondary Cu-sulfides and gypsum (Lapakko et al., 2004b). Iron-rich coatings/ precipitates were also noted in the field and by SEM.

## 1.7 Operational-scale test piles- Dunka Pit stockpiles

Iron mining operations at the Dunka mine stripped mineralized Duluth Complex rock starting in the 1960s to access underlying taconite (iron) ore. The waste material was separated into eight piles on site. MDNR reported that the piles contained a mix of rock types including iron formation, Virginia Formation, and Duluth Complex. The drainage chemistry is typically acidic and metal-rich albeit seasonally variable (Lapakko, 2012; Lapakko and Olson, 2015). No weathering product characterization work has been published on the Dunka material.

## 1.8 Generalized conceptual model of Duluth Complex waste rock weathering

Previous studies collectively provide a general framework for understanding environmental behavior of Duluth Complex rock. Major aspects of this framework include:

1. Oxidation of primary sulfide minerals releases acidity, sulfate, iron, and trace metals.
2. Dissolution of mafic silicates and plagioclase produces alkalinity which can raise pH that would otherwise be depressed by acid derived from sulfide oxidation and atmospheric $CO_2$.
3. Rock containing less than 0.22 wt. percent S consistently generates drainage pH above 6 in small scale tests. Sulfur content is a suitable metric to segregate acid producing and non-acid producing rock at a future mine site (Day and Kennedy, 2015). Generally, sulfur content also controls trends in sulfate and trace metal concentrations in all test environments.
4. The field test pile work shows that geochemical environments in large scale systems can form a variety of weathering products including common weathering products (gypsum, clay, and poorly crystalline iron oxides) and well as less common minerals (native copper, native sulfur, secondary Cu-sulfide minerals and malachite). Trace metal attenuation clearly occurs even under bulk acidic conditions, but especially when drainage pH is neutral to alkaline.
5. Metal:sulfate ratios in test cell leachates suggest trace metal attenuation is occurring to a large degree here under circum-neutral conditions.

## 1.9 Problem statement

Test systems of various sizes and complexities have provided some data for predicting the response of Duluth Complex rock to subaerial exposure. A detailed study into how weathering products control metal concentrations in water associated with low sulfur, non-acid producing rock that would likely make up the bulk of any waste produced at a future Duluth Complex mine has not been completed. This represents a significant gap in our current understanding, as most attenuation mechanisms are pH-dependent (e.g. sorption onto ferrihydrite, precipitation of metal-hydroxides/ carbonates). Many of the methods used thus far lack detailed solid-phase characterization of poorly crystalline secondary iron oxides, so the results of previous studies may not be sufficiently precise to evaluate the influence of these phases on water quality under mine site conditions.

In this study, weathering products were characterized using conventional mineral characterization techniques including light microscopy, XRD, and SEM as well as high-resolution chemical analysis by synchrotron methods. The results have been interpreted in the context of the current understanding of the environmental behavior of Duluth Complex rock. Exploratory numerical modeling was used to further investigate possible controls on trace metal concentrations- especially at circumneutral pH. A conceptual geochemical model is presented to summarize the work.

# 2 Materials and Methods

The following section describes sampling and characterization methods utilized for this study. The research conducted for the present thesis represents one phase of a larger technical program, with the overall objective of characterizing and interpreting the significance of weathering products on exposures of rock at the Mesaba Project site. In addition to the research conducted for the thesis, a preliminary phase of work was designed and coordinated by consultants at SRK and Barr Engineering, with the analyses executed by contract labs. Selected work conducted in the preliminary phase by contract labs is included in the method sections below, and designated as such. Samples were collected from rock exposures on the Mesaba site. Bulk chemistry and solid phase characterization was conducted through a set of complementary analytical methods, which provided multiple lines of evidence for weathering product identity.

## 2.1 Field sampling

Rock sampling on Teck's Mesaba property occurred on September, 17th 2013 (M-SM series) and June 2nd 2014 (BS-series). Three areas (shown in Figure 2-1, Figure 2-2) were sampled:

| | |
|---|---|
| Area 1 | natural outcrop exposed near a swamp (collected September, 17th 2013) |
| Area 2 | historic railroad cut (collected September, 17th 2013) |
| Area 3 | surface material near the 2008 Teck bulk sample collection area (collected June 2nd 2014) |

At Areas 1 and 2, two types of grab samples were collected. "Type 1" included small clasts (typically < 2-5 cm) that occurred at the base or face of outcrops. The clasts (totaling ~1 kg) were collected from a several foot area around exposures to increase sample representation (i.e. reduce nugget effect). "Type 2" samples were removed from exposures using a rock hammer; each sample weighed approximately 1 kg. All samples

were placed in labelled polyethylene sample bags. Sample locations were recorded using an ETREX 10 handheld GPS. Sample selection utilized an opportunistic sampling strategy; i.e. samples were selected that showed visual evidence of weathering, with an effort to capture range of weathering products at each outcrop. However, the assortment of rocks sampled at each exposure is not necessarily representative of the entire rock comprising that outcrop. Examples of weathered exposures are provided in Figure 2-3.

Area 3 samples were collected from area surrounding Teck's 2008 bulk metallurgical sample site. Rocks were collected in the vicinity of the southern portion of the presently reclaimed blast site, and were presumably exposed during bulk sample collection (Severson personal communication, 2014). A summary of the samples collected is provided in Table 2-1.

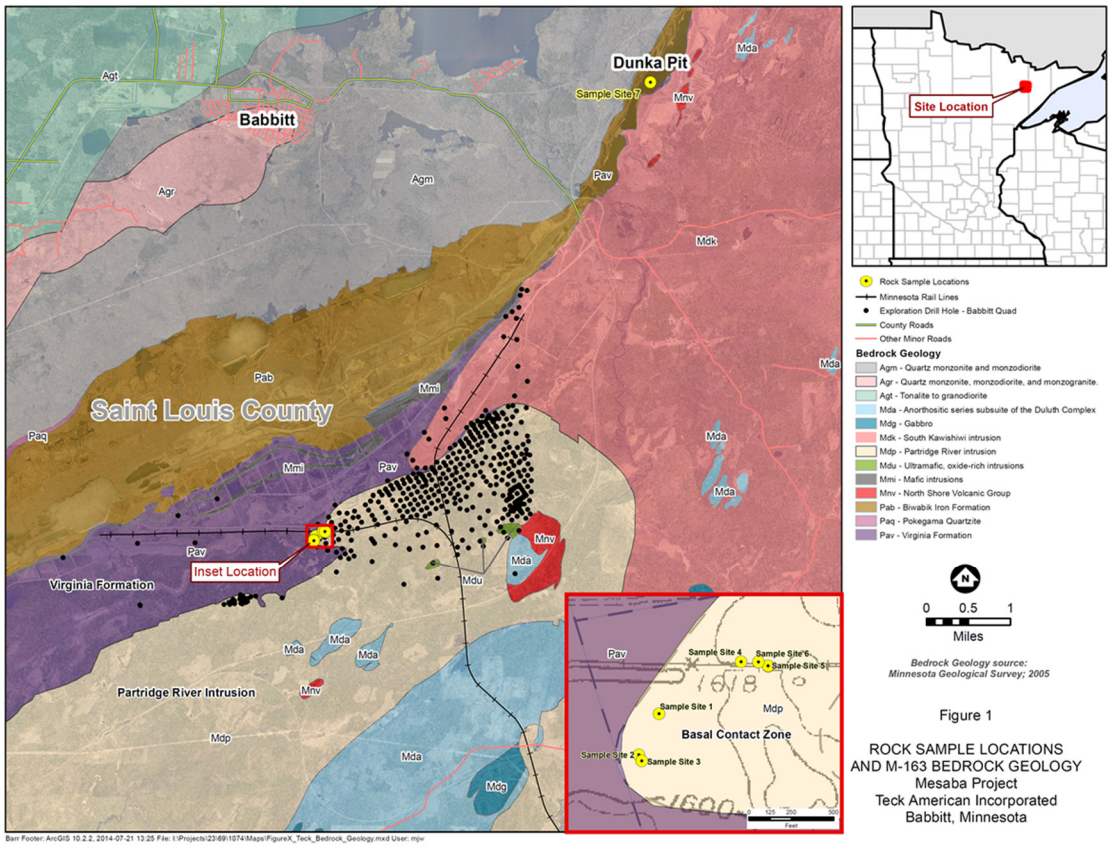


Figure 2-1. Map showing sample locations in relation to local geological and geographical features. From Barr and SRK, 2014 using M-163 bedrock geology (Jirsa et al., 2005).

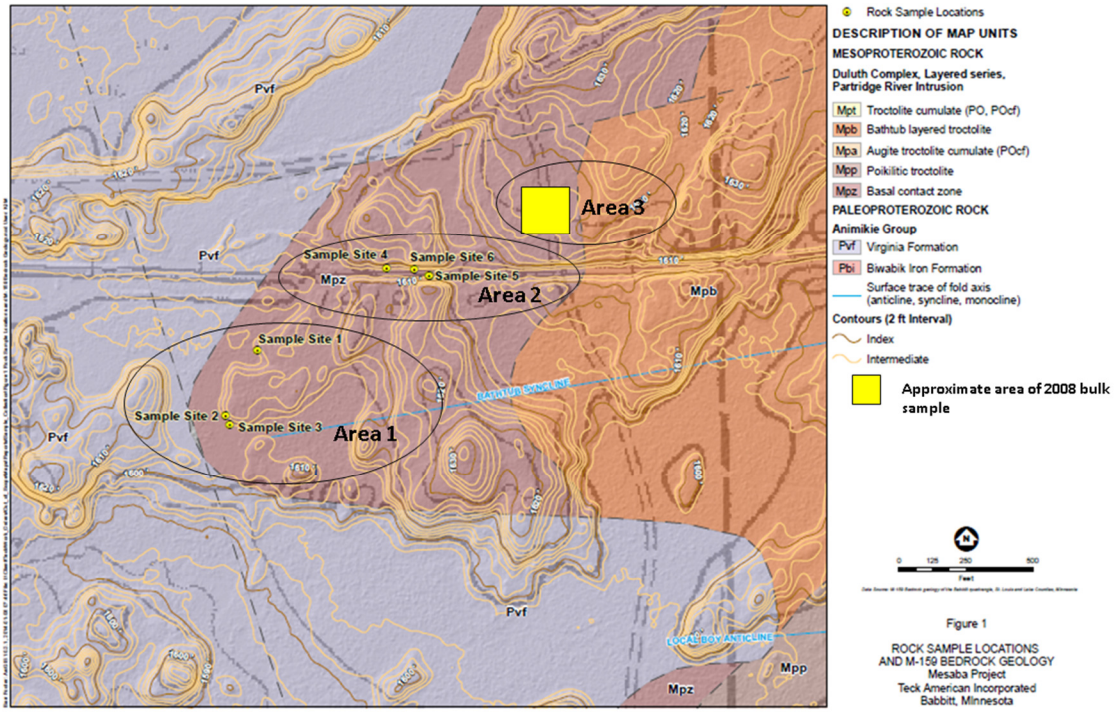


Figure 2-2 Detailed map showing sample locations on M-159 (Miller and Severson, 2005) bedrock geology map with 2-foot LiDAR based topography (modified after Barr and SRK, 2014).

Figure 2-3. Sample site M-SM-006 (historic rail cut) showing the accumulation of efflorescent salts (left). Sample site M-SM-001 showing highly weathered natural outcrop with lichen (right).

Table 2-1. Sample summary. Geochemistry samples analyzed for Barr/SRK 2014.

| Sample ID | UTM | | Date | Site Description | Observations | Thin Section(s) | Geochemisry Sample(s) |
|---|---|---|---|---|---|---|---|
| | East | North | | | | | |
| M-SM-001 | 580328 | 5276473 | 9/16/2013 | Outcrop, Area 1 | Naturally weathered outcrop on western edge of deposit, near contact with Virginia Fm. | M-SM-001-b<br>M-SM-001-b-syn | M-SM-001 A<br>M-SM-001 B<br>M-SM-001 C |
| M-SM-002 | 580296 | 5276386 | | Outcrop, Area 1 | Similar to M-SM-001, slightly north | none | M-SM-002 A<br>M-SM-002 B<br>M-SM-002 C |
| M-SM-003 | | | | | Virginia Formation xenolith sample for Phase I (Barr/SRK, unpublished) | none | M-SM-003 A<br>M-SM-003 B<br>M-SM-003 C |
| M-SM-004a | 580467 | 5276560 | | Railroad gossan - west, Area 2 | White sulphate (?) mineral collected | none | M-SM-004-a |
| M-SM-004b | | | | | Grab samples of rubble collected across intensely weathered exposure. | none | M-SM-004c A<br>M-SM-004c B<br>M-SM-004c C |
| M-SM-004c | | | | | Heavily oxidized (covered in rusty coatings) hand sample. | M-SM-004-c | none |
| M-SM-005 | 580521 | 5276556 | | Railroad gossan - south-east, Area 2 | Shaded side of outcrop - weathering appears less intense, more competent rock | M-SM-005-b<br>M-SM-005-syn | M-SM-005 A<br>M-SM-005 B |
| M-SM-006a | | | | Railroad gossan - north-east, Area 2 | North side far more oxidized, with white sulphate (?) mineral present | M-SM-006-a | none |
| M-SM-006b | | | | | Grab samples of rubble collected across exposure. Intense weathering. | none | M-SM-006b A<br>M-SM-006b B<br>M-SM-006b C |
| BS-001-w | ~580688 | ~5276600 | 7/2/2014 | Site 1- Teck, 2008 bulk sample, Area 3 | Hand sample appears extensivly weathered, paleoweathering. Blue-green (malachite?) coating. | BS-001-w | none |
| BS-002-w | | | | | Hand sample appears to be non-weathered based on unaltered sulfides on rock | BS-002-w | none |
| BS-003-w | | | | | Hand sample appears to be weathered (paleoweathering), but less than BS-001-w. | BS-003-w | none |
| BS-004-w | | | | | Hand sample visually non-weathered based on abundant unaltered sulfides on sample surface. Significant mineralization 3-5% sulfide. | BS-004-w | none |

## 2.2 Static testing and bulk chemical analysis

As a part of the preliminary phase of work, samples selected for geochemical analysis (Table 2-1) were shipped to SGS-Canada for a series of chemical analysis which constitute “static tests” of mine wastes, termed as such because these tests do not evaluate the reactivity of rock over time (Price, 2009). These analyses included, sulfur speciation, carbon, paste pH, rinse pH, conductivity as well as bulk chemistry.

### 2.2.1 Sulfur analyses

Sulfur speciation included total sulfur and two sulfur-as-sulfate analyses described below. Total S was determined using the LECO furnace method (Price, 2009). In the LECO method, the furnace is operated at or above 1650 °C. At this temperature all sulfur species are volatilized in the presence of oxygen to sulfur dioxide. The gaseous sulfur dioxide is measured by an infrared spectrometric cell (Price, 2009). The limit of detection is 0.01 wt. percent sulfur.

Sulfur as sulfate was determined by two different leach methods and analyzed by inductively coupled plasma mass spectrometry (ICP-MS). Ideally, the solvents only dissolve sulfur from specific mineralogical phases. However, uncertainty exists in the specificity of these analyses because sulfur bearing minerals can be dissolved completely, partially, or not at all. For example, if a sulfur bearing mineral is occluded in an impervious gangue, its complete extraction will be more difficult than if it occurs as large, exposed grains (Price, 2009).

Sulfur as sulfate was determined by leaching the sample with diluted HCl and analyzing the resulting liquid by ICP-MS. Mineral species that could contribute sulfur to this leach include:

1. Highly soluble sulfate salts, such as melanterite and epsomite and less soluble sulfate species such as gypsum (complete dissolution)
2. Relatively insoluble iron and aluminium hydroxyl sulfates (e.g. jarosite and alunite) and organic matter (partial dissolution)

Sulfur as sulfate was determined by ICP-MS analysis of a dilute $Na_2CO_3$ leach. Mineral species that could contribute sulfur to this leach include:

1. Highly soluble sulphate salts, such as melanterite and epsomite and less soluble sulphate species such as gypsum (complete dissolution)
2. Relatively insoluble iron and aluminium hydroxyl sulphates (e.g. jarosite and alunite), as well as some sulphur from organic matter (partial dissolution, although greater than HCl leach)

Sodium carbonate will not dissolve barite (Lapakko, 2002 in Price, 2009).

### 2.2.2 Carbon analyses

Total C was determined using the LECO furnace method. For total C analysis, mineralogical (e.g. graphite, calcite) and biological forms of carbon (e.g. lichen) were volatilized in the presence of oxygen to carbon dioxide and analyzed by infrared spectrometric cell (Price, 2009). The limit of detection (LOD) is 0.01 wt. percent.

Total carbonate was determined using coulometry. The crushed sample was digested in hot perchloric acid and the amount of carbon dioxide exsolved during the digestion was measured. Minerals that could report measurable carbon to this test include calcite, dolomite, and siderite. The LOD is 0.01 wt. percent.

### 2.2.3 Mine waste tests

The Sobek method of rinse pH test and electrical conductivity (EC) was conducted on particles that were dry sieve sorted, but had not undergone comminution (i.e. crushing/grinding). The < 2 mm fraction was rinsed with enough distilled water as to allow accurate measurement of pH and EC by an electrode.

The paste pH/EC test was conducted on particles that had undergone comminution creating 100 µm size or smaller fragments. The comminution step could have exposed potentially reactive surfaces that may have been occluded in the Sobek rinse described above. Comminution also increases sample surface area, potentially allowing slowly reacting phases (both primary and secondary) to have a greater contribution to solution chemistry. The solid:water mass ratio used was 1:1; pH and EC were determined by electrode methods.

### 2.2.4 Bulk chemistry: metals by aqua regia- ICP-MS

The *SGS- Metals by Aqua Regia Digestion with ICP-MS Finish* method was used to measure the concentrations of 42 elements contained in aqua regia soluble phases. Aqua regia is a 3:1 combination of full-strength HCl:$HNO_3$ acids and is known to preferentially attack sulfide minerals, but typically partially dissolves many other rock-forming minerals. Silicon is not reported as it is volatilized during digestion.

## 2.3 Powder X-ray diffraction

X-ray powder diffraction (XRD) was conducted to detect and identify any weathering products that are present as crystalline phases. Powder X-ray diffraction scans were performed on both the bulk samples and on samples that had been subjected to a procedure that isolated the weathered portions of the sample. Bulk scans provided an overall sense of the crystalline phases present.

For analyses of the bulk samples, large grab samples were smashed with a hammer. From the resulting clasts, several small pieces (< 1$cm^3$) were randomly selected.

Pieces were then loaded in a hammer crusher and pulverized to approximately fine-sand size. Samples were then ground under acetone with an agate mortar and pestle and mounted in bulk holders.

For the samples with the isolated weathering products, hand specimen-sized clasts were viewed under a binocular microscope to identify visually distinct weathered areas. Rusty alteration coatings were scraped with a stainless steel pick onto a plastic weigh boat. While viewing the granular scrapings under a binocular microscope, materials that appeared to be primary mineral grains were removed. Samples were ground under acetone with an agate mortar-and-pestle and mounted on zero-background plates. Where whitish efflorescent salts or fine greenish-blue materials occurred, these phases were lightly scraped directly onto the zero-background holder to avoid sample loss during grinding.

All samples were analysed with a Phillips XPert MPD diffractometer at the University of Minnesota-Duluth (UMD) with a Cu Kα radiation source. Each sample was scanned between 5° and 65° 2θ at a scan rate of 0.05 deg. /min. X-rays were refined with a graphite monochromator, 1° divergence slit, incident and diffracted Stoller slits and a 10 mm mask. The X-rays were collected with a point scintillator detector and the X-ray tube was operated at 40 kV and 40 mA. Long collection times (~15 hrs.) were used to increase signal to noise ratios. Diffraction data were processed with X-Pert HighScore software and compared to mineral patterns in the International Centre for Diffraction Data (ICDD 2007) database.

## 2.4 Petrographic thin section preparation and analysis

Type 2 samples were smashed using a rock hammer. A representative piece of the larger hand sample was then cut into a rough thin section billet with a water-cooled diamond saw at UMD. A second representative piece of the same original hand sample was selected, and a section of interest was delineated using a permanent marker for diamond sawing under kerosene at Vancouver Petrographic. Final preparation (sawing, polishing, etc.) on all samples was completed using oil or kerosene by Vancouver

Petrographic. All thin sections were polished to 'probe-quality'. Thin sections designated by 'syn' in the name were not subjected to water during preparation at any point during sample preparation (Table 2-1). Thin sections were prepared using a low temperature epoxy (EPO-TEK 301) without the use of heat for curing. Quartz was used as the slide material because it does not contain trace quantities of arsenic which would create false positives during synchrotron analyses. All sections were thinned to ~30 µm.

Each thin section was examined using reflected and transmitted light petrographic microscopes. Grains of interest were noted for future observation using other methods. Transmitted light microscopy was used to document rock types using the scheme presented in Miller et al., 2002 for mafic intrusive rock classification (Figure 1-2). Modal mineral abundance was evaluated using visual approximation. Textural relationships were documented using the cumulate code method (Miller et al., 2002). Reflected light microscopy was used to approximate, by visual estimation, the relative abundance of sulfide minerals, their identities, and weathering/alteration attributes.

## 2.5 Scanning electron microscopy

A JEOL JSM-6590LV scanning electron microscope (SEM), combined with an INCA X-ACT energy dispersive spectroscopy system (EDS) and complementary INCA software, was operated at UMD. Thin sections were carbon coated (~15 nm). Operating conditions were optimized for chemical analysis in EDS mode: 15 kV accelerating voltage, objective aperture: 30 µm, spot size: 61, working distance: 10mm. EDS calibration in INCA was performed on metallic copper. A small piece of copper tape was placed on each thin section and spectra were collected with the quant optimization function. Each thin section was viewed under a range of magnifications, typically between 100 and 1000 times. Grains of interest included grains that had obvious weathering features such as alteration rims and iron rich precipitates occurring as fracture fillings. EDS spectra were collected at several locations on the secondary phases as well as adjacent phases. Line scans provided compositional data across weathering features. Ten or more areas on each thin section were documented to provide a library of location

targets for later synchrotron-based analyses. Because of the micro-scale size and sub-micron to micron-scale heterogeneity of the weathering products, considerable uncertainty as to the accuracy of the chemical results produced by EDS is introduced. Even under optimal conditions, with the best standardization practices, EDS analysis is considered semi-quantitative (Goldstein and Newbury, 2012). Adding the small scale of the weathering features (where interaction volume can be larger than the area of interest), their likely-hydrous nature, and a lack of suitable standards adds further uncertainty. A reduction in accelerating voltage acts to decrease the analytical volume however, detection limits are also increased especially at energies below the K-alpha energy of the element(s) of interest. Spatial resolution for the EDS analysis is on the order of 1 μm at 15 kV. Energy dispersive spectroscopy analysis is sufficiently precise to allow meaningful comparisons between analyses because operating conditions were held constant, however the reported compositions should be interpreted with the above caveats in mind (Goldstein and Newbury, 2012).

## 2.6 Synchrotron-based micro-analysis

Synchrotron based micro-scale X-Ray fluorescence (μXRF) and X-ray absorption spectroscopy (XAS) analyses were conducted at the Stanford Synchrotron Radiation Lightsource (SSRL) in Menlo Park, California on beamline 2-3 in May 2015. Dr. Andrea Foster (USGS) and Dr. Sam Webb (SSRL) provided guidance for the beamline set-up, data collection, and processing. X-rays of requested energy were delivered by a Si (111) double crystal monochromator which were microfocused to an approximately 2x2 μm spot by Kirkpatrick-Baez mirrors.

### 2.6.1 Micro- X-ray fluorescence element mapping

Micro-XRF signals are processed to produce ‘heat maps’, where the relative abundance of elements of interest are displayed as images where higher concentrations are displayed as warmer colors. The colors are assigned based on the number of counts recorded by the detector for a given spot. Seven maps were collected at 13,000 eV from

regions of interest (ROI) on two thin sections using pixel (step) size of 2 or 10 µm and dwell times of 30 or 50 milliseconds. Pixel size was matched to beam diameter to generate the finest-scale element map possible. Emitted X-ray fluorescence was collected by a Vortex Si drift detector oriented at 45 degrees to the sample. Fluorescence from 15 elements (Table 2-2) was monitored in windowed energies as counts, but full per-pixel multi-channel analyzer (MCA) spectra were also collected for each ROI for additional analysis, if required.

MicroToolkit v 1.1 (S. Webb, 2011) was used to process and analyze µXRF maps. Detector dead time was assessed by plotting incoming versus outgoing counts, and determined to be negligible using the XPRESS data processing system (Quantum Detectors). Per-pixel element fluorescence (windowed channel) counts were normalized by the per-pixel incident beam counts (measured from an $N_2$-filled gas ionization chamber placed upstream of the sample).

Unlike SEM-EDS analysis, photons produced during synchrotron X-ray analysis have an escape depth that is greater than the thickness of a standard thin section (30 µm) (Brown and Sturchio, 2002). Therefore, the analytical volume at a single spot is roughly cylindrical with a ~2 µm diameter and 30 µm depth. A comparison of the merits of SEM and synchrotron methods is provided in Table 2-3.

Elemental overlap of windowed fluorescence counts was assessed by analyzing mapped ROIs of single-element XRF standards, and was found to be insignificant for the elements of interest in this study. We did however identify a problem of false positive signal for As, Cr, and Ni in the mapped regions. The false positive signal was approximately of the same magnitude as real signal (producing approximately the same color on a heat map), and was only identified after attempts to collect an XAS spectrum at these points of interest (POI) yielded no edge for the element of interest. Comparison of the full MCA spectrum at false and true positive POIs indicated that false positives for these elements manifest because the baseline fluorescence signal at false positive POIs is

approximately the same magnitude as the true fluorescence signal measured at other POIs. Since the two signals are approximately the same magnitude, they are assigned approximately the same color in the μXRF map, leading to false positive assignments. The concentration of Fe (and therefore the magnitude of the Fe K-shell fluorescence peaks) appears to be the main control on the magnitude of the background signal in the MCA spectrum, so the false positive problem is partly a function of Fe concentration, and indeed was observed only in regions where earlier analysis indicated the predominance of iron rich coatings in the POI. However, the problem is also a function of the very low abundance of As, Cr, and Ni overall in maps where false positive signals were observed. In other words, in order for false positive signal to be observed, high Fe as well as low As, Cr, and/or Ni must be present in the mapped ROI. False positive signals prevent meaningful interpretations of certain elements in the μXRF maps as a standalone method, however where addition information has been gained from other methods (i.e. SEM, μXAS) the data can be used confidently.

Although the data required for semi-quantification of elements in ROIs was collected, the procedure was not performed, because SEM semi-quantitative information was available for the ROIs.

Table 2-2. Elements widowed by the multi-element Si-drift EDS detector.

| **Channel** | **Element** |
|---|---|
| 1 | As |
| 2 | Se |
| 3 | Cr |
| 4 | Fe |
| 5 | Al |
| 6 | Si |
| 7 | Co |
| 8 | S |
| 9 | K |
| 10 | Ca |
| 11 | Ti |
| 12 | Mn |
| 13 | Ni |
| 14 | Cu |
| 15 | Zn |
| 16 | Znb |

Table 2-3. Analytical metrics of synchrotron and SEM methods used. Z is atomic number. Data compiled from Calvin, 2013 (synchrotron) and Goldstein and Newbury, 2012 (SEM).

| **Property** | **SSRL Beamline 2-3 μXRF** | **UMD SEM-EDS** |
|---|---|---|
| Elements detected | See Table 2-2 | Z >3 |
| Elements quantified | Qualitative | Semi-quantitative (Z >10) |
| Elemental detection limit (mg/kg) | ~1 | ~2000 |
| Approximate spot size (diameter-μm) | 2 | 2 |
| Analytical depth (μm) | 30+ | ~5 |
| Theoretical 3D shape of analytical area | Cylinder | Onion |
| Count rate ($10^3$ counts/sec) | 500+ | 15 |
| Sample condition | Ambient conditions | Vacuum |

### 2.6.2 X-ray absorption spectroscopy (XAS)

X-ray absorption spectra were collected from POI identified within the mapped ROIs. For reference, spectral regions are labeled in Figure 2-4 for a generic spectra. The energy range, step size, and count time parameters for element-specific XAS spectra are listed in Table 2-4.

Spectral processing and analysis was performed in SixPack v 1.1 (Webb, 2005) and WinXAS v3.11 (Ressler, 1998). Spectral energy calibration was performed in SamView (part of SixPack) by comparing the 4 –point smoothed 1$^{st}$ derivative of model and sample spectra, and shifting spectral unknowns in accordance with published values (Table 2-5). Spectra were smoothed to remove monochromator crystal glitches and spectral noise. WinXAS was used to apply the Golay-Savitsky filter to XAS spectra from which Extended X-Ray Absorption Fine Structure (EXAFS) was extracted using a polynomial of 4/5 order, smoothing interval of 10 points, and 5 iterations. All spectra were

normalized to a single point, which varied with element (see Table 2-5). X-ray Absorption Near Edge Structure (XANES) analysis was conducted on unsmoothed spectra.

Principle components analysis (PCA) was conducted on Cu XANES data. While the initial goal was to combine PCA and linear combination fitting, a lack of suitable standards prevented successful execution of the latter. In total, twelve high quality spectra were included for PCA.

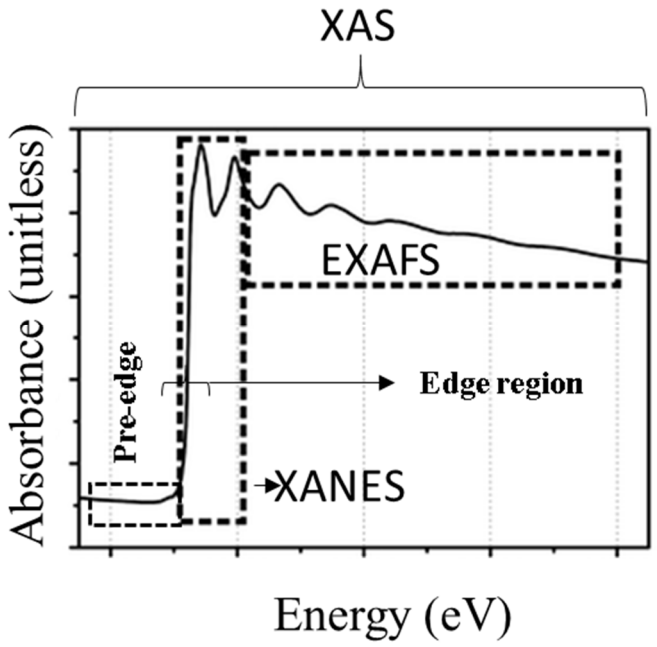


Figure 2-4. Diagram showing the spectral regions in a generic XAS spectra. Acronyms: XAS= X-ray absorption spectrum XANES= Extended X-Ray Absorption Fine Structure EXAFS= X-ray Absorption Near Edge Structure.

Table 2-4. XAS spectra collection procedure.

| Element | Energy range | Pre-edge region [1] | Edge Region[2] | EXAFS region[3] |
|---|---|---|---|---|
| Fe | 6942-7497 | 6882- 7092 | 7092-7142 | 7142-7497 |
| Cu | 8809-9365 | 8809-8959 | 8959-9009 | 9009-9365 |
| Ni | 8103-8444.5 | 8103-8313 | 8313-8364 | 8364-8444.5 (step only to 1.85) |
| As | 11634-12272 | 11634-11844 | 11844-11894 | 11894-12273 |

1. 10 eV Step, 1 second count time
2. 0.35 eV Step, 1 second count time
3. 0.6-4 eV step, 2-5 second count time

Table 2-5. XAS spectra normalization values.

| Element | Calibrant | Reference Energy | Shift Required |
|---|---|---|---|
| Fe | Fe(0) | 7112[1] | -0.125 |
| Cu | CuS | 8984.4[2] | none |
| Ni | Ni(0) | 8333 [1] | -2.29 |
| As | As(0) | 11867 [1] | -1.83 |

1. Thompson and Vaughan, 2001

2. Kumar et al., 2013

# 3 Results

The results from chemical analyses, petrographic studies, and spectroscopy are reported here. Chemical analyses were selected to provide a reference point to previous studies that used rock composition (and other tests) to predict mine waste behavior. Petrography and spectroscopy were essential in determining the presence of weathering products, their characteristics, and interpretation of their significance in limiting metal mobility. The information is separated by analysis type.

## 3.1 Static testing and bulk chemical analysis

Results of static test analyses are reported in Table 3-2 and Table 3-1. Table 3-3 is a table of Pearson correlation factors generated using Excel©. The full result for the static tests are provided in Appendix A. Collectively, the static tests show sulfur becomes oxidized during paragenesis, but can be attenuated in the form of water soluble phases. The static tests also confirm the general absence of carbonate minerals in Duluth Complex deposit rocks. The sulfur as sulfate and pH analyses showed that subaerial weathering promotes considerable S attenuation. The Sobek method of rinse pH and EC showed that all samples contained phases that depressed leachate pH (compared to distilled water in equilibrium with atmospheric $CO_2$, pH 5.6). This indicates very soluble acidic salts were probably present on the surface of all samples. Carbon analysis confirmed previous studies that carbonate minerals are not a major component of Duluth Complex rock, however, organic carbon is present, probably as graphite.

### 3.1.1 Sulfur analyses

Total sulfur was determined by LECO analyzer. The results show samples contain a range of sulfur contents (0.09 to 1.04 wt. %) typical of mineralized Duluth Complex material. Comparing total sulfur values of the weathered samples to material that has been subjected to kinetic test work is possible. Using a <0.22 wt. percent S as the cut-off for non-acid producing material, samples M-SM-001 and M-SM-002 likely were associated with neutral pH drainage during their history of exposure (Table 3-1). The

other samples were likely acid-generating. Both acid forming and acid neutralizing phases hosted in the weathered samples may have altered reactivity due to the accumulation of weathering products on the surface. In light of this fact, the comparison with earlier kinetic test work on Duluth Complex rock is tenuous. Furthermore, highly soluble secondary minerals including sulfate salts and carbonate minerals may dominate initial pH and metal release upon water saturation of weathered material.

All samples contained significant HCl and $Na_2CO_3$ leachable sulfur: between 5 and 57 percent and 10 to 63 percent of total S respectively. $Na_2CO_3$ leached S was always higher than by HCl leach consistent with the notion that $Na_2CO_3$ is a more aggressive rinse (Price, 2009).

### 3.1.2 Carbon analyses

All samples contained C above the 0.01 wt. percent LOD; Total C ranged from 0.03 to 0.46 wt. percent (Table 3-2). Carbonate concentrations were below detection limits in all samples. Assuming very low concentrations of carbonate minerals (indicated by the non-detects for inorganic carbon), the major carbon bearing solids were probably graphite and biological forms of carbon (e.g. lichen). While the relative contribution of each is unknown, graphite has been reported to occur at about 2 volume percent quantities in Mesaba rocks (Al-Alawi, 1985).

### 3.1.3 Mine waste tests

The Sobek rinse pH results show all samples had acidic rinse pH when compared to distilled water at equilibrium with the atmosphere (~5.6). The pH of the rinsates ranged from 3.9 to 4.9. As expected, rinse pH was negatively correlated ($\rho$ = -0.69) with total S (i.e. more sulfur, lower pH).

Generally rinse EC was low < 315 µS/cm except for sample M-SM-004a (EC = 8222 µS/cm) which contained salty encrustations (field observations, Table 2-1). Rinse EC was positively correlated with total S as sulfate determined by both HCl leach and $Na_2CO_3$ leach ($\rho$ = 0.87 and 0.84 respectively).

The Sobek paste pH results show samples had pH ranging from 4.9 to 6.1. Rinse pH was negatively correlated ($\rho$ = -0.90, 0.89) with total sulfate and to a lesser degree ($\rho$ = - 0.16) with total S. Paste pH values were generally higher than rinse pH values.

Paste EC values were generally two to four times higher than values reported in rinse EC tests although paste EC was highly positively correlated with rinse EC ( $\rho$= >0.99).

Table 3-1. Results from S and mine waste tests. Bold total S values indicate neutral pH could be associated with the sample based on previous kinetic studies by MDNR.

| Sample ID | S(T) % | S(SO4) % | S(SO4) % | NP | Fizz Test |
|---|---|---|---|---|---|
| Method Code | CSA06V | HCl Leach | $Na_2CO_3$ Leach | Modified | Sobek |
| LOD | 0.01 | 0.01 | 0.01 | 0.5 | #N/A |
| M-SM 001 A | **0.09** | 0.03 | 0.04 | 5.6 | None |
| M-SM 001 B | **0.09** | 0.03 | 0.04 | 6.3 | None |
| M-SM 001 C | **0.10** | 0.03 | 0.04 | 4.2 | None |
| M-SM 002 A | **0.15** | 0.03 | 0.04 | 9.7 | None |
| M-SM 002 B | **0.17** | 0.03 | 0.04 | 12.0 | None |
| M-SM 002 C | **0.20** | 0.03 | 0.05 | 11.0 | None |
| M-SM 004a | 0.54 | 0.31 | 0.34 | 3.2 | None |
| M-SM 004b A | 0.80 | 0.09 | 0.10 | 8.3 | None |
| M-SM 004b B | 0.70 | 0.07 | 0.09 | 7.8 | None |
| M-SM 004b C | 0.73 | 0.09 | 0.10 | 7.6 | None |
| M-SM 005 A | 0.81 | 0.04 | 0.08 | 12.1 | None |
| M-SM 005 B | 0.91 | 0.05 | 0.10 | 11.4 | None |
| M-SM 005 C | 1.04 | 0.05 | 0.10 | 11.7 | None |
| M-SM 006b A | 0.59 | 0.14 | 0.17 | 12.5 | None |
| M-SM 006b B | 0.58 | 0.14 | 0.17 | 12.5 | None |
| M-SM 006b C | 0.57 | 0.09 | 0.13 | 12.1 | None |
| Duplicates | | | | | |
| M-SM 001 A | | | | 5.8 | None |
| M-SM 002 C | | | 0.05 | | |
| M-SM 006b B | | | 0.18 | | |
| M-SM 006b C | | | | 12.6 | None |
| QC | | | | | |
| GTS-2A | 0.34 | | | | |
| PD-1 | | 4.19 | | | |
| RTS-3A | | | 1.44 | | |
| NBM-1 Reference | | | | 38.4 | Slight |
| Expected Values | 0.35 | 4.27 | 1.34 | 42 | Slight |
| Tolerance +/- | 0.03 | 0.30 | 0.10 | 4 | |

Table 3-2. Results from pH and mine waste tests.

| Sample ID | Rinse pH<br>SU | Rinse EC<br>µS/cm | Paste pH<br>SU | Paste EC<br>µS/cm | Total Inorganic C<br>% | CaCO3<br>NP | C(T)<br>% |
|---|---|---|---|---|---|---|---|
| Method Code<br>LOD | Sobek<br>0.2 | Sobek<br>1 | Sobek<br>0.2 | Sobek<br>1 | CSB02V<br>0.01 | Calc.<br>#N/A | CSA06V<br>0.01 |
| M-SM 001 A | 4.85 | 112.6 | 5.75 | 253 | <0.01 | <0.8 | 0.11 |
| M-SM 001 B | 4.86 | 71.5 | 5.88 | 267 | <0.01 | <0.8 | 0.11 |
| M-SM 001 C | 4.87 | 87.6 | 5.82 | 308 | <0.01 | <0.8 | 0.11 |
| M-SM 002 A | 4.86 | 84.1 | 5.72 | 355 | <0.01 | <0.8 | 0.08 |
| M-SM 002 B | 4.82 | 87.3 | 5.75 | 350 | <0.01 | <0.8 | 0.08 |
| M-SM 002 C | 4.79 | 97.0 | 5.71 | 367 | <0.01 | <0.8 | 0.09 |
| M-SM 004a | 4.09 | 8222 | 4.61 | 4850 | <0.01 | <0.8 | 0.48 |
| M-SM 004b A | 4.43 | 315 | 5.18 | 648 | <0.01 | <0.8 | 0.06 |
| M-SM 004b B | 4.37 | 226 | 5.22 | 606 | <0.01 | <0.8 | 0.08 |
| M-SM 004b C | 4.33 | 223 | 5.13 | 623 | <0.01 | <0.8 | 0.09 |
| M-SM 005 A | 4.29 | 211 | 6.12 | 611 | <0.01 | <0.8 | 0.03 |
| M-SM 005 B | 4.33 | 213 | 5.97 | 667 | <0.01 | <0.8 | 0.03 |
| M-SM 005 C | 4.34 | 238 | 5.97 | 620 | <0.01 | <0.8 | 0.04 |
| M-SM 006b A | 3.93 | 250 | 4.93 | 634 | <0.01 | <0.8 | 0.16 |
| M-SM 006b B | 3.92 | 228 | 4.95 | 640 | <0.01 | <0.8 | 0.16 |
| M-SM 006b C | 3.90 | 203 | 5.38 | 762 | <0.01 | <0.8 | 0.11 |
| Duplicates | | | | | | | |
| M-SM 001 A | 4.88 | 93.9 | 5.79 | 256 | | | |
| M-SM 006b C | | | 5.26 | 786 | | | |
| QC | | | | | | | |
| GTS-2A | | | | | | | 1.98 |
| PD-1 | | | | | | | |
| RTS-3A | | | | | | | |
| SY-4 | | | | | 0.91 | | |
| NBM-1 | | | | | | | |
| Reference | | | | | | | |
| Expected Values | | | | | 0.95 | | 2.01 |
| Tolerance +/- | | | | | 0.06 | | 0.15 |

Table 3-3. Correlation matrix for ABA tests. Highlighted cells indicate values of 0.90 or greater.

| | Rinse pH | Rinse EC | Paste pH | Paste EC | C(T) | S(T) | $S(SO_4)$ | $S(SO_4)$ | NP |
|---|---|---|---|---|---|---|---|---|---|
| Rinse pH | 1.00 | | | | | | | | |
| Rinse EC | -0.28 | 1.00 | | | | | | | |
| Paste pH | 0.61 | -0.55 | 1.00 | | | | | | |
| Paste EC | -0.39 | 0.99 | -0.58 | 1.00 | | | | | |
| C (T) | -0.31 | 0.93 | -0.69 | 0.91 | 1.00 | | | | |
| S (T) | -0.69 | 0.06 | -0.16 | 0.16 | -0.14 | 1.00 | | | |
| S $(SO_4)^1$ | -0.65 | 0.87 | -0.84 | 0.90 | 0.90 | 0.26 | 1.00 | | |
| S $(SO_4)^2$ | -0.74 | 0.84 | -0.77 | 0.89 | 0.84 | 0.38 | 0.98 | 1.00 | |
| NP | -0.38 | -0.50 | 0.20 | -0.43 | -0.50 | 0.38 | -0.26 | -0.15 | 1.00 |

[1] Sulfate determined by HCL leach

[2] Sulfate determined by $Na_2CO_3$

### 3.1.4 Bulk chemistry: metals by aqua regia- ICP-MS

All samples contained concentrations of metals that are typical for Duluth Complex rocks (e.g. SRK, 2007). Because aqua regia can dissolve both sulfide and silicate phases, the results are a sum of the contributions of both. For example, if the samples contained 10% (by weight) olivine containing 1500 mg/kg Ni we can approximate that 150 mg/kg of the reported Ni is associated with olivine. Olivine hosts a significant portion of Ni for low-S samples. Selected results are provided in Table 3-4.

Table 3-4. Selected results from aqua regia chemical analyses.

| **Sample ID** | **S** **%** | **Cu** **mg/kg** | **Ni** **mg/kg** | **Co** **mg/kg** | **Zn** **mg/kg** | **As** **mg/kg** |
|---|---|---|---|---|---|---|
| Method Code | ICM14B | ICM14B | ICM14B | ICM14B | ICM14B | ICM14B |
| LOD | 0.01 | 0.5 | 0.5 | 0.1 | 1 | 1 |
| M-SM 001 A | 0.08 | 2310 | 361 | 36.9 | 56 | 5 |
| M-SM 001 B | 0.08 | 2230 | 363 | 38.9 | 60 | 3 |
| M-SM 001 C | 0.09 | 2390 | 404 | 41.1 | 61 | 3 |
| M-SM 002 A | 0.15 | 1670 | 292 | 44.0 | 72 | 4 |
| M-SM 002 B | 0.16 | 1750 | 290 | 44.5 | 71 | 4 |
| M-SM 002 C | 0.20 | 1970 | 301 | 46.8 | 74 | 5 |
| M-SM 004a | 0.55 | 4830 | 870 | 82.8 | 72 | 5 |
| M-SM 004b A | 0.79 | 5470 | 663 | 64.9 | 87 | 5 |
| M-SM 004b B | 0.71 | 5140 | 708 | 66.2 | 87 | 5 |
| M-SM 004b C | 0.73 | 5310 | 700 | 65.9 | 85 | 5 |
| M-SM 005 A | 0.81 | 4530 | 529 | 58.8 | 88 | 3 |
| M-SM 005 B | 0.87 | 4970 | 533 | 56.4 | 81 | 3 |
| M-SM 005 C | 0.97 | 4890 | 770 | 66.1 | 80 | 4 |
| M-SM 006b A | 0.58 | 3260 | 472 | 57.2 | 74 | 5 |
| M-SM 006b B | 0.58 | 3290 | 439 | 56.6 | 73 | 5 |
| M-SM 006b C | 0.56 | 3040 | 425 | 58.8 | 78 | 4 |
| Duplicate | | | | | | |
| M-SM 006b B | 0.56 | 3300 | 453 | 56.7 | 72 | 5 |
| QC | | | | | | |
| CH4 | 0.70 | 2020 | 48.6 | 24.1 | 201 | 8 |
| Certified Values | 0.73 | 2000 | 49.57 | 22.8 | 189.4 | 8.14 |
| Tolerance (%) | 13.4 | 10.1 | 12.5 | 11.1 | 11.3 | 13.1 |

### 3.3 Powder X-Ray diffraction

X-Ray diffraction on powdered bulk rock samples produced results consistent with previous studies that determined the identity of primary silicate and oxide minerals in Duluth Complex rocks. Samples contained plagioclase, olivine, pyroxene, ilmenite, biotite, and chlorite. Sulfide minerals were not identified in most samples (except for sample M-SM-006, cubanite), however, their low abundance, as indicated by sulfide sulfur analysis of the bulk material would suggest that primary sulfide content of the samples is at or below the detection limit for powder XRD; especially with potential self-absorbance of X-rays when using a Cu X-ray source (personal communication, Foster, 2015). Weathering products were not identified in bulk scans, consistent with low abundance, poor crystallinity, and complex crystal structures (e.g. clay minerals) typical for many weathering products

X-ray diffraction of weathering products that were isolated and analyzed on zero-background holders identified three secondary minerals:

1. A white salt encrustation was identified as rozenite (Figure 3-1).
2. A green/ blue precipitate was identified as malachite (Figure 3-2).
3. Material sampled from a sulfide replacement pit was identified as poorly-crystalline goethite (Figure 3-3).

Many attempts were made to analyze the ubiquitous rust colored coatings, especially prevalent on the most weathered samples however, XRD did not consistently yield a definitive secondary iron oxide mineral match. Scans of this type can be found in Appendix B. Instead, broad 'humps' roughly corresponding to peak positions of goethite and/or ferrihydrite were observed, which is consistent with an interpretation that the rusty coatings are amorphous to poorly crystalline hydrous iron oxide minerals. Sharp XRD peaks in scans from samples with abundant rusty coatings are the result of minor contamination from primary silicates and oxides (see Figure 3-4); these peaks act to further complicate secondary iron mineral identification.

The presence of highly soluble acidic sulfate minerals was determined by directly by XRD (rozenite) for one sample and indirectly by rinse tests. The presence of these phases indicates a non-oxide sink for iron and a source of stored acidity.

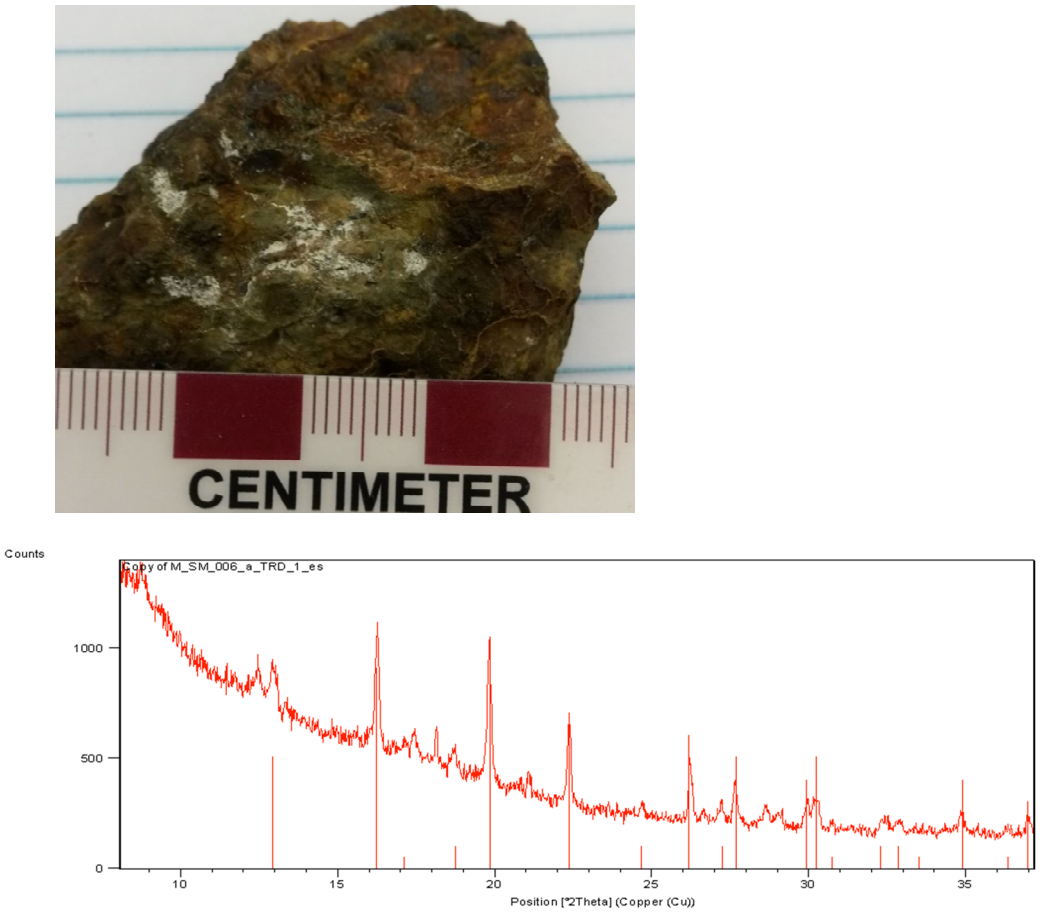


Figure 3-1. Hand sample showing efflorescent salt on sample M-SM-006-a (upper). Corresponding diffraction pattern of the selectively sampled white precipitate with the matched pattern (vertical lines) from ICDD 2007 database for rozenite (ID card 000160699) (lower).

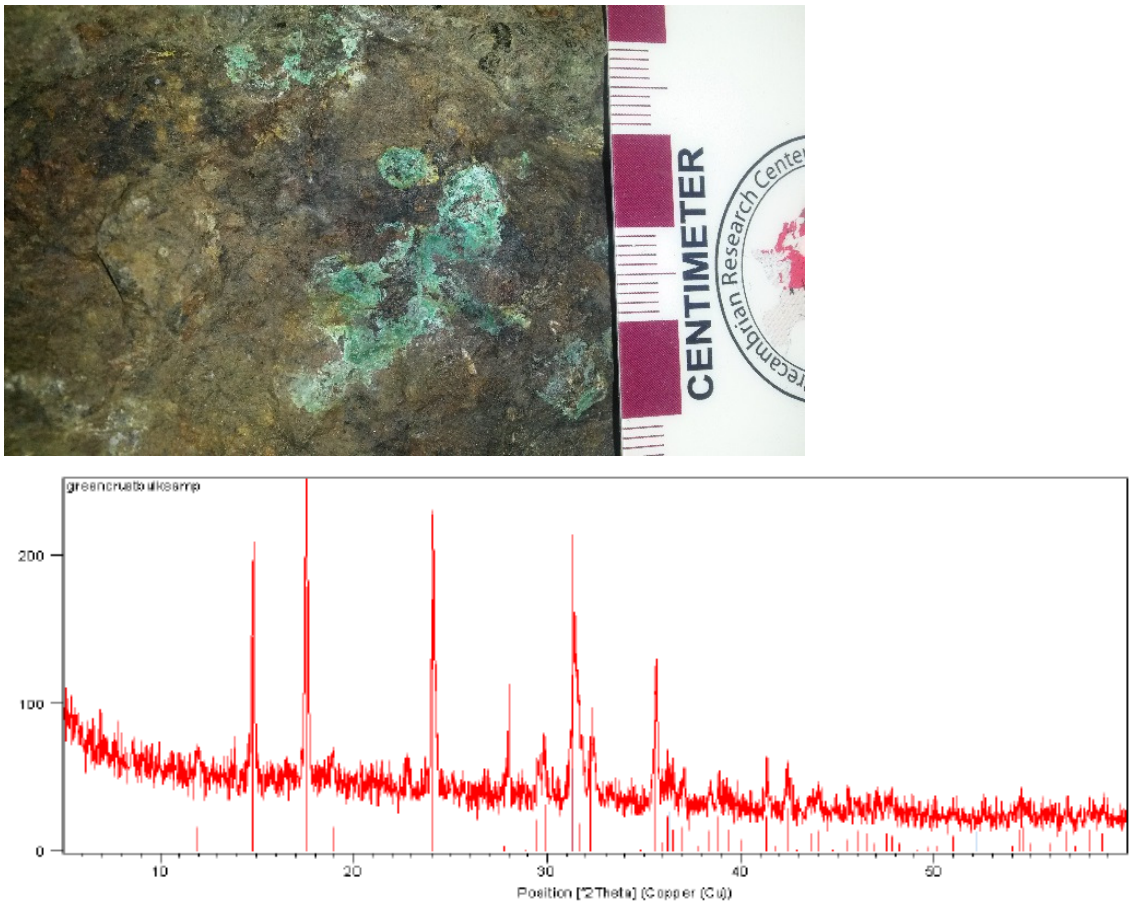


Figure 3-2. Photo of green/blue precipitate on the surface of hand sample BS-001-W (upper). Diffraction pattern of the selectively sampled precipitate with the pattern (vertical lines) from ICDD 2007 database for malachite: ID card 00-056-0001 (lower).


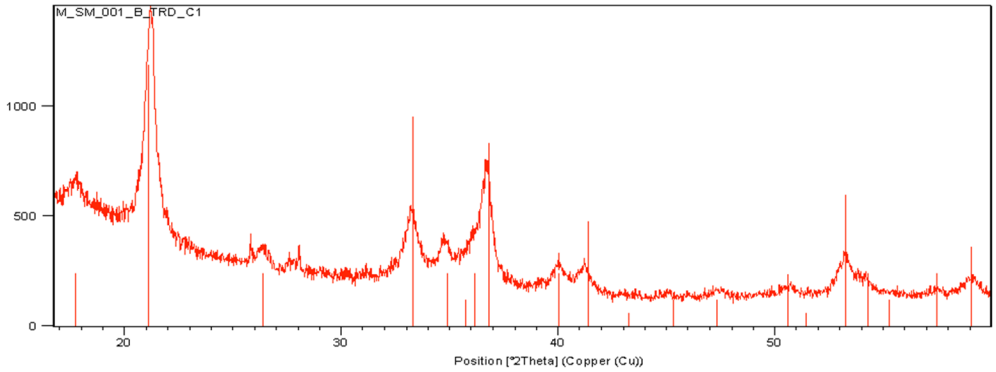


Figure 3-3. Hand sample showing a rust-coloured sulfide replacement pit. Corresponding XRD pattern of the selectively sampled area with the matched pattern (vertical lines) from ICDD 2007 database for goethite: ID card 000080097 (lower).

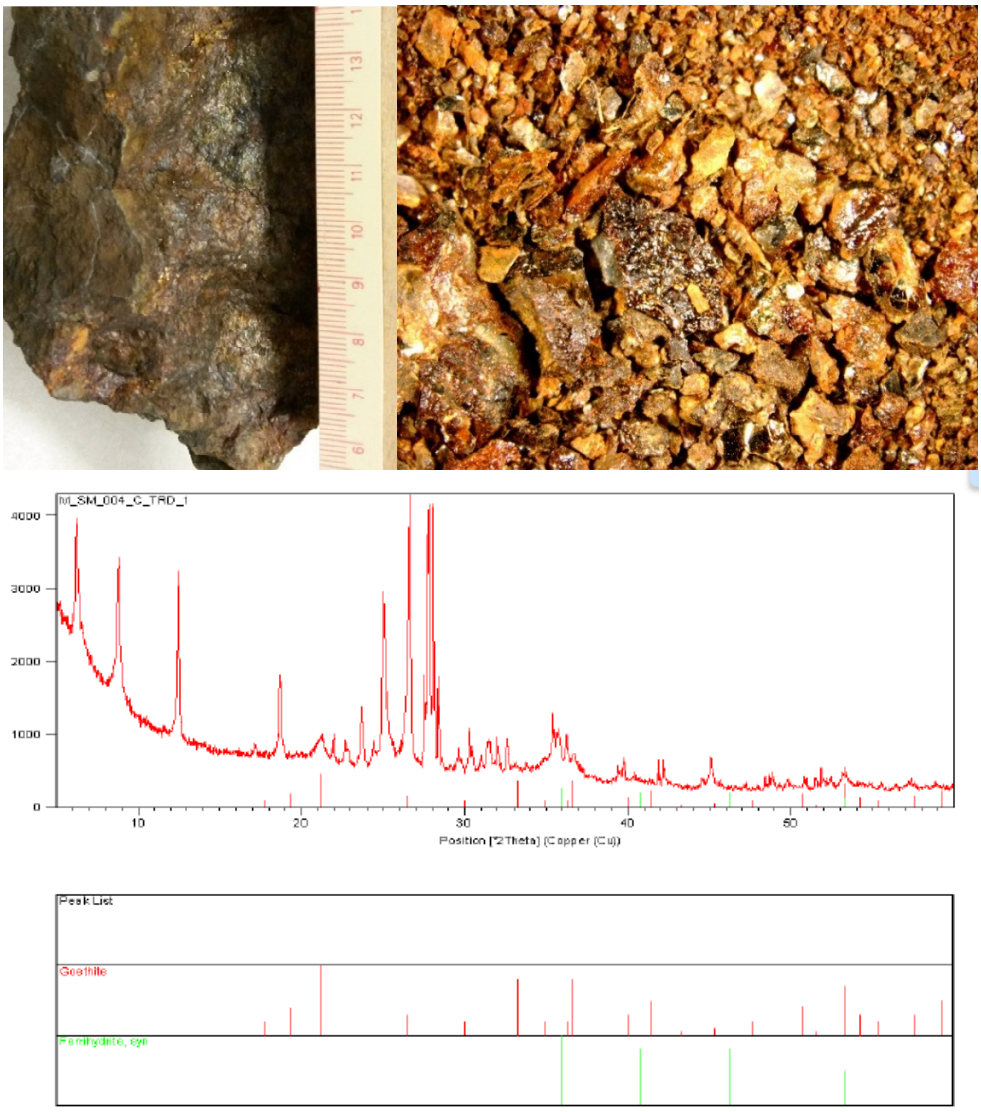


Figure 3-4. Hand sample photo showing pervasive secondary iron oxide coatings (top, left). Binocular microscope photo of selectively sampled rusty coatings found on sample M-SM-004-c length of view= 0.5 cm (top, right). Corresponding XRD pattern from the rusty material. Red vertical lines are for goethite (ID: 00-002-0272) and green lines are for ferrihydrite (ID 00-009-0721) other sharp peaks are the result of primary mineral contamination.

## 3.4 Petrographic analysis by light microscopy

Petrographic observations were made on ten thin sections from the three sample sites ("Type 2" samples) using both transmitted and reflected light microscopy. Observations related to rock type, mineral texture, primary alteration, and degree of physical and chemical weathering were documented. Petrographic description sheets are provided in Appendix C and D.

### 3.4.1 Transmitted light petrography

All samples were determined to be heterogeneous oxide/ sulfide bearing mafic intrusive rocks (i.e. variations of "gabbro"), Table 3-5 summarizes the findings. The samples contain between 50-60% euhedral plagioclase which is commonly normally zoned and contains oxide inclusions. Plagioclase is not typically altered although weak-moderate saussurite alteration was noted on several samples. Olivine exhibits highly variable crystal size (fine to coarse grained) and habit (euhedral to poikilitic), and is locally altered to iddingsite. Clinopyroxene content is around 10% and is medium to coarse grained, sub-ophitic to ophitic. Orthopyroxene is typically less abundant than clinopyroxene and commonly occurs as reaction rims around olivine or as small intercumulus grains. Pyroxene grains are typically unaltered. Samples contain less than 5 volume percent combined biotite, apatite, chlorite and zeolite minerals. Biotite commonly rims opaque phases (sulfide and Fe-Ti oxides) and is locally altered to chlorite (varying from partial to complete replacement). Chlorite occurs as pseudomorphs after olivine and biotite. Apatite occurs as euhedral elongate crystals. Minor micrographic intergrowths of feldspar and quartz were also observed. Opaque phases occur as interstitial phases and as small (micro-scale) inclusions in silicates, especially plagioclase. Rust colored weathering products commonly occur along grain-boundaries and cross cutting primary minerals.

Table 3-5. Transmitted light petrography results.

| Site | Sample | Rock type | Cumulate Code | Notes: |
|---|---|---|---|---|
| Area 1 | M-SM-001-b<br>M-SM-001-b-syn | Biotitic Apatitic Olivine Gabbro Norite | mPciofb | cm-scale clinopyroxene oikocrysts; weak saussurite, iddingsite alteration |
| Area 2 | M-SM-004-c | Vari-textured Olivine Gabbro Norite | mPOicfb | euhedral and sub-poikilitic olivine; variable plagioclase grain size (<1mm-~5mm); weak chlorite alteration |
| | M-SM-005-b<br>M-SM-005-syn | Vari-textured Augite Troctolite | cP(O/o)cifb | variable olivine habit euhedral to poikilitic; oxide inclusions in plagioclase, very weak alteration |
| | M-SM-006-a | Biotitic Augite Troctolite | mPocifb | oxide inclusions in plag; weak saussurite, chlorite, iddingsite alteration; + hornblende? |
| Area 3 | BS-001-w | Biotitic Olivine Gabbro Norite | mcPOcifb | abundant opaques; moderate saussurite. alteration |
| | BS-002-w | Biotitic Augite Troctolite | mPOcifbα | highly altered chlorite, amphibole saussurite.; oxide inclusions in plagioclase |
| | BS-003-w | Olivine Gabbro | mPcoifb | weak-moderate iddingsite, saussurite. alteration |
| | BS-004-w | Augite Troctolite | mcPocfα | extensive saussurite, iddingsite amphibole, chlorite, alteration + zeolite |

Notionally, the outer surface of hand-samples that were exposed during weathering could provide the most representative regions of the samples. To this end, efforts were made to preserve this outer edge during thin section preparation. However, during inspection of the thin-sections it became apparent that the true outer-most edge was likely destroyed during cutting, epoxy mounting, and grinding (Figure 3-5). This is important because it seems plausible that the redox state, pH, and the availability of other components (e.g. $CO_2$) may be different in the 'inner-sample' environment compared to strictly 'open atmosphere' scenarios. Furthermore, it seems possible that fine-grained precipitates (e.g. sulfate and carbonate minerals) may have become dislodged from the sample during thin section preparation so some weathering products could have been missed in the methods that characterized phases in thin-section.


Figure 3-5. Thin section scan of thin section M-SM-001-b. Note absence of rust colored coatings around outer edge. Slide dimensions = 27 × 46 mm.

Oxidation appears to be facilitated by grain-boundary influx of water as evidenced by rust-colored fractures and partially oxidized sulfide minerals in the interior part of the samples (Figure 3-6 Figure 3-7 and Figure 3-8). This was observed microscopically, in thin sections, and also upon breaking of pieces of exposure with a hammer. The interior portions of the weathered rocks are also rusty. Clearly, physical and chemical weathering are coupled processes.

Transmitted light petrography confirmed previous studies that the basal portions of Mesaba are quite heterogeneous with respect to alteration, mineral habit, and rock type. This has been observed by studies done at a range of scales including field-scale mapping (Miller and Severson, 2005), meter-scale core logging (Severson & Hauck, 2008), and microscopic-scale studies (Ripley and Alawi, 1986; Ripley et al., 1993; Ripley, et al., 2007).

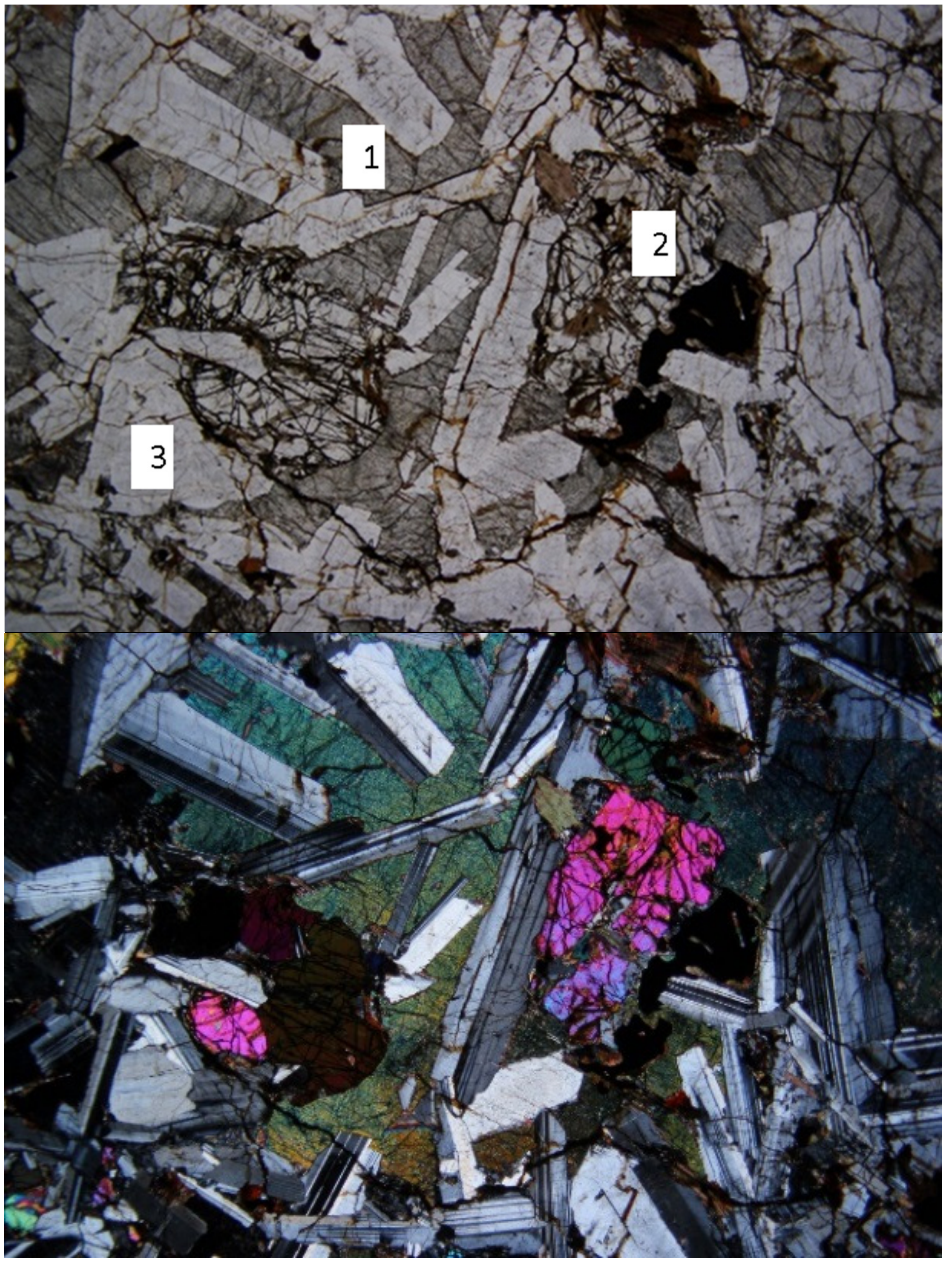


Figure 3-6. Photomicrographs showing typical primary silicate textures- ophitic clinopyroxene (1), euhedral plagioclase (2) and euhedral olivine grains (3). Sample M-SM-001-b Magnification = 1.25 x. Width of view = 1.5 cm. Top = plane polarized light, bottom = cross polarized light.

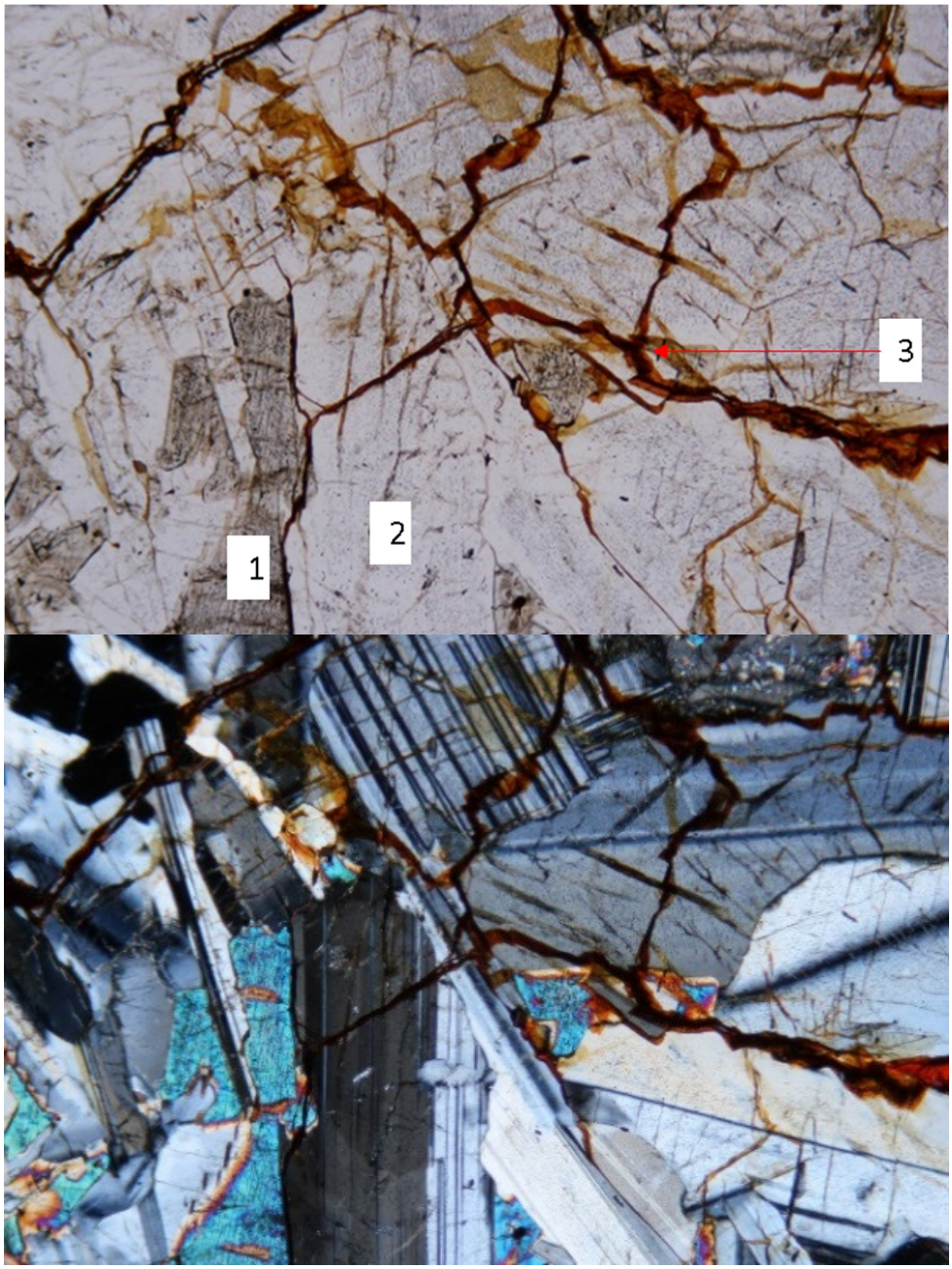


Figure 3-7. Photomicrographs showing primary sample characteristics (1) subophitic clinopyroxene (2) non-foliated plagioclase and (3) secondary iron oxides fill fractures along grain boundaries and cross-cutting fractured primary grains Width of view = 1.5 cm. M-SM-001-b Magnification = 1.25x. Top = plane polarized light, Bottom = cross polarized light.

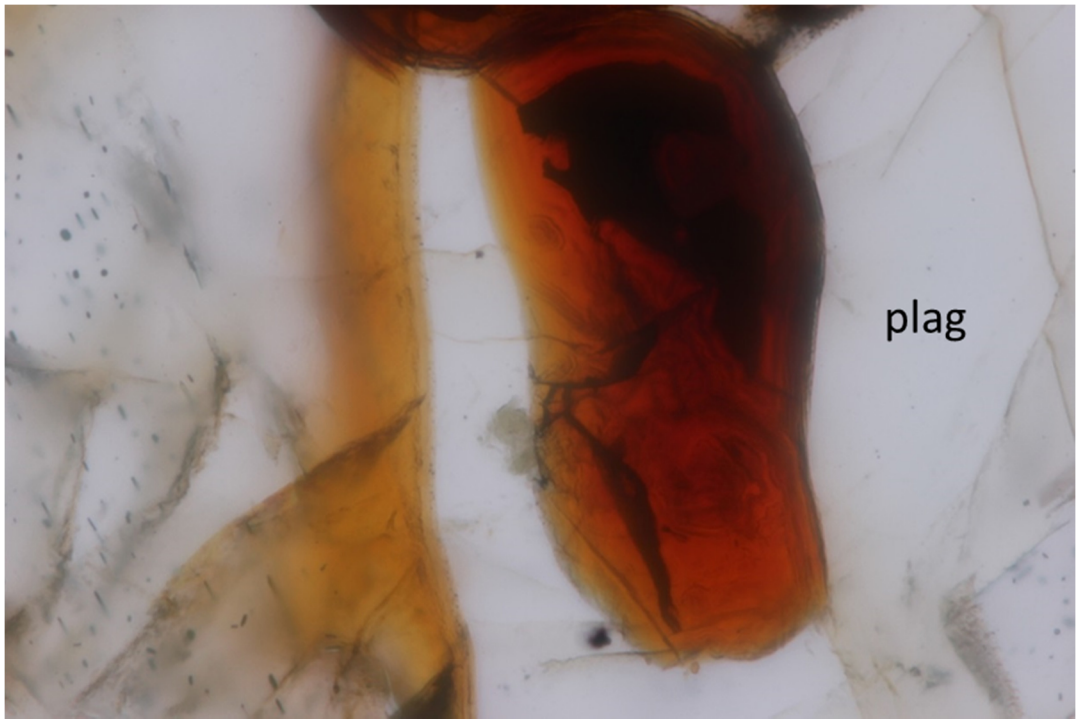


Figure 3-8. Highly magnified (~600x) image of commonly observed texture of iron-rich coatings (sample M-SM-001-b-syn). Note subtle banding in oxide phases surrounding the primary sulfide (opaque) and fractured plagioclase with iron oxide filling the fracture (left of sulfide grain).Width of view is approximately 250 µm.

### 3.4.2 Reflected light petrography

While studying the samples under reflected light, emphasis was placed on documenting sulfide minerals and their reaction products- other opaque phases including primary oxides were commonly observed, but not documented in detail. Sulfide minerals show wide variability with respect to texture, grain size, primary and surficial alteration, and modal abundance (Table 3-6). The most common sulfide mineral assemblage is cubanite-chalcopyrite-pyrrhotite which occurs as disseminated, interstitial masses and veinlets (Figure 3-9). Sulfide minerals also occur as secondary replacement phases probably due to sulfur mobilization by late sulfidic fluids, and as inclusions in primary silicates (Figure 3-10). Samples commonly show evidence of both primary (magmatic) and surficial alteration (Figure 3-10, left and Figure 3-11 respectively). A common

primary alteration texture is hematite? rimmed primary grains with emanating sulfide veinlets. Samples with lower sulfide mineral content were generally observed to have higher proportions of chalcopyrite, while more mineralized thin-sections had greater relative proportions of cubanite and pyrrhotite. Surficial weathering was evidenced by banded pseudomorphs of iron oxide surrounding sulfide minerals, however reflected light microscopy had limited utility for assessing weathering product identity or presence.

Table 3-6. Reflected light petrography results.

| Site | Sample | Mineralization | Relative abundance | Notes: |
|---|---|---|---|---|
| Area 1 | M-SM-001-b<br>M-SM-001-b-syn | very weak | Cub≈Cpy>Po | Abundant secondary iron oxide, 'shrinking core textures', fine grain fresh sulfides (occluded by silicates?) |
| Area 2 | M-SM-004-c | moderate | Cub>Cpy>Po | Sulfide minerals occur interstitially and in veins, minor chalcocite/covellite? |
| | M-SM-005-b<br>M-SM-005-syn | intense | Cub>Cpy>Po>Pn | Mostly non-oxidized sulfide, coarser grained sulfide grain size (0.5-4mm), some vein sulfide, Pn ~5-10%? of total sulfide |
| | M-SM-006-a | moderate | Cpy>Cub>Po | Iron oxide-sulfide weathering+ taknakhite? |
| Area 3 | BS-001-w | intense | Cpy>Cub>Po>Pn | Extensive oxidation, box work sulfide replacement textures +covellite? |
| | BS-002-w | weak | Cpy=Cub=Po | Deuteric alteration of sulfide? Occluded grains? Fine grained Cu-sulfide |
| | BS-003-w | very weak | Po>Cub=Cpy | Low sulfide abundance- S remobilization? |
| | BS-004-w | intense | Cub>Po>Cpy | Primary sulfide alteration- absence of secondary iron oxide |

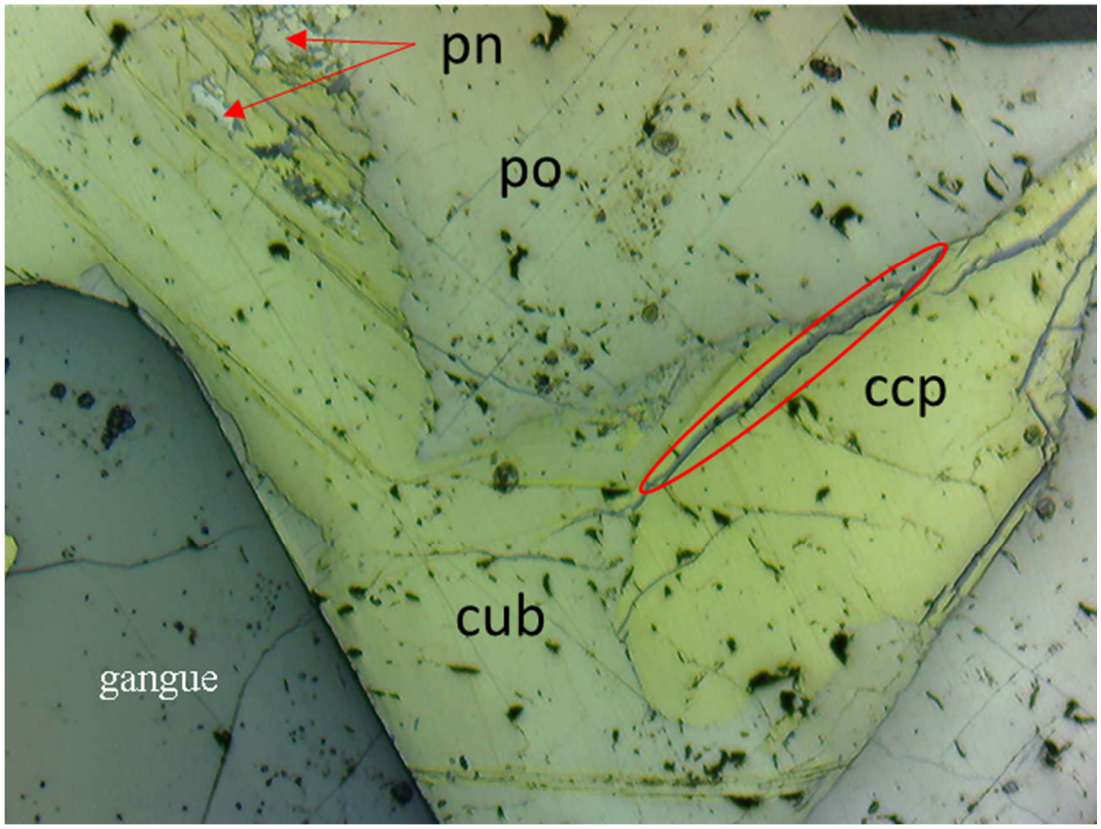


Figure 3-9. Reflected light photomicrograph showing primary sulfide habit typical for Mesaba samples. Note complex intergrowth of chalcopyrite (ccp), cubanite (cub), pyrrhotite (po), and pentlandite (pn) and inferred primary alteration (oval and similar) Sample: M-SM-005-b, Length of view= ~0.5 cm.

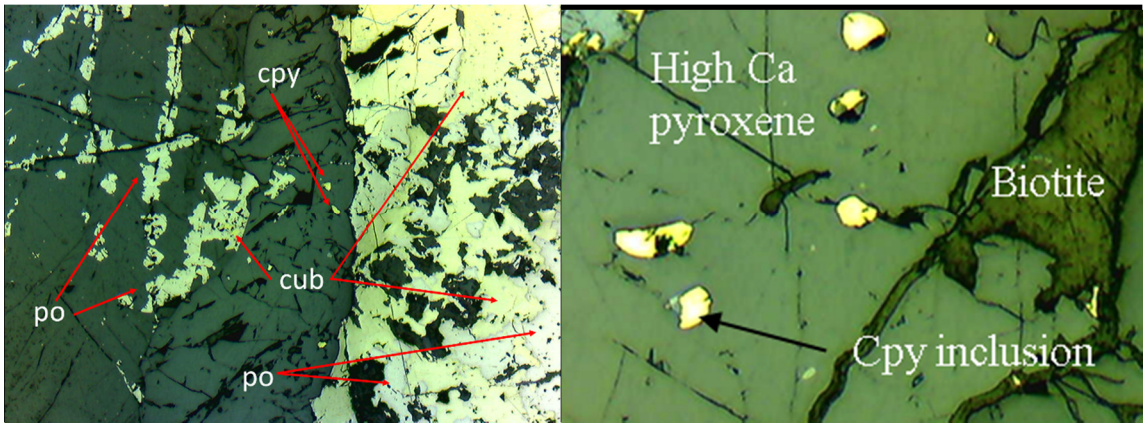


Figure 3-10. Reflected light photomicrographs. Left, showing late stage magmatic sulfide alteration texture with ragged grain boundaries. Sample BS-002, length of view= ~0.5cm. Right, showing chalcopyrite inclusions in pyroxene. Sample M-SM-004-C, length of view= 200um.

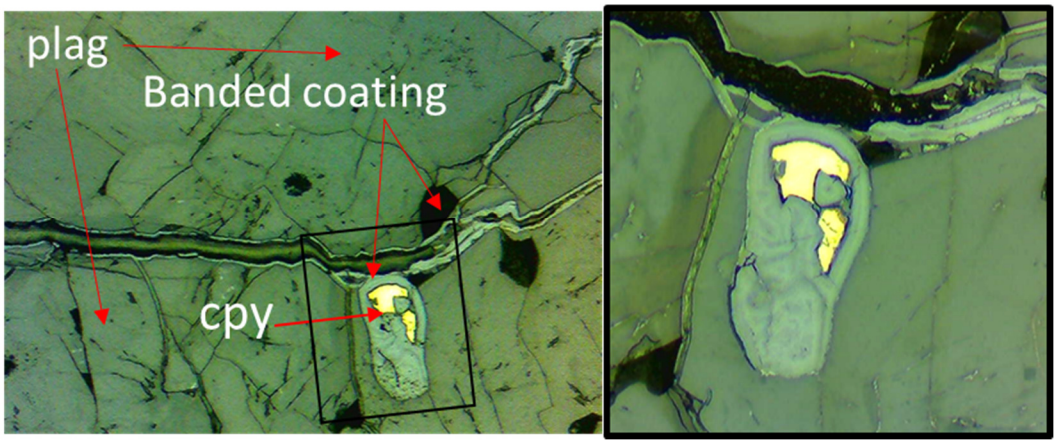


Figure 3-11. Reflected light photomicrograph (plane polarized) showing typical oxidation of primary sulfide (chalcopyrite) by surficial processes as indicated by fracture filled with iron oxide and banded 'shrinking core' texture. Sample M-SM-001-b-syn, length of view, left = ~ 1.5 cm., right (inset) = ~ 0.6 cm.

## 3.5 Scanning electron microscopy

Analysis by SEM showed clear evidence of sulfide oxidation weathering product formation occurring as iron-rich banded phases. Also, Cu and Ni enriched sheet silicates were documented. Observations are presented as SEM-BSE images with accompanying semi-quantitative chemical composition data generated by EDS. Supporting data can be found in Appendix E.

### 3.5.1 Banded iron rich coatings

Back-scattered electron (BSE) images showed weathering products both replace primary sulfide grains and form in fractures and along grain boundaries. In both cases, the weathering products have a banded morphology; because the contrast in BSE images is a function of average atomic number (Z), the banding observed is due to compositional variation between bands (Figure 3-12). Chemical composition data gathered by EDS show the coatings commonly contain Fe and Si as major components in addition to Al, S, and Cu as minor elements (Figure 3-13). The amount of copper contained in the coatings is highly variable at the micron-scale (within the same SEM field of view) and the centimeter scale (within one thin-section) (Figure 3-14).

More intensely weathered samples contain more banded iron weathering products, but no clear trends could be determined sample-to-sample. Said differently, higher sulfur content does not strictly dictate the composition of the banded iron oxides. For some analyses, the copper content was below the detection limit of the instrument under the operating conditions described (approximately 0.2 wt. %), however where Cu was above the detection limit, low weight percent quantities were observed (Figure 3-15). Other elements of interest (Ni, Co, Zn, As) were not present in concentrations sufficient to produce a measurable EDS signal. The SEM-BSE images show the width of individual layers within the layered iron oxide-rich features range from approximately < 1-3 μm.

Upon the identification of banded iron rich coatings, attempts were made to characterise the variation in Cu concentration from band-to-band (i.e. at a scale finer that individual band width). This is important because if Cu is concentrated in the iron-rich

domains of the bands it would support the notion that sorption/coprecipitation onto ferrihydrite is an active attenuation mechanism. While this still is the favored hypothesis, the methods employed had analytical volumes detection limits too great to discover any small scale variations in Cu abundance (Figure 3-13). Because iron and silicon occurred at higher concentrations, EDS measurements were able to capture the compositional variation. The banded nature suggests that variations in solution chemistry (cyclic chemical compositions) caused the layered morphology of these features (Lin, 1996; Fix et al., 2015).

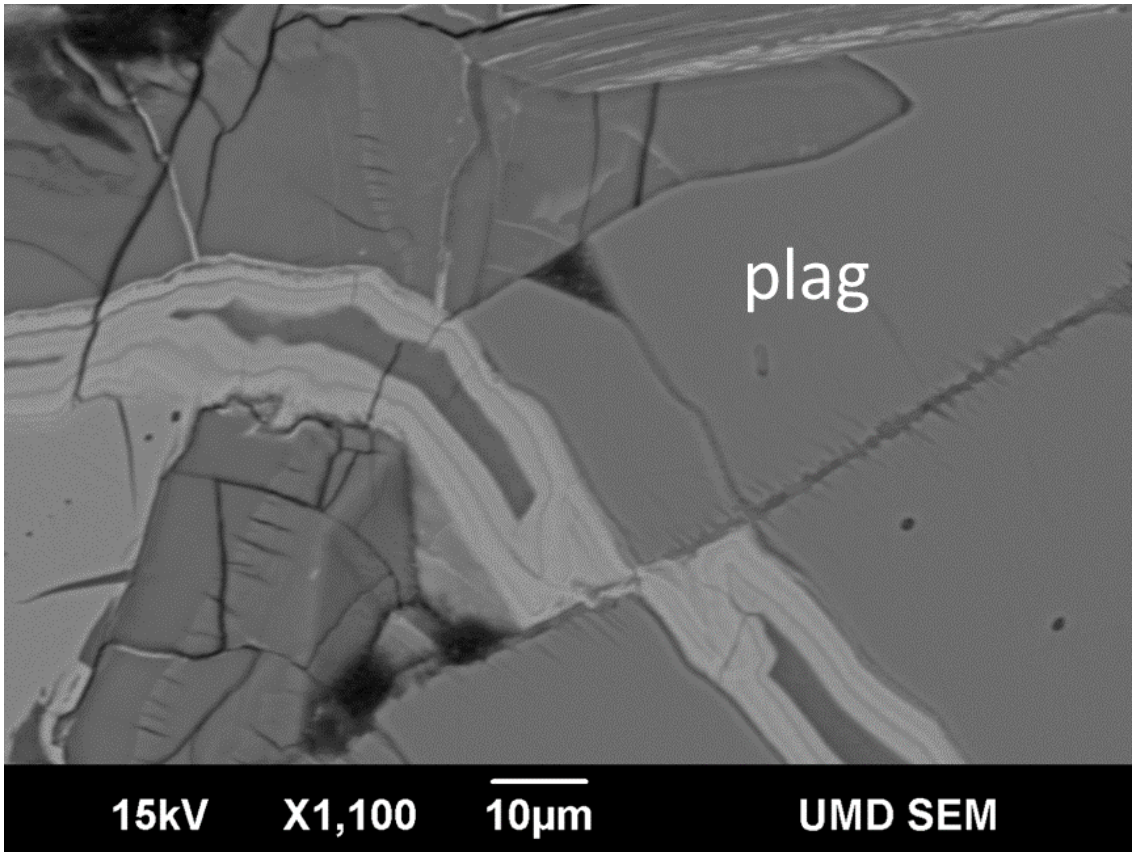


Figure 3-12. SEM-BSE image of iron rich banded fracture filling (M-SM-001-syn). Note offset by fractured (weathered?) plagioclase grain.

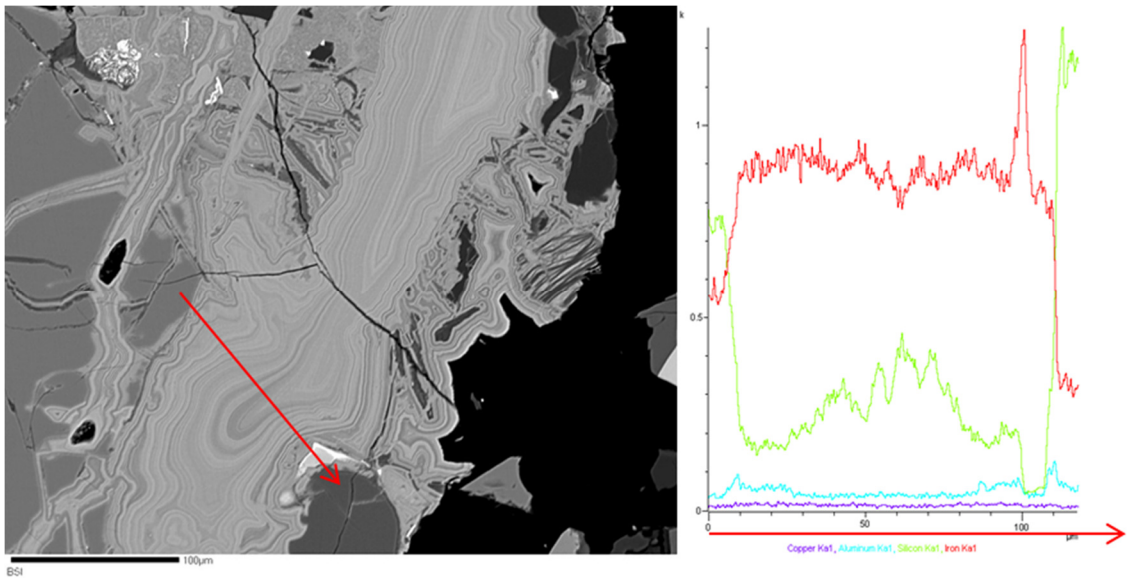


Figure 3-13. BSE image and location of cross-section line scan (red) of an iron-rich coating from sample M-SM_005-b (left). Relative chemical abundance plot Fe (red) and Si (green) Al (blue) and Cu (purple) showing variation across the feature (right).

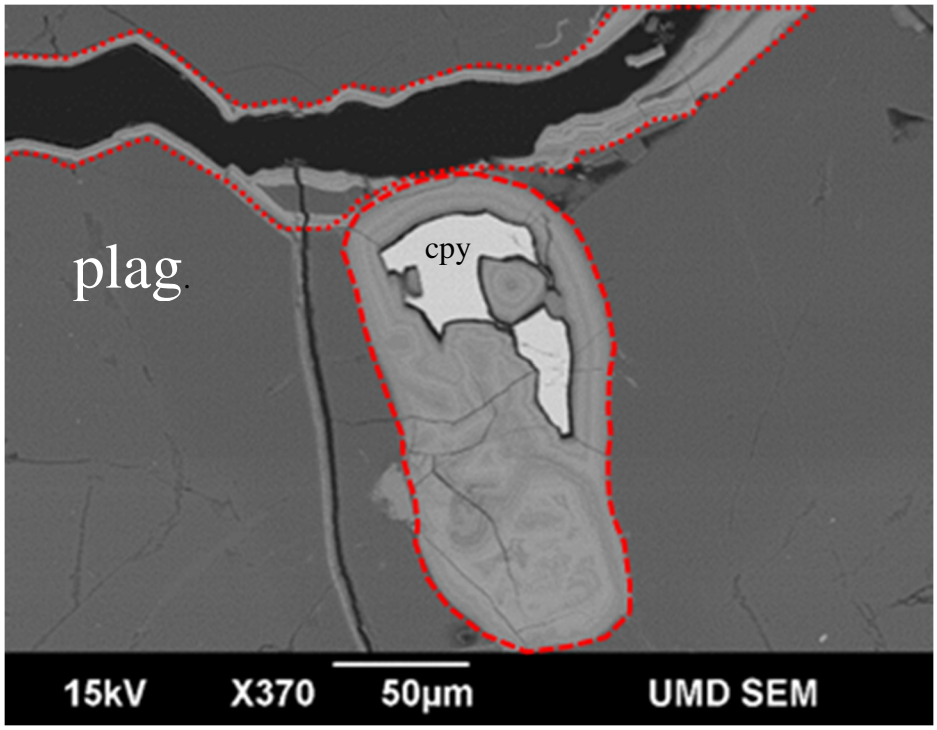


| Area | Element | Average (wt. %) |
|---|---|---|
| Sulfide replacement | Fe | 51 |
| | Si | 11 |
| | Al | <1 |
| | S | 0.5 |
| | Cu | 7 |
| Fracture | Fe | 54 |
| | Si | 9 |
| | S | 0.5 |
| | Al | 2 |
| | Cu | 3 |

Figure 3-14. SEM-BSE image showing iron-rich sulfide oxidation texture (surrounding chalcopyrite grain, long dashed outline) and associated banded iron rich fracture precipitate (top of image, short dashed outline). Host mineral is plagioclase. Table shows average compositions of multiple analyses in respective regions (oxygen not reported). Note the higher Cu concentration in sulfide replacement area. Sample M-SM-001-b-syn.

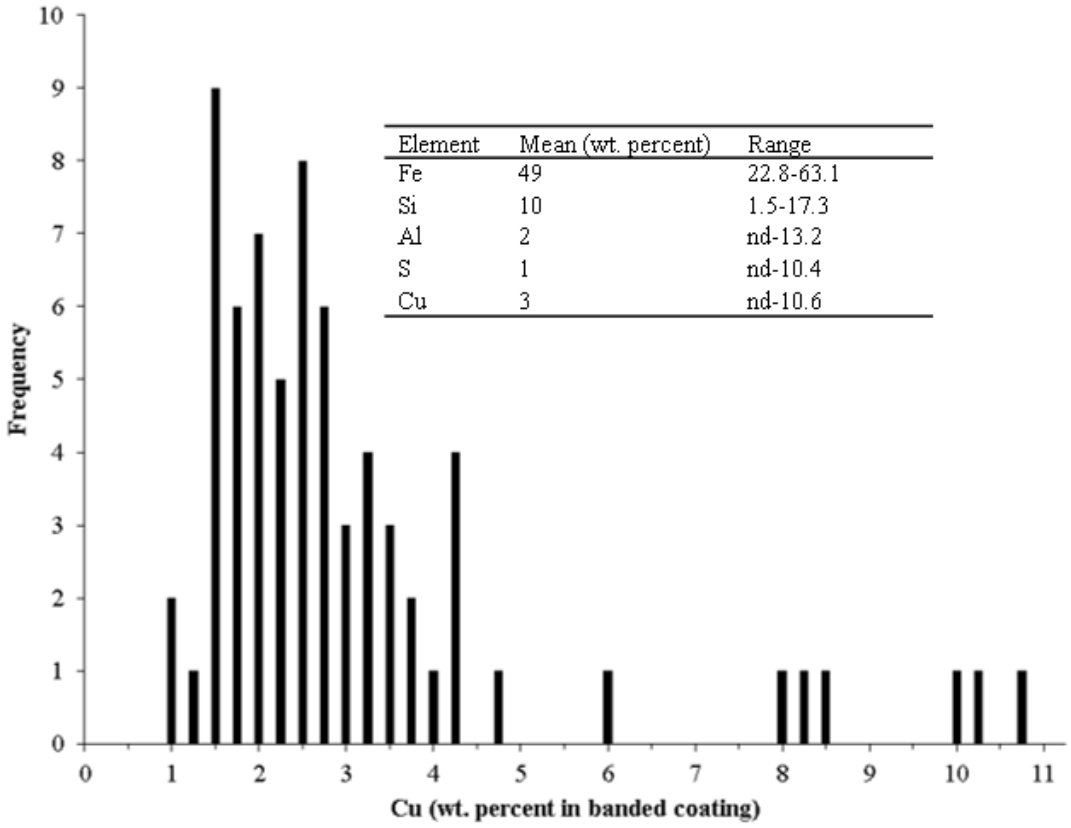


| Element | Mean (wt. percent) | Range |
|---|---|---|
| Fe | 49 | 22.8-63.1 |
| Si | 10 | 1.5-17.3 |
| Al | 2 | nd-13.2 |
| S | 1 | nd-10.4 |
| Cu | 3 | nd-10.6 |

Figure 3-15. Histogram and associated statistics showing the observed Cu concentrations (wt. percent Cu) in banded coatings for various samples N=69.

During exploratory analysis, it became apparent that certain phases and textures that were observed, may not have been the products of surface weathering. Alteration following primarily mineral crystallization, but prior to exposure on surface, can occur in mafic rocks (e.g. Ripley et al., 1993). For example, sulfur remobilization processes by late stage fluids can mantle primary sulfides in a hematite/ magnetite coating. Cervin (2011) showed, for NorthMet material, that some sulfide mineral grains had been altered-evidenced by reaction halos (Figure 3-16). Similar textures were observed in our weathered samples (Figure 3-17). Upon the recognition of these features that are deemed to be likely due to late-stage deuteric processes, additional consideration was conducted as to the criteria that would distinguish between deuteric alteration and subaerial

weathering alteration. Evidence that the banded coatings are the product of surficial weathering origin include: (1) the proximity/association of coatings with field exposures; (2) coatings are more abundant for samples that appeared more weathered (field observation); and, (3) the coatings have not been reported in any of the previous studies (on non-weathered Duluth Complex material) (e.g. Al-Alawi, J., 1985; Ripley et al., 1993; Miller et al., 2002, Ripley et al, 2007; Cervin, 2011; Steiner, 2014). Furthermore, similar phases have been observed on weathered mine waste in the literature and were determined to be of secondary origin (e.g. Lin, 1996; Carbone et al., 2012). Therefore, we conclude that the banded features are almost certainly a product of surficial weathering.

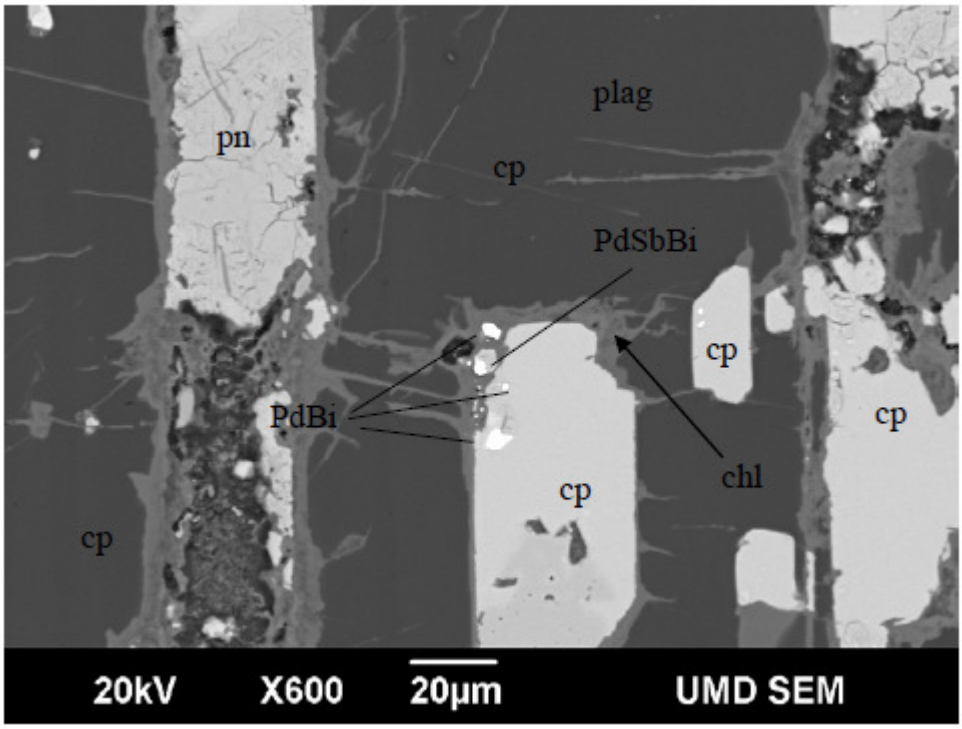


Figure 3-16. Figure 20c from Cervin, 2011 (pg. 59) showing altered sulfide minerals found in drill core samples (not exposed to surficial weathering).

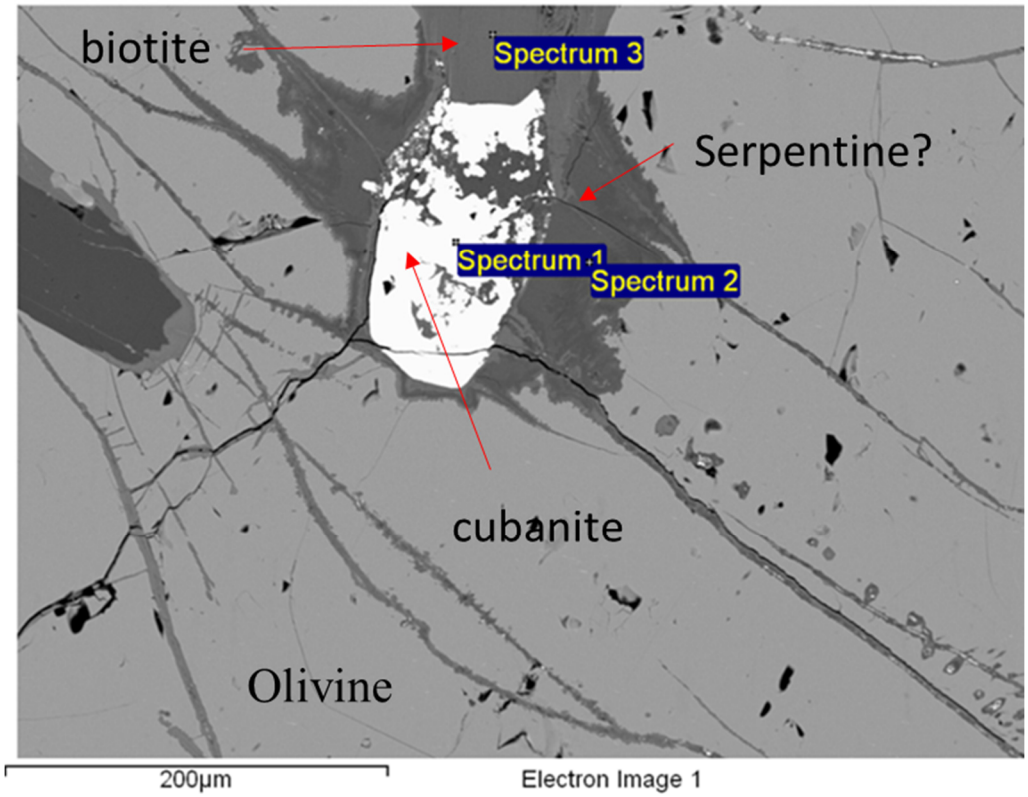


Figure 3-17. Cubanite grain (spectrum 1) from sample M-SM-005b showing primary dissolution textures. Dark phase surrounding sulfide grain (spectrum 2) and similar shaded veins have components consistent with serpentine. In general textures are similar to Figure 3-16. Mineral at Spectrum 3 is biotite.

### 3.5.2 Copper and nickel enriched sheet silicates

Biotite and chlorite-like phases locally contain significant concentrations of Cu and/or Ni. The metal-enriched sheet silicates commonly occur in close proximity to the previously mentioned banded weathering products, but not in all cases. The enrichment in Cu and Ni is was commonly associated with biotite grains that show K deficiency which is transitional to a chlorite-like (based on composition and morphology) phase (Figure 3-18). The provenance of the Ni and Cu enriched sheet silicates remains unresolved, however µXAS spectra did provide the additional insight that Ni and Cu contained in these phases is oxidized. Some studies have suggested that Ni can be incorporated into

the interlayers of sheet silicates as reduced species. For example, in a study by Suárez et al. (2012) Cu and Ni enriched sheet-silicate phases (chlorite, serpentine and talc) from the weathered portion of the Aguablanca Ni-Cu-PGE deposit in Spain were investigated. Previous studies on materials from weathered Cu porphyry deposits have shown that Cu can be incorporated into the interlayer region of biotite through the precipitation of native Cu nano-particles (Ilton and Veblen, 1988; Ilton et al., 1992; Ilton and Veblen, 1993). The study suggested that surficial weathering processes cause the enrichment though the precipitation of native Cu nano-particles and Ni-Fe alloys in the sheet silicate interlayers. Electron microprobe results from NorthMet deposit sheet silicates (mostly biotite) did not showed that Cu/Ni was not enriched in these Duluth Complex sheet silicates (SRK, 2007). Other microprobe studies on Duluth Complex rocks have not reported Cu/Ni enriched sheet silicates, however it is not known if these elements were analyzed in the phases of interest (e.g. Al-Alawi, 1985).

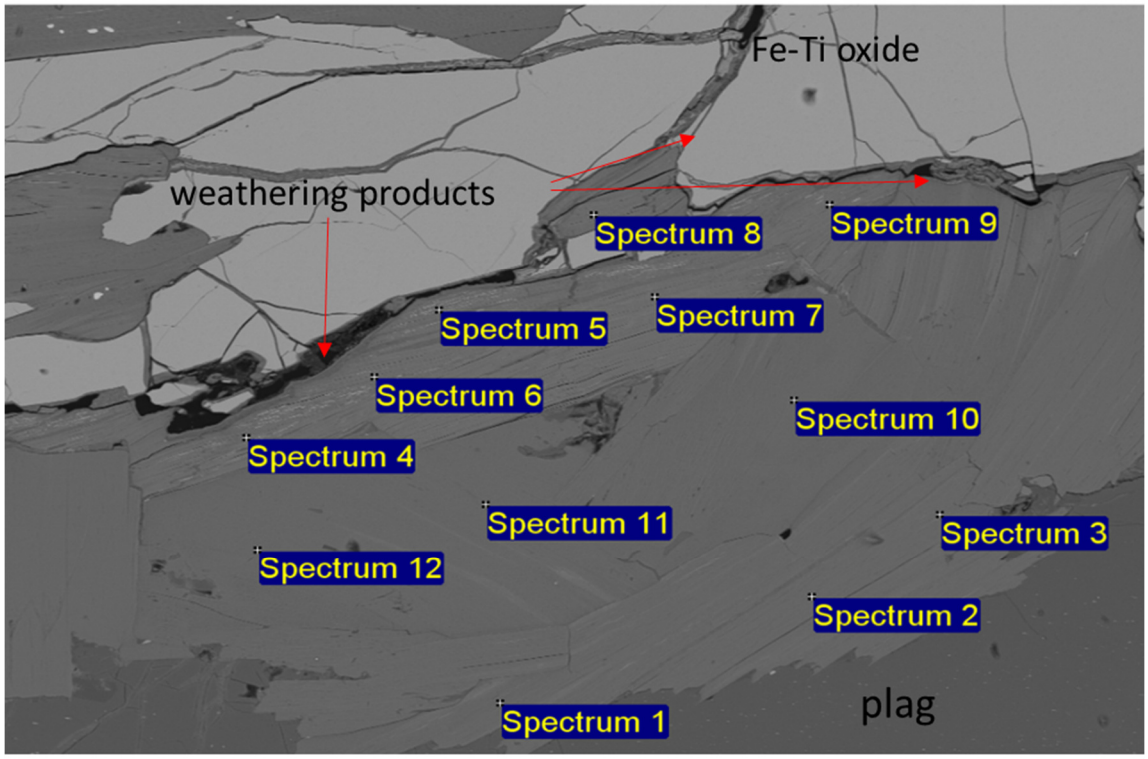


| Spectrum | Na | Mg | Al | Si | Cl | K | Ca | Ti | Cr | Fe | Ni | Cu | O | Total |
|---|---|---|---|---|---|---|---|---|---|---|---|---|---|---|
| Spectrum 1 | | 10.15 | 8.27 | 17.84 | | 7.28 | | 2.79 | 0.31 | 12.06 | | | 41.31 | 100.00 |
| Spectrum 2 | | 9.45 | 7.92 | 17.46 | | 6.97 | | 2.90 | 0.33 | 13.63 | 0.60 | | 40.74 | 100.00 |
| Spectrum 3 | | 7.94 | 7.25 | 15.37 | | 4.54 | | 2.27 | | 22.94 | 0.59 | 0.57 | 38.51 | 100.00 |
| Spectrum 4 | | 7.11 | 7.13 | 15.01 | | 0.25 | | 1.85 | | 26.59 | 2.60 | 1.37 | 38.08 | 100.00 |
| Spectrum 5 | | 7.30 | 7.16 | 16.15 | | | | 1.83 | | 23.58 | 3.50 | 1.58 | 38.90 | 100.00 |
| Spectrum 6 | | 8.21 | 7.16 | 15.43 | | | | 2.12 | | 22.72 | 4.58 | 1.02 | 38.77 | 100.00 |
| Spectrum 7 | | 8.26 | 7.01 | 14.94 | | | | 2.27 | | 22.34 | 4.33 | 2.44 | 38.40 | 100.00 |
| Spectrum 8 | | 8.57 | 7.45 | 14.98 | 0.26 | 0.29 | | 1.98 | 0.28 | 23.12 | 3.62 | 0.79 | 38.65 | 100.00 |
| Spectrum 9 | | 7.91 | 7.01 | 14.42 | | | | 2.13 | 0.31 | 25.81 | 3.79 | 0.61 | 38.02 | 100.00 |
| Spectrum 10 | | 9.69 | 8.02 | 17.57 | | 7.99 | | 3.00 | 0.34 | 12.49 | | | 40.90 | 100.00 |
| Spectrum 11 | | 9.50 | 8.33 | 17.40 | | 6.91 | 0.73 | 2.95 | | 13.23 | | | 40.95 | 100.00 |
| Spectrum 12 | 0.29 | 9.85 | 7.95 | 17.49 | 0.21 | 7.94 | | 2.82 | 0.31 | 12.37 | | | 40.77 | 100.00 |

Figure 3-18. Sheet silicate phases found in sample M-SM-001-b-syn and EDS results. Semi-quantitative compositional analyses suggest biotite has been altered to chlorite. Spectra showing chlorite-like compositions tend to have greater metal (Cu and Ni) contents. Note arrows pointing to a fracture filled with secondary iron phases in close proximity to the sheet silicates.

## 3.6 Synchrotron-based micro-analysis

Synchrotron-based analyses are grouped into µ-XRF maps and µXAS analyses; the results of each are presented below. A combination of false positives and low concentrations of metals in the weathering products posed major limitations to this portion of the study. The µ-XAS analyses provided data on the redox state of arsenic associated with the banded iron-rich coatings.

### 3.6.1 Micro-X-Ray fluorescence element mapping (µXRF)

Micro-XRF maps show the distribution of elements of interest for approximately 1 $mm^2$ areas at a spatial resolution of 2 $\mu m^2$ in the form of 'heat maps', where hotter colors indicate higher concentrations of the element of interest. The XRF data presented are limited to areas where supporting data from XAS and/or SEM-EDS support the presence of the element displayed (see 2.6.1 for method analytical challenges).

Consistent with the results from SEM, Cu was found to be present in iron oxide rich weathering products. Figure 3-19 shows that Cu is retained in weathering products that directly replaced, in this case, chalcopyrite as well as in banded coatings that occur in a fracture that cross cuts plagioclase grains. Concentrations of Cu are greatest in the area that is close to the partially oxidized chalcopyrite grain, however, banded coatings above the sulfide grain also contain significant amounts of Cu (Figure 3-20). Overall, the high degree of variability emphasizes the heterogeneous nature of weathering products caused by the micro-geochemical environments.

Figure 3-21 shows results for Cu and Ni from an area on thin section M-SM-001-b-syn that contains both banded coatings and Cu/Ni enriched sheet silicates. By comparing the Cu and Ni heat maps it is apparent that the geochemical behavior of these two elements is quite different. Copper is concentrated in secondary iron-rich weathering products and sheet silicate minerals. Nickel is concentrated in sheet silicate minerals but not found in the iron rich weathering products. Interestingly, the weathered portions of the olivine grain show an apparent depletion of Ni and enrichment of Cu compared to the "fresher" portions of the grain (Figure 3-21).

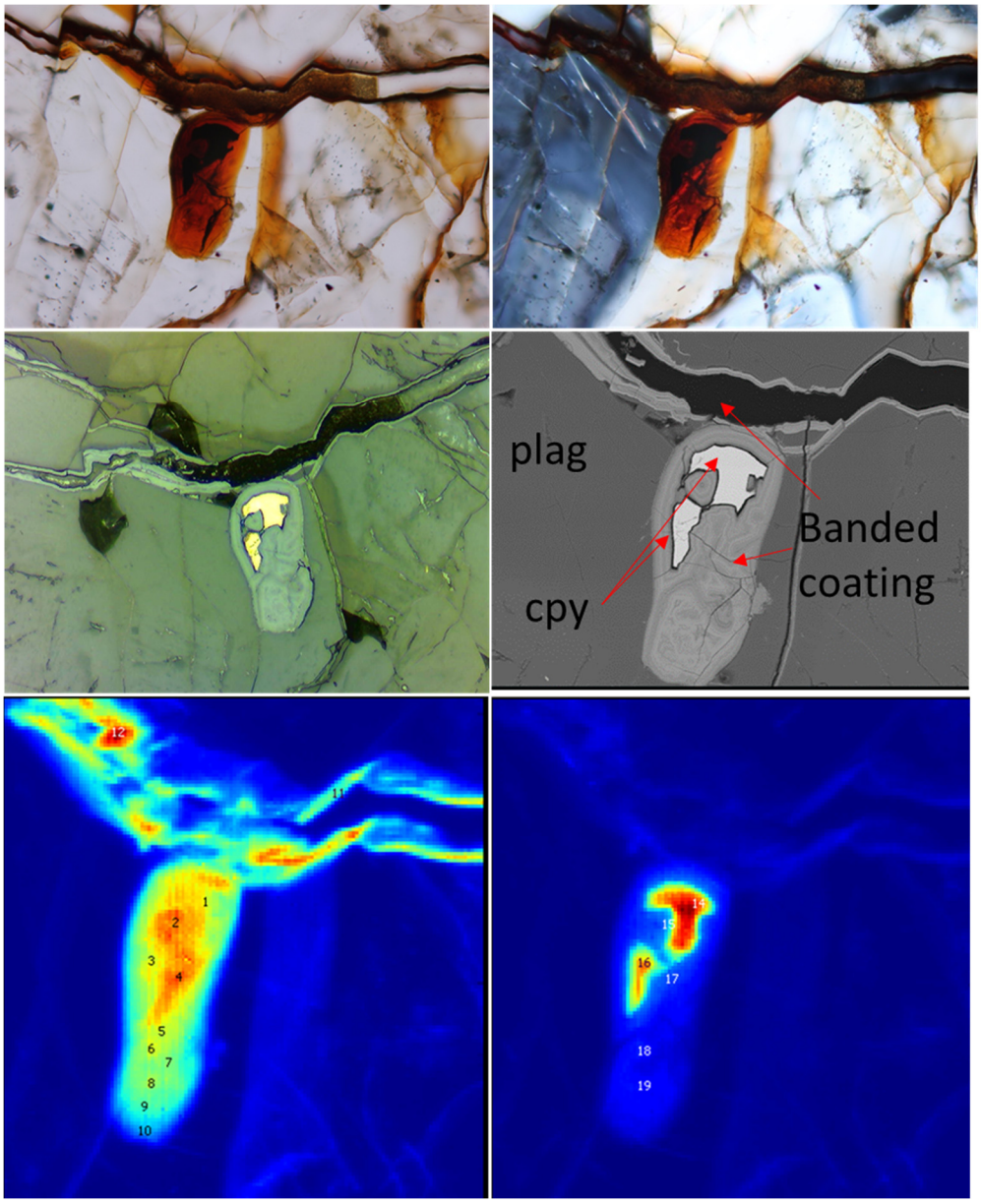


Figure 3-19. Images and synchrotron µXRF element maps of sample M-SM-001-b-syn. Top left: Transmitted, plane polarized light. Top right: Transmitted cross-polarized light. Middle left: Reflected plane polarized light. Middle right: SEM-BSE image. Bottom left: µXRF map for iron. Bottom right: µXRF map for copper. Warmer colors indicate higher relative abundance. Numbers on µXRF maps indicate the locations of XAS spot analyses. The field of view in each image is approximately 350 µm.

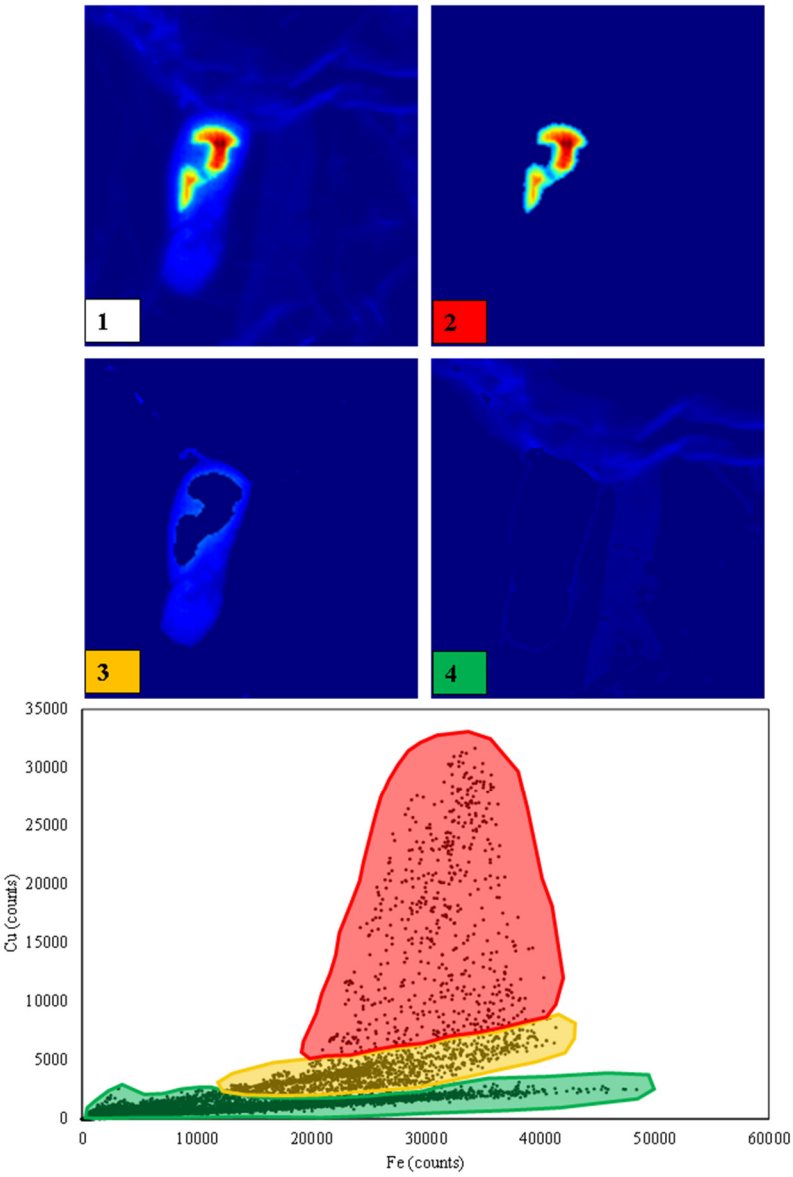


Figure 3-20. Synchrotron µXRF maps showing variation in Cu:Fe ratios from different domains (Sample M-SM-001-b-syn). Images were created using the mask feature in SMAK (Webb, 2014). Top left 1]: Raw copper map. Top right [2]: masked region with high Cu:Fe associated with "non-reacted" chalcopyrite grain. Bottom left [3]: masked region associated with intermediate Cu:Fe ratios associated with proximal iron oxide replacement surrounding chalcopyrite grain. Bottom right [4] masked areas associated with low Cu:Fe ratios associated with banded iron oxides phase(s) filling fractures. The field of view in each image is about 350 µm. Bottom chart shows masked data points selected to generate the above images.

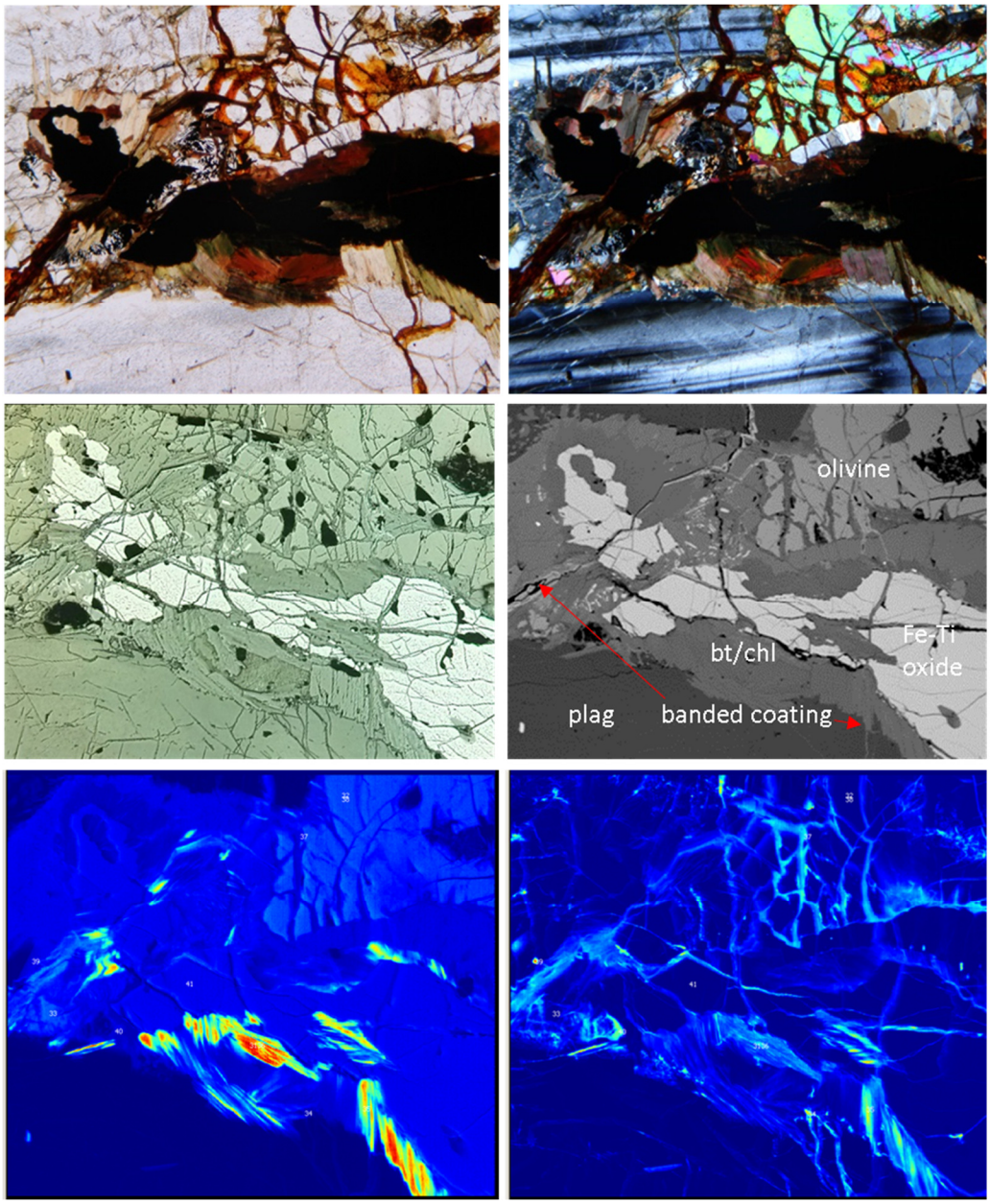


Figure 3-21. Images and synchrotron µXRF element maps (sample M-SM-001-b-syn). Top left: Transmitted, plane polarized light. Top right: Transmitted cross-polarized light. Middle left: Reflected plane polarized light. Middle right: SEM-BSE image. Bottom left: µXRF map for nickel. Bottom right µXRF map for copper. Warmer colors indicate higher relative abundance. Each field of view is ~ 2 mm.

### 3.6.2 X-ray absorption spectroscopy (µXAS)

Micro-XAS spectra were used for two purposes. In the raw form, spectra were used to confirm the presence of a particular element of interest that could not be confirmed based on the µXRF map or SEM data. Where high quality spectra were collected the spectra were processed to evaluate the oxidation state(s) of the element of interest. Poor quality spectra were excluded from further analyses. A set of Cu µXAS spectra were analyzed using principle components analysis (PCA).

Figure 3-22 shows an example of how false positive errors were investigated and the results from model fitting arsenic µXAS spectra. In the raw µXRF element map, it appears that arsenic is concentrated in the primary sulfide (chalcopyrite), the iron oxide replacement surrounding the sulfide grain, and in the banded coatings in the fracture at the top of the image. Upon further analysis of the MCA spectra, one can see that the baseline counts are very close in magnitude to the real arsenic signal. The background is elevated in areas with high iron concentrations (e.g. around spot 23) creating a deceptive element map. Micro-XAS spectra collected at the two points in the banded coating area (20 and 21) show; in fact, arsenic was present in these areas. In the fitting routine, a combination of 30 percent As (III) and 70 percent As (V) model species gave the best fit results. The precision of this determination is on the order of +/- 10 percent (Foster, 1998). The µXAS point collected on the chalcopyrite grain however, did not generate a usable µXAS spectrum for arsenic because arsenic is not present in the sulfide. This suggests chalcopyrite is not a “primary source” of arsenic in Duluth Complex rock.

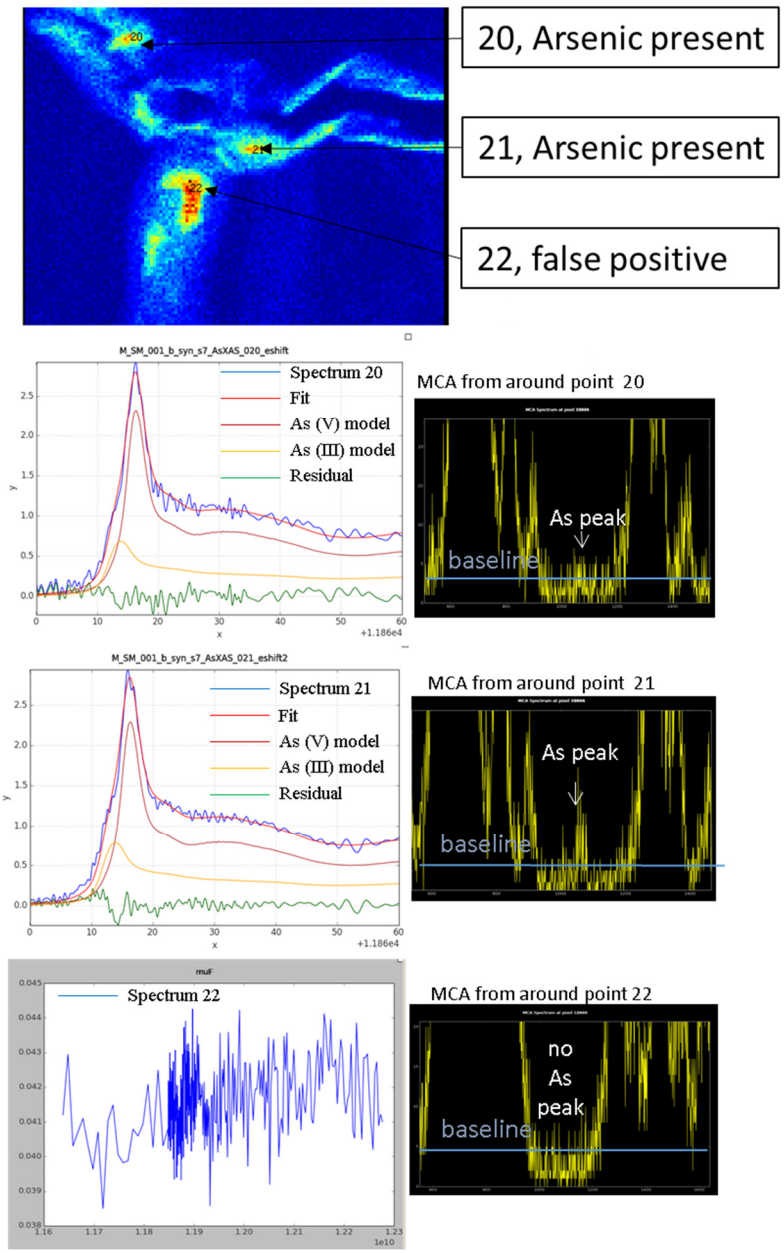


Figure 3-22. Summary of As XAS data from sample M-SM-001-b-syn. A reconstruction routine in SixPack using As (III) and As (V) models showed 30% of the two specta can be attributed to As (III) while the majority is As (V). Note false positives for arsenic where baseline counts in the µXRF map were discovered by viewing the MCA data (lower). Field of view top µXRF map is about 350µm, see Figure 3-19 and Figure 3-20 for additional context.

Principle components analysis of the high-quality copper spectra suggest that three species describe 98 percent of the variance in the sample set. Principle components analysis does not indicate what the components are, just the number. Following PCA, we attempted to fit model spectra to the sample spectra to elucidate the identities of the three 'components'. The fitting routines did not provide usable results, possibly because of the limited library of model compounds available, and the marginal quality of some of our spectra.

Our μXAS data suggest that the form of Cu in the sheet silicates is not reduced, and it remains unclear whether the enrichment of sheet silicates in Cu is due to a weathering process (Figure 3-23).

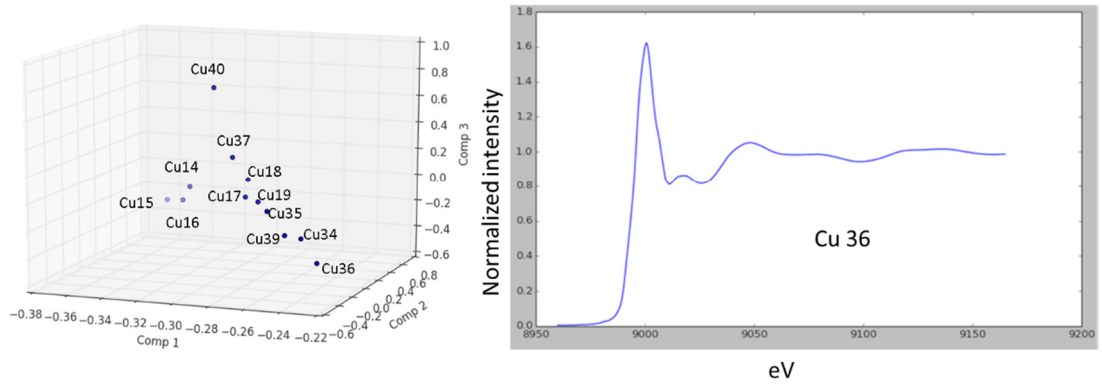


Figure 3-23. PCA cube plot (left), Cu spectrum 36 (right) from a Cu enriched sheet silicate mineral showing oxidized nature (shifted to higher energy compared to 8984.4 eV CuS calibrant energy).

SEM-EDS and µXRF mapping showed that Ni is concentrated in sheet silicate phases. A µXAS spectrum collected at a POI where a high-Ni sheet silicate mineral occurs showed that, in this case, Ni occurs in the divalent state (Figure 3-24). It remains unclear as to the mineral identity of this phase and weather surficial processes caused the enrichment.

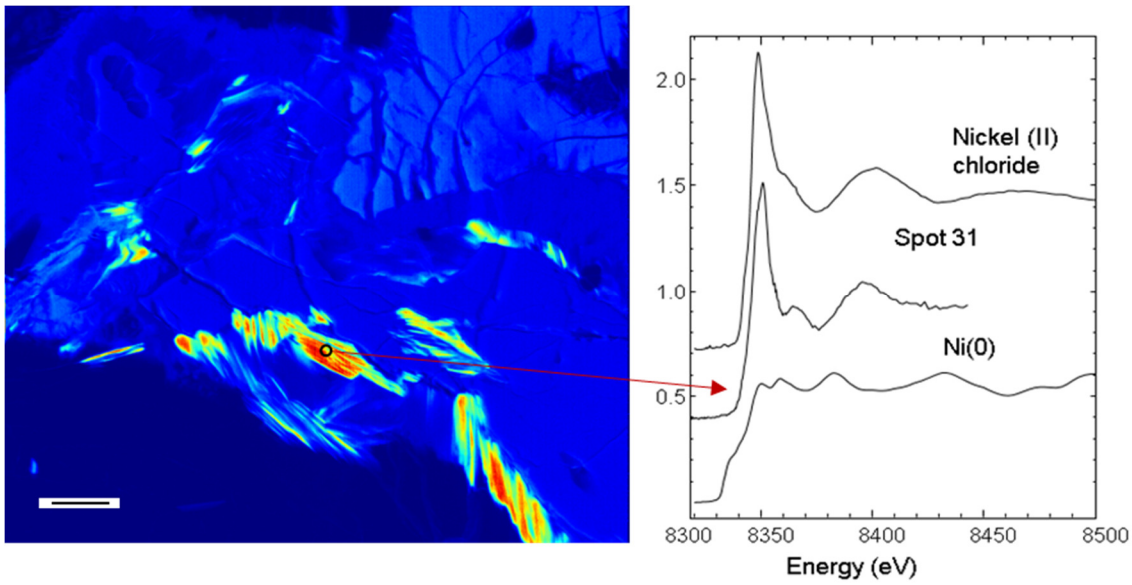


Figure 3-24. Micro-XRF image for Ni (see Figure 3-21 for additional context) for thin section M-SM-001-b-syn Comparison of XAS spectra number 31 (see Figure 3-21) compared to Ni (II) chloride and elemental Ni (metallic, zero valent). The spectrum suggests, for this case, Ni associated with sheet silicates occurs in the divalent state. SEM data suggest sheet silicates are inter-grown biotite and chlorite. Field of view in µXRF map is approximately 2mm.

## 3.7 Conclusions from characterization work

The major findings from the solid state characterization work are:

1. Products of subaerial weathering of Duluth Complex rock include: malachite, rozenite, and banded iron-silica-alumina-rich coatings.

2. XRD of concentrated iron-rich coatings yield patterns that are consistent with goethite and/or ferrihydrite; however, other patterns suggest that the coatings are poorly crystalline.

4. Copper is concentrated up to several weight percent (semi-quantitative) in the banded coatings for samples with both low total sulfur (e.g. M-SM-001) and higher sulfur (M-SM-004). No strict correlation between bulk sulfur content and coating composition was observed.

5. Chemical heterogeneity was observed in coatings at the sub-micron scales, suggesting fluctuation in micro-scale geochemical environments.

6. Fractures that cross cut iron oxide-filled fractures suggest physical weathering (e.g., freeze/thaw) plays an important role in providing conduits for oxidizing fluids to interior sulfide minerals.

7. XAS data prove that Cu occurs in an oxidized form (i.e. $Cu^{++}$) within the banded iron oxides however, the crystal chemistry could not be determined.

8. A mixture of As (III) and As (V) was observed within the iron oxide coatings.

9. Sheet silicates can be highly enriched in Cu and/or Ni (i.e. contain several weight percent Cu, Ni by SEM-EDS). The metals appear to occur in the divalent state (μXAS). However, the source of metal enrichment in sheet silicates remains unresolved. Importantly, these phases will either act as either a source or a sink for metals during weathering.

# 4 Geochemical modeling and discussion

This section primarily focuses on exploratory geochemical modeling done for the metals of interest (Cu, Ni, Co, Zn, As). A conceptual model that describes weathering product controls on metal mobility in water associated with mineralized Duluth Complex rock is also presented. The conceptual model incorporates the conclusions drawn from both characterization work and modeling.

## 4.1 Geochemical modeling

Geochemical modeling was employed to investigate the theoretical control exerted by weathering products on aqueous metal concentrations. To avoid redundancy, the general method is described below and element-specific results are presented in the following sections.

Metal concentrations calculated from the solubilities of specific mineral assemblages were directly compared to concentrations observed in the AMAX drainage and from the Mesaba barrels. This assessment of geochemical equilibrium works to support the contention made in the introduction that weathering products act to limit the concentrations of environmentally-important solutes through solid phase solubility and adsorption reactions. Visual estimation of the fit between the observed values and the theoretical solubility limit allowed a conceptual evaluation of reasonable secondary mineral controls for the constituents of interest. The modeling methodology follows a review paper in Applied Geochemistry by Eary (1999) titled *Geochemical and equilibrium trends in mine pit lakes*.

Geochemical equilibrium modeling was performed using Geochemist's Workbench- Version 7 (Bethke, 2008). Models were generated in order to produce 'solubility curves' which were then plotted alongside drainage chemistry, following the general form of Eary (1999). Solubility curves were generated for both observed weathering products (e.g. malachite) and reasonable, but not observed phases (e.g. $Ni(OH)_2$), and were generated using the MINTEQ.tdat thermodynamic data (unmodified). When noted, different databases were used because the MINTEQ.tdat dataset did not contain data for all of the phases of interest.

Metal concentrations in equilibrium with specific hydroxide and oxide phases were calculated using theoretical a 0.021 M $Na_2SO_4$ solution in equilibrium with atmospheric $O_2$ (0.20 atm.) and $CO_{2(g)}$ ($10^{-3.5}$ atm.). Temperature was held at 25° C. To generate curves from pH 3 to 9, a sliding pH command was used and the solution was charge balanced on $Na^+$. Solubility curves for sulfate minerals were performed with gypsum as the $SO_4$ controlling phase. Solubility curves for silicates were made with chalcedony as the Si controlling phase. Additional documentation can be found in Appendix F.

## 4.2 Modeling results and discussion by element

### 4.2.1 Copper

Copper concentrations in waste rock are elevated due to primary sulfides especially chalcopyrite and cubanite. Two copper bearing weathering products were identified for Mesaba samples: malachite and Cu associated with secondary banded iron phases (inferred to be incorporated by sorption on ferrihydrite).

#### 4.2.1.1 Equilibrium trends for copper

Copper concentrations in low pH drainage (pH 3- 4.5) from the AMAX pile are very high, exceeding 100 mg/L (Figure 4-1). Comparisons of the solubilities of the modeled solid species to the low pH observations (where no solid phase limits concentration) suggest that Cu concentrations in AMAX drainage were limited by sulfide mineral oxidation kinetics. At neutral to alkaline pH, observed AMAX concentrations show large variability, however, the data tend to generally track the malachite curves. Malachite also appears to bound the upper limit of the Mesaba barrel data. Tenorite is too insoluble to match the data, while $Cu(OH)_2$ represents a truer upper limit. The modeled ferrihydrite sorption curves indicate that, while sorption/coprecipitation reactions are expected to remove Cu from solution, they are not expected to strictly limit concentrations.

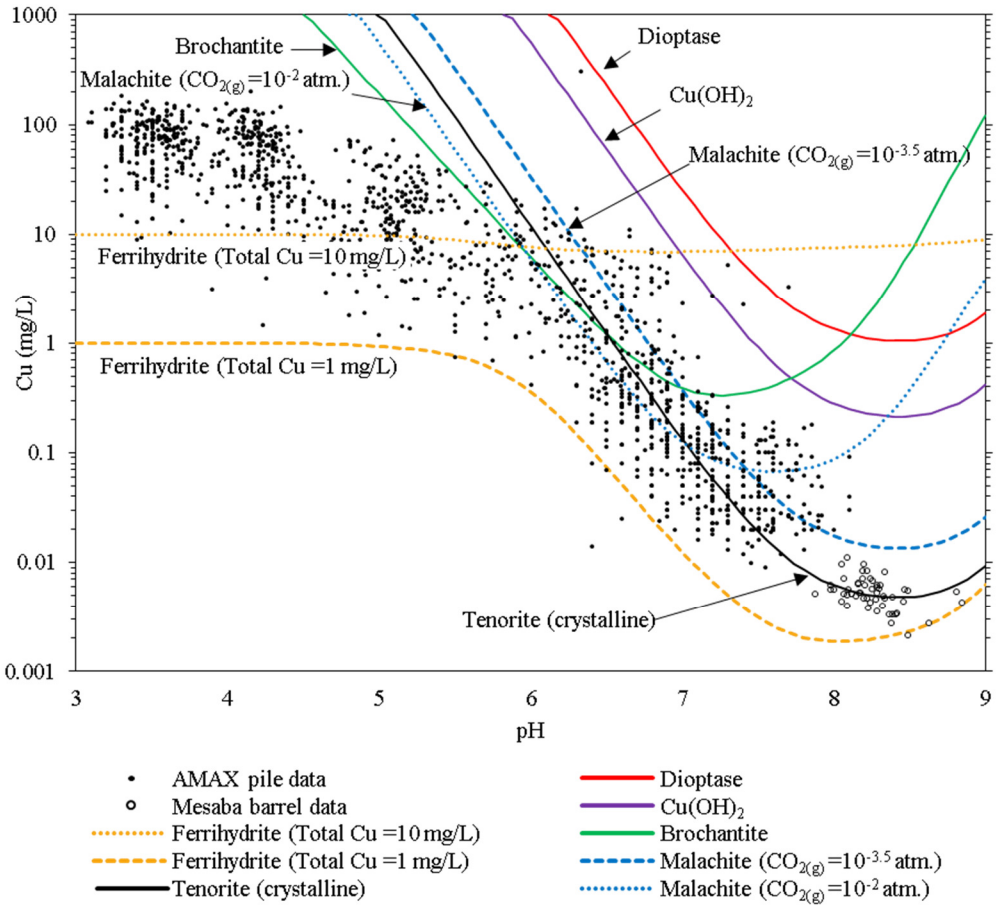


Figure 4-1. Concentrations of Cu [total Cu] in AMAX pile drainage and Mesaba barrel leachate compared to the solubilities of Cu-bearing solids in a theoretical 0.021 M $Na_2SO_4$ solution charge balanced on Na in equilibrium with atmospheric $O_2$ (0.20 atm.) and $CO_{2(g)}$ ($10^{-3.5}$ atm.). Solubility curves for brochantite shown at equilibrium with gypsum, for dioptase at equilibrium with chalcedony, and for malachite, an additional curve is shown at equilibrium with $CO_{2\ (g)}$ at $10^{-2}$ atm. Two ferrihydrite adsorption curves are shown both for 1 mg/L *free* ferrihydrite and either 1 mg/L total Cu or 10 mg/L total Cu. All curves were generated using Geochemist's Workbench© (version 7) and the MINTEQ.tdat thermodynamic data except for dioptase which was plotted using the V8R6+.tdat thermodynamic data because dioptase is not included in MINTEQ.tdat dataset.

### 4.2.2 Nickel

The prediction of Ni concentrations in mine waters are especially difficult due to its multiple primary sources and relatively high solubility in neutral to alkaline pH water. Furthermore, Ni is a known contaminant in contaminated neutral drainage (CND).

Nickel is hosted by both sulfide and silicate phases. Two sulfide sources are pentlandite and pyrrhotite; in the case of pyrrhotite, Ni substitutes for Fe at up to weight-percent quantities. Olivine is a significant silicate host of Ni; concentrations in olivine have been observed to show wide variability ranging from 10s to 1000s of mg/kg (Al-Alawi, 1985; SRK, 2007).

#### 4.2.2.1 Equilibrium trends for nickel

Nickel concentrations in low pH (3- 4.5) AMAX pile drainage are very high, approaching 1000 mg/L (Figure 4-2). Comparisons of the solubilities of the modeled solid species do not bound any of the low pH observations suggesting these concentrations were limited by sulfide/silicate mineral oxidation/dissolution kinetics. For neutral to alkaline pH, observed concentrations show large variability, however the data tend to generally track the $NiCO_3$ (gaspeite) curve. Crystalline $Ni(OH)_2$ (theophrasite) represents an upper limit as it bounds all of all observations. The modeled ferrihydrite sorption curves indicate that, while sorption is expected to be removing Ni from solution, it is not expected to be the dominant mechanism. It has also been suggested that nickel silicates may act as secondary mineral controls. This is a difficult hypothesis to test because of the dearth of thermodynamic data for these phases, and the possible kinetic constraints.

Mine waste investigations have frequently noted Ni concentrations in kinetic tests show increasing flux over time (Nicholson et al., 1999; Maest et al., 2005; Rinker et al. 2003; Geochimica, 2005; SRK, 2007). However, several recent papers by researchers from Université du Québec en Abitibi-Témiscamingue (UQAT)- Research Institute of Mining have presented results of detailed investigations on the geochemical behavior of Ni, especially under neutral pH conditions. The mentioned studies suggested that

$Ni(OH)_2$ sorption onto primary mineral surfaces is an important secondary phase controlling Ni concentrations. The delay in observed nickel leaching rates in their system was attributed to primary mineral surfaces becoming saturated with $Ni(OH)_2$ over time, leading to gradually diminishing attenuation potential (Plante et al. 2010; Plante et al.2011a; Plante et al. 2011b; Plante et al. 2014).

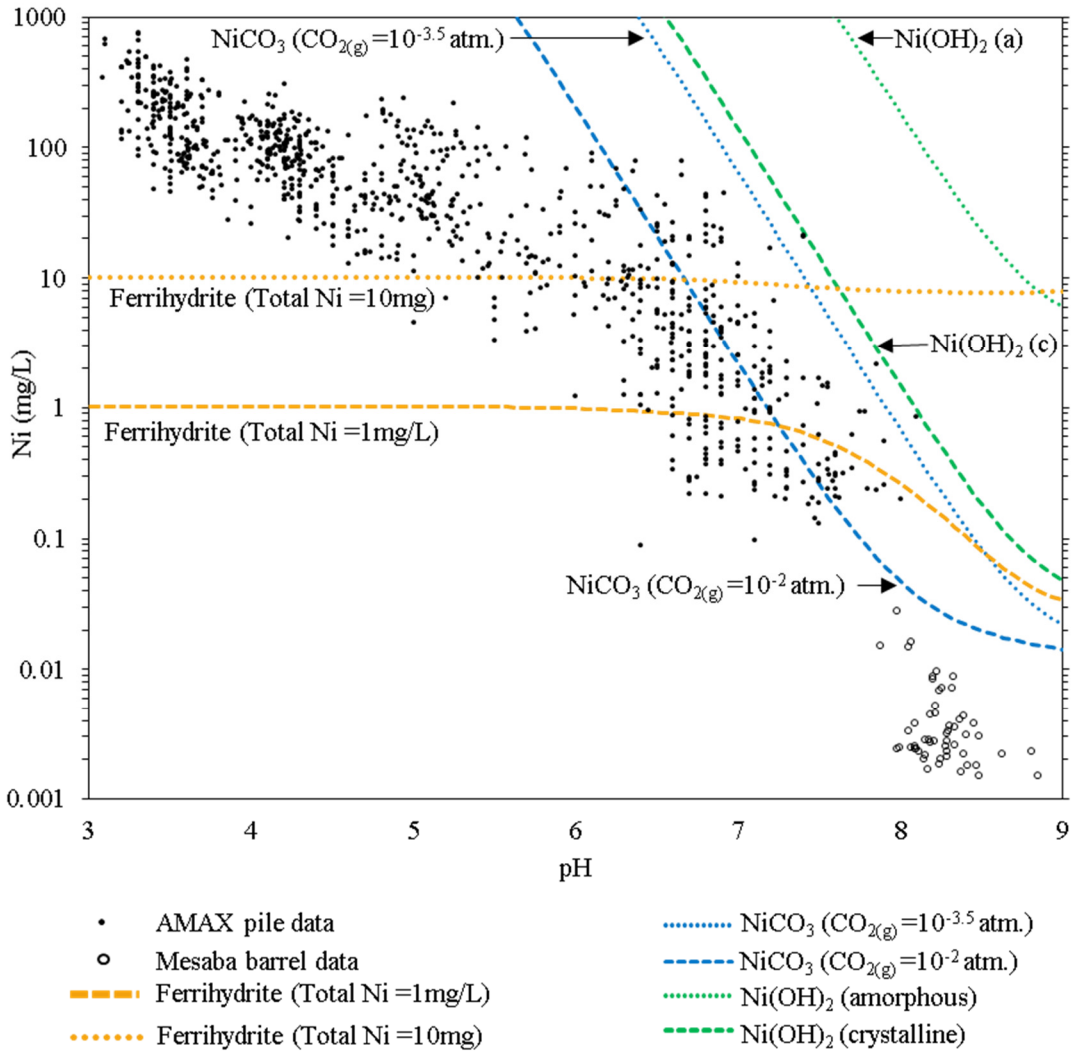


Figure 4-2. Concentrations of Ni [total Ni] in AMAX pile drainage and Mesaba barrel leachate compared to the solubilities of Ni-bearing solids in a theoretical 0.021 M $Na_2SO_4$ solution charge balanced on Na in equilibrium with atmospheric $O_2$ (0.20 atm.) and $CO_{2(g)}$ ($10^{-3.5}$ atm.). For $NiCO_3$, an additional curve is shown at equilibrium with $CO_{2\ (g)}$ at $10^{-2}$ atm. Two ferrihydrite adsorption curves are shown both for 1 mg/L *free* ferrihydrite and either 1 mg/L total Ni or 10 mg/L total Ni. All curves were generated using Geochemist's Workbench© (version 7) and the MINTEQ.tdat thermodynamic data.

### 4.2.3 Cobalt

Cobalt is a commonly enriched in mafic rocks and is a known environmental contaminant (e.g. from Dunka stockpiles). Cobalt in Duluth Complex rock can be hosted by minor cobalt arsenide and sulfide phases and can also occur in pentlandite at several weight percent quantities (SRK, 2007). No Co-bearing weathering products were identified for Mesaba samples.

#### 4.2.3.1 Equilibrium trends for cobalt

Cobalt concentrations in low pH (3- 4.5) AMAX pile drainage are high, approaching 100 mg/L, although lower than Ni or Cu concentrations (Figure 4-3). The lower concentrations probably reflect the much lower Co concentrations in the rock. Comparisons of the solubilities of the modeled solid species do not bound any of the low pH observations. For neutral to alkaline pH, observed concentrations show large variability, however the data are bounded at the upper limit by the $CoCO_3$ (sphaerocobaltite) curve. The modeled ferrihydrite sorption curves indicate, that while sorption is expected to be removing Co from solution, it is not expected to be the dominant mechanism. Cobalt concentrations are very low in barrel test leachate and are not fit by any of the solubility curves suggesting that here, Co concentrations were release rate controlled.

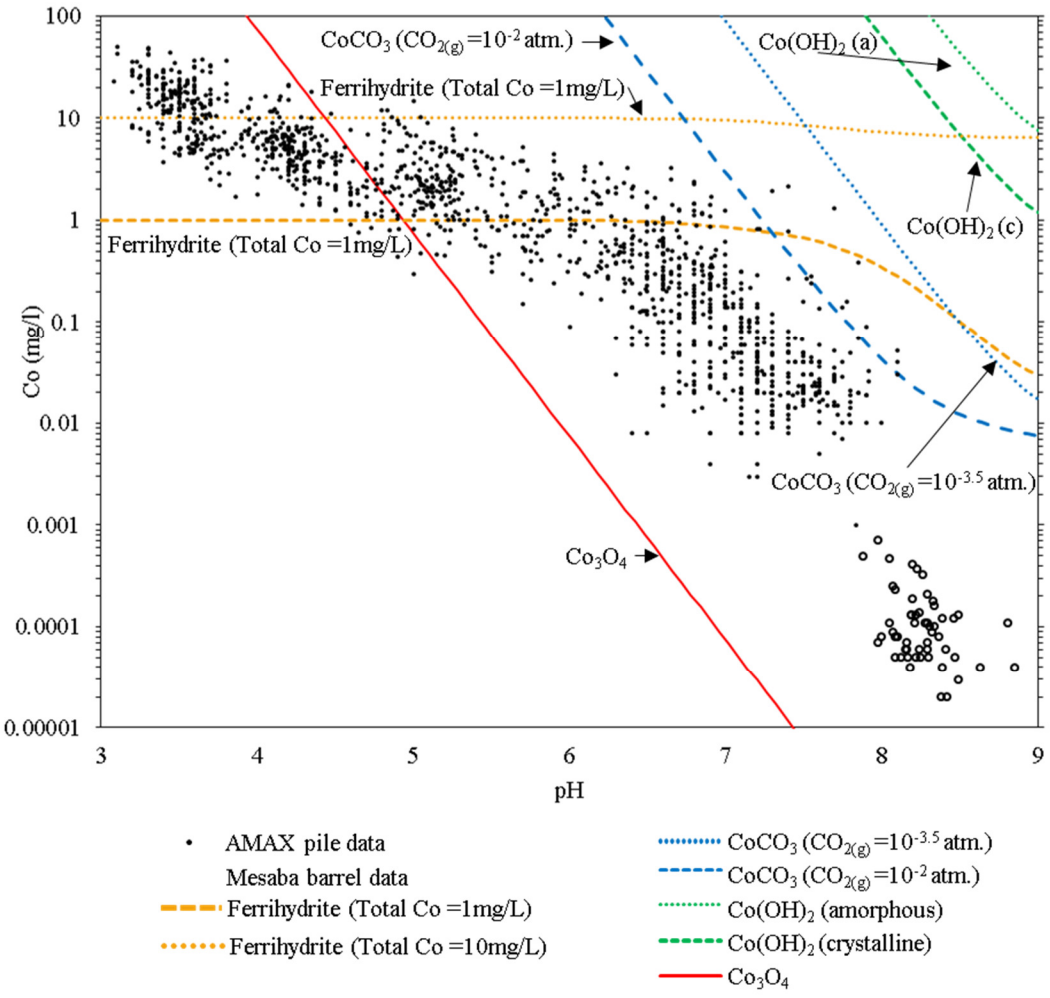


Figure 4-3 Concentrations of Co [total Co] in AMAX pile drainage and Mesaba barrel leachate compared to the solubilities of Co-bearing solids in a theoretical 0.021 M $Na_2SO_4$ solution charge balanced on Na in equilibrium with atmospheric $O_{2(g)}$ (0.20 atm.) and $CO_{2(g)}$ ($10^{-3.5}$ atm.). For $CoCO_3$, an additional curve is shown at equilibrium with $CO_{2\ (g)}$ at $10^{-2}$ atm. Two ferrihydrite adsorption curves are shown both for 1 mg/L *free* ferrihydrite and either 1 mg/L total Co or 10 mg/L total Co. All curves were generated using Geochemist's Workbench© (version 7) and the MINTEQ.tdat thermodynamic data. One data point from a Mesaba barrel was below the 0.02 µg/L Co detection limit and is plotted at the detection limit. It appears that some of the AMAX data points are also at the detection limit, but this is unknown based on the author's knowledge of the data.

### 4.2.4 Zinc

Zinc is an element of concern because it is relatively soluble in circumneutral pH mine waters. Zinc concentrations in Duluth Complex rocks are low, however sphalerite was observed as microscopic grains associated with sheet silicates in the Mesaba samples. No Zn-bearing secondary phases were identified for Mesaba samples.

#### 4.2.4.1 Equilibrium trends for zinc

Zinc concentrations in low pH (3- 4.5) AMAX pile drainage are high, approaching 25 mg/L, although generally lower than Ni, Cu, and Co concentrations (Figure 4-4). The lower concentrations probably reflect the low Zn concentrations in the rock. Comparisons of the solubilities of the modeled solid species do not bound any of the low pH observations. For neutral to alkaline pH, observed concentrations show large variability, however the data trend with the smithsonite ($ZnCO_3$) curve and are bounded at the upper limit by the willemite ($Zn_2SiO_4$) curve. The modeled ferrihydrite sorption curves indicate, that while sorption is expected to be removing Zn from solution, it is not expected to be the dominant mechanism. Zinc concentrations are very low in barrel test leachate and are not fit by any of the solubility curves possibly because the barrel chemistry was release-rate controlled. At higher pH, the AMAX data appear to trend with possible low-level detection limits (concentrated data points at a single low concentration).

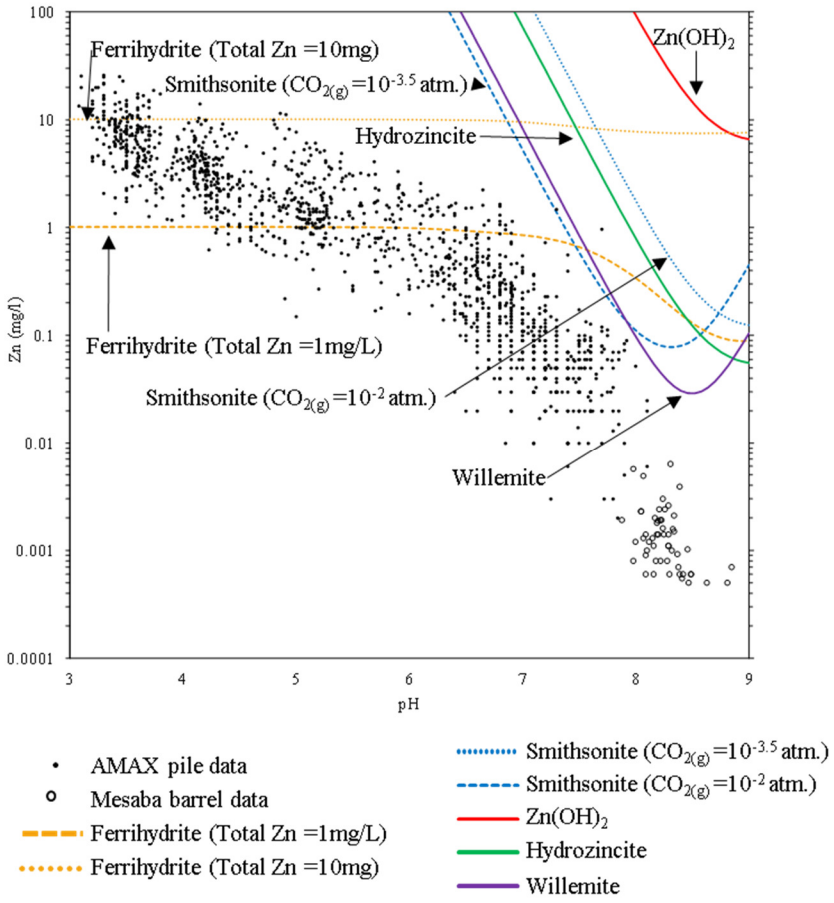


Figure 4-4. Concentrations of Zn [total Zn] in AMAX pile drainage and Mesaba barrel leachate compared to the solubilities of Zn-bearing solids in a theoretical 0.021 M $Na_2SO_4$ solution charge balanced on Na in equilibrium with atmospheric $O_2$ (0.20 atm.) and $CO_{2(g)}$ ($10^{-3.5}$ atm.). Solubility curves for willemite are at equilibrium with chalcedony, and for smithsonite, an additional curve is shown at equilibrium with $CO_{2\ (g)}$ at $10^{-2}$ atm. Two ferrihydrite adsorption curves are shown both for 1 mg/L *free* ferrihydrite and either 1 mg/L total Zn or 10 mg/L total Zn. All curves were generated using Geochemist's Workbench© (version 7) and the MINTEQ.tdat thermodynamic data except for willemite which was plotted using the PHREEQC.tdat thermodynamic data because willemite is not included in MINTEQ.tdat dataset. Three data points from the Mesaba barrels were below the 0.5 µg/L Zn detection limit and are plotted at the detection limit. It appears that some of the AMAX data points are also at the detection limit, but this is unknown based on the author's knowledge of the data.

### 4.2.5 Arsenic

Arsenic is a common contaminant associated with mine waste in general, however Duluth Complex rock generally contains low concentrations of arsenic. In these rocks, small grains of arsenic-bearing minerals have been observed (e.g. sperrylite -$PtAs_2$) (Teck, 2008). The low abundance of arsenic presents significant difficulties in determining its distribution among different primary minerals weathering products.

Sorption/ coprecipitation are the commonly reported control mechanisms for arsenic concentrations in mine waste systems except in unique, high arsenic systems (Bowell et al., 2014). Unlike the previously mentioned elements, arsenic typically occurs as an oxyanion (e.g. $H_2AsO_4$-) in solution (Figure 4-5) making the pH-dependence of sorption processes unlike the metals mentioned above. For example, the efficiency of arsenic sorption onto ferrihydrite is less at higher pH, and in the presence of competing sulfate, chloride (competing anions) in solution (Eary, 1999).

The only secondary arsenic-bearing phase identified for Mesaba samples was a banded iron oxide coating that occurred in a fracture (analyzed by µXAS). The analyzed points showed that arsenic was partially (~30 %) in the form of As (III) while the remainder was in As (V), the most oxidized form.

Micro-system redox disequilibrium can explain the presence of both As (III) and As (V) species adsorb/coprecipitated with secondary iron oxides (Foster, personal communication, 2015). Studies have shown that arsenic redox disequilibrium is common in natural systems, and can be often be attributed to microbial activity (Bowell et al., 2014 and references therein). Figure 4-5 shows predominant arsenic species in a theoretical fluid for a given Eh and pH conditions. When arsenic occurs in aqueous environments in the trivalent state, it is considered to be more mobile because it has a lower tendency to sorb onto mineral surfaces.

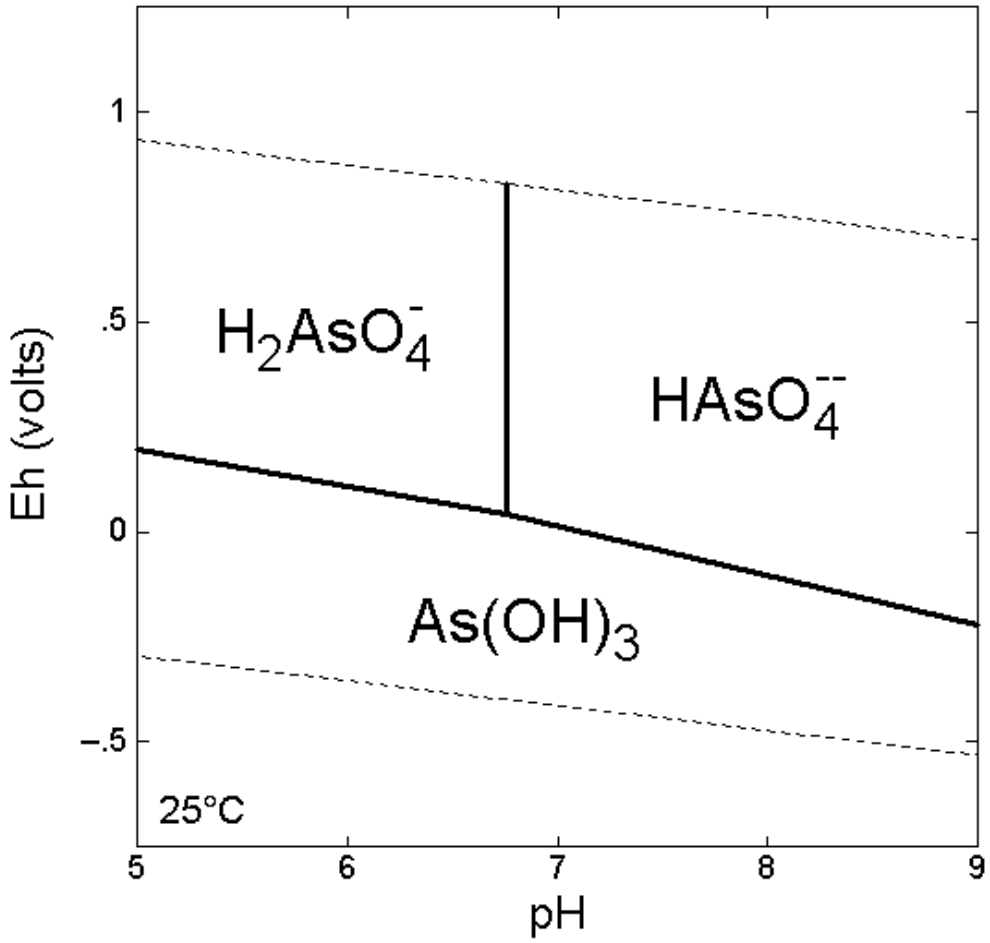


Figure 4-5. Pourbaix diagram for arsenic plotted using Geochemist's Workbench.

## 4.3 Conclusions and a Duluth Complex conceptual model for metal mobility

The modeling and solid phase characterization results suggest secondary minerals and other weathering products significantly attenuate metals and metalloids of interest in these systems. In summary, Cu, Ni, Co, and Zn will be strongly attenuated in scenarios where pH is circumneutral (Figure 4-6. Much greater uncertainty exits around the fate of arsenic because it was not measured in AMAX pile drainage and is not concentrated Duluth Complex rock.

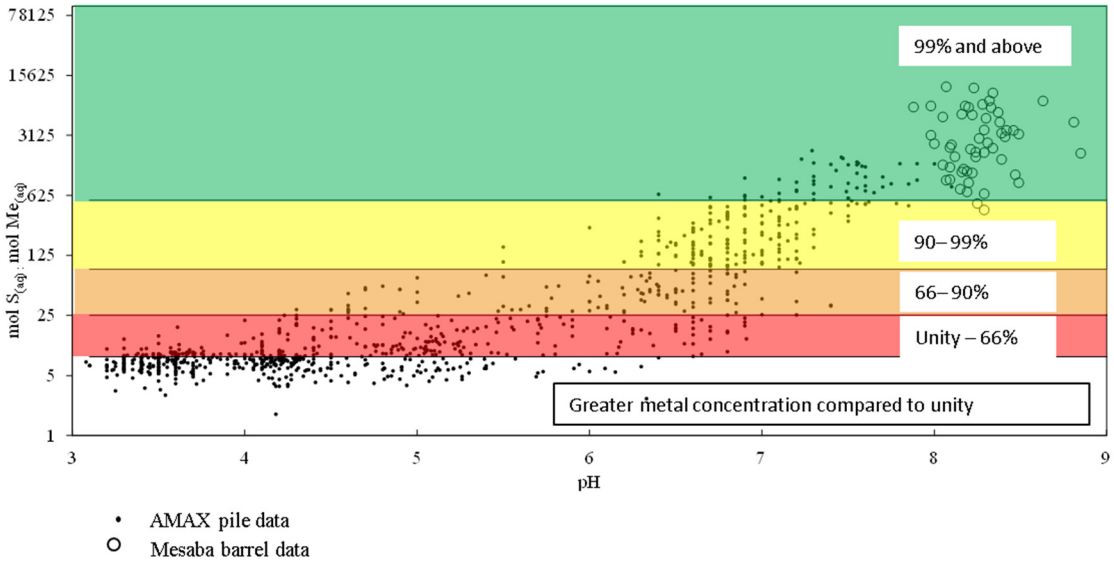


Figure 4-6. Calculated molar ratios of aqueous S (measured as sulfate) and metals (aqueous concentrations of Cu+Ni+Co+Zn) versus pH from AMAX pile and barrel leachate. The transition between areas of white and colored areas shows the calculated unity line. Unity (8.2) is calculated as the mean molar ratio between pH 3 and 4.5 (below solubility limits and sorption edges for metals of interest) for AMAX data. Colored regions are delineated for the stated ranges (mass percent) of calculated attenuation. Note significant attenuation of metals at pH 6.5 and higher.

The weight of evidence from characterization of weathering products and modeling informed the following conceptual model for mobility of metals released during weathering of Duluth Complex rock.

1. During weathering of Duluth Complex rock, a balance between acid generated by sulfide oxidation and alkalinity produced by silicate dissolution, primarily controls drainage pH.

2. Oxidized iron produced during sulfide mineral oxidation can remain near the sulfide grain (iron oxide replacement) or can be mobilized short distances resulting in rusty coatings. In both cases, but especially in the later, iron, silicon, aluminium, copper, and sulfur can form compositionally distinct bands at the microscopic scale (several micrometres wide). The banded morphology may be result of variable solution chemistry that influences the effectiveness of coprecipitation and/or adsorption onto ferrihydrite.

3. Metal mobility will be highly dependent on pH however, the dominant mechanisms controlling metal mobility may be element specific. The results from characterization suggest malachite solubility and sorption/ coprecipitation reactions may limit copper mobility. Weathering products controlling nickel, cobalt, and zinc were not observed directly but may be partially explained by the solubilities of secondary carbonate, hydroxide, and/or silicate phases.

4. For arsenic, sorption/coprecipitation on iron-bearing weathering products could be an important control, however complex redox kinetics may allow coexisting As (III) and As (V) species in both waters and the weathering products. The pH and ionic strength of the coexisting fluids may also influence ultimate arsenic mobility.

5. During evaporation, dissolved constituents can precipitate as sulfate salts. In one case rozenite (an acid sulfate) precipitated suggesting that, under certain low water:rock ratio conditions acidity can be stored temporarily. Wetter conditions cause highly soluble phases to dissolve.

6. The water chemistry of drainage associated with exposed Duluth Complex rock produced by potential future mining will likely be variable and dependent on many system parameters.

# 5 Conclusion and future studies

This research utilized a complementary suite of characterization methods, supported by geochemical modeling and evaluation of observed water quality from field-scale weathering experiments to refine the conceptual model for the mobility of metals released during weathering of Duluth Complex rock. The major conclusions of this study are:

1. The environmental behaviour of Duluth Complex rock is dependent on a suite of chemical and physical processes. Precipitation of weathering products is an important control on water chemistry.
2. The secondary minerals goethite, malachite, and rozenite were identified by XRD included.
3. Malachite solubility represents a reasonable control for copper concentrations in future mine waters.
4. The presence of rozenite and results from static test work (e.g. rinse pH) suggest acidity can be retained as highly soluble salts in acidic, low water:rock ratio settings.
5. Secondary iron oxide weathering products form on Duluth Complex rocks as banded iron rich coatings that can contain copper and arsenic suggesting at least a partial control mechanism for these elements. Assuming sorption processes incorporated the metals associated with the banded coating, solution characteristics (e.g. pH, ionic strength) will be important in actual attenuation efficacy. Secondary iron oxides may be attenuating other metals at low levels, below the detection limits of the methods used.
6. Modeling has shown metals of interest may have been precipitated as pure-phase secondary minerals in the AMAX experimental piles. The trace metal concentration of AMAX waters were highly dependent on pH, but showed significant variability at any pH.
7. Further work is required to characterize weathering products that are responsible for the control of several metals, most importantly, nickel.

The questions posed for this thesis research could benefit by additional characterization of the mineralogical identity of the banded iron oxides. Synchrotron based micro-XRD may be able to determine the crystallinity and mineralogical makeup of the banded coatings. Electron microprobe analysis (EMPA) of the banded coatings would provide quantitative results at a detection limits below that of SEM-EDS and the 'degree of hydration' could be evaluated based on reported EMPA totals (Jambor, 1998).

Studying weathering products that formed in humidity cell test (or similar) environments could be useful to improve our understanding of the geochemistry in these systems. Interpretations would benefit from knowledge of pH over time and complete system mass balance. In addition, weathering product characteristics from materials subjected to lab-based weathering could be compared to the findings from this study. For example: Do iron coatings precipitate in a banded morphology under controlled conditions?

# 6 References


Al-Alawi, J., 1985, Petrography, Sulfide Minerology and Distribution, Mass Transfer, and Chemical Evolution of the Babbitt Cu-Ni Deposit, Duluth Complex, Minnesota. Unpublished Ph.D. Indiana University.

ASTM International- D5744-13, 2013, Standard test method for laboratory weathering of solid materials using a humidity cell. In Annual book of ASTM Standards, 11.04. American Society for Testing and Materials, West Conschohocken, PA. 19 p.

Barr Engineering Company and SRK Consulting (Canada) Inc., 2014, Mesaba Project Secondary Mineral Characterization- Phase 1 DRAFT.

Belzile, N., Chen, Y., Chi, M., Li, Y., 2004, A review of pyrrhotite oxidation. Journal of Geochemical Exploration. vol. 84. pp 65-76.

Bethke, C. M., 2008, Geochemical and biogeochemical reaction modeling. Cambridge University Press.

Blowes, D. W., Jambor, J. L., Alpers, C. N., 1994, The environmental geochemistry of sulfide mine-wastes (Vol. 22). Mineralogical Association of Canada.

Bowell, R., Alpers, C., Jamieson, H. Nordstrom, K., Majzlan, J., editors. 2014, Arsenic: Environmental Geochemistry, Mineralogy, and Microbiology Reviews in Minerology and Geochemistry: Volume 79.

Brantley S.L., 2008, Kinetics of mineral dissolution. *In*: Kinetics of water-rock interaction. Brantley S.L, Kubicki J.D, White A.F (eds.). Springer Science 834p.

Brown, G.E., Sturchio, N.C. 2002. An overview of synchrotron radiation applications to low temperature geochemistry and environmental science. Reviews in Mineralogy and Geochemistry. 49, 1-115.

Calvin, S. 2013. XAFS for Everyone. CRC Press.

Caraballo, M. A., Michel, F. M., Hochella, M. F., 2015, The rapid expansion of environmental mineralogy in unconventional ways: Beyond the accepted definition of a mineral, the latest technology, and using nature as our guide. American Mineralogist, 100(1), 14-25.

Carbone, C., Marescotti, P., Lucchetti, G., Martinelli, A., Basso, R., Cauzid, J., 2012, Migration of selected elements of environmental concern from unaltered pyrite-rich mineralizations to Fe-rich alteration crusts. Journal of Geochemical Exploration, 114, 109-117.

Cervin, D.O., 2011, Characterization of Precious Metal Mineral Occurrences in the Northmet Deposit of the Partridge River Intrusion, Duluth Complex, Minnesota, USA. Unpublished M.S Thesis. University of Minnesota- Duluth. p.166.

Cornell, R. M., & Schwertmann, U, 2006, The iron oxides: structure, properties, reactions, occurrences and uses. John Wiley & Sons.

Day, S. and Kennedy, C., 2015, Setting ARD management criteria for mine wastes with low sulfide content. 10th ICARD (International Conference on Acid Rock Drainage). Santiago, Chile.

Dzombak, D.A. and Morel, F.M.M., 1990, Surface Complexation Modeling – Hydrous Ferric Oxides. Wiley, New York

Eary, L. E., 1999, Geochemical and equilibrium trends in mine pit lakes. Applied Geochemistry, 14(8), 963-987.

Eary, L.E., Williamson M.A., 2006, Simulations of the Neutralizing Capacity of Silicate Rocks in Acid Mine Drainage Environments, 7th ICARD (International Conference on Acid Rock Drainage) St. Louis, Missouri.

Fix, P., Diedrich, T., Kennedy, C., Day, S., 2015, Characterization of weathering products and controls on metal mobility at a Cu, Ni, PGE deposit. Paper and presentation at 10th ICARD (International Conference on Acid Rock Drainage). Santiago, Chile.

Foster, A., 2015, Personal communication.

Foster, A. L., Brown Jr, G. E., Tingle, T. N., Parks, G. A., 1998, Quantitative arsenic speciation in mine tailings using X-ray absorption spectroscopy. American Mineralogist, 83(5), 553-568.

Geochimica, Inc., 2005, Phase II Eagle Project Geochemistry Study. 45 p.

Goldstein, J., Newbury, D. E., 2012, Scanning electron microscopy and X-ray microanalysis: a text for biologists, materials scientists, and geologists. Springer Science & Business Media.

International Centre for Diffraction Data (ICDD), 2007.

Ilton, E.S., Veblen, D.R., 1988, Copper inclusions in sheet silicates from porphyry copper deposits. Nature, 334, 516–518.

Ilton, E.S., Earley III, D., Marozas, D., Veblen, D.R., 1992, Reaction of some trioctahedral micas with copper sulfate. Economic Geology. 87, 1813–1829.

Ilton, E.S., Veblen, D.R., 1993, Origin and mode of copper enrichment in biotite from rocks associated with porphyry copper deposits: a transmission electron microscopy investigation. Economic. Geology. 88, 885–900.

INAP, 2009, The International Network for Acid Prevention. Global Acid Rock Drainage Guide (GARD Guide). http://www.gardguide.com/. Accessed October 2015.

Jambor, J.L., Blowes, D.W., 1998, Theory and applications of mineralogy in environmental studies of sulfide-bearing mine wastes. *In*: Cabri, L.J., Vaughan, D.J. (Eds.), Modern Approaches to Ore and Environmental Mineralogy, Short Course Series, vol. 27. Mineralogical Association of Canada, Ottawa, pp. 367–401.

Jambor, J. L., Dutrizac, J. E., 1998, Occurrence and constitution of natural and synthetic ferrihydrite, a widespread iron oxyhydroxide. Chemical Reviews, vol. 98, pp. 2549–2586.

Jambor, J.L., 2003, Mine-waste mineralogy and mineralogical perspectives of acid– base accounting. *In:* Jambor, J.L., Blowes, D.W., Ritchie, A.I.M. (Eds.), Environmental Aspects of Mine Wastes, Short Course Series, vol. 31. Mineralogical Association of Canada, Ottawa, pp. 117–145.

Jamieson, H.E., 2011, Geochemistry and Mineralogy of Solid Mine Waste: Essential Knowledge for Predicting Environmental Impact. Elements 7, 381-386.

Jamieson, H. E., Walker, S. R., Parsons, M. B., 2015, Mineralogical characterization of mine waste. Applied Geochemistry, 57, 85-105.

Jerz, J. K., Rimstidt, J. D., 2004, Pyrite oxidation in moist air. Geochimica et Cosmochimica Acta, 68(4), 701-714.

Jirsa, M. A., Chandler, V. W., Lively, R. S., 2005, Bedrock geology of the Mesabi Iron Range. Minnesota: Minnesota Geological Survey Miscellaneous Map Series M-163, I sheet, scale, 1:100,000.

Kelsey, P., 1996, Weathering of Cu-Ni Mineralized Mine Tailings from the Duluth Complex, Minnesota. Unpublished M.S. Thesis. Colorado School of Mines. 91p.

Kuipers, J.R., Maest, A.S., MacHardy, K.A., Lawson, G., 2006, Comparison of Predicted and Actual Water Quality at Hardrock Mines: The reliability of predictions in Environmental Impact Statements. Report prepared for Earthworks.

Kumar, P., Nagarajan, R., & Sarangi, R., 2013, Quantitative X-ray absorption and emission spectroscopies: electronic structure elucidation of $Cu_2S$ and CuS. Journal of Materials Chemistry C, 1(13), 2448-2454.

Lapakko, K. A., 1980, The kinetics and mechanisms of the oxidative dissolution of metal sulfide and silicate minerals present in the Duluth Gabbro. M. S. Thesis, Univ. MN, Minneapolis, MN. 199 p. plus appendices.

Lapakko, K. A., 1993b, Field dissolution of test piles of Duluth Complex rock: Report to the US Bureau of Mines Salt Lake City Research Center. Coop. Agreement No. C0219003. MN Dept. Nat. Resour., Div. of Minerals. St. Paul, MN. 41p

Lapakko, K.A., Antonson, D.A., Folman, J.T., Johnson, A.M., 2002a, Assessment of test methods for waste rock dissolution and laboratory drainage quality from Duluth Complex rock. Final report on Contract BLM JSP012002 to the U.S. Bureau of Land Management, Salt Lake City Office. 63 p. plus appendices.

Lapakko, K. A., Engstrom, J., Antonson, D. A., 2004a, Long term dissolution testing of mine waste. Report on Contract No. DACW45-02-P-0205 to US Army Corps of Engineers by the Minnesota Department of Natural Resources. 154 p. plus appendices.

Lapakko, K.A., Antonson, D.A., Engstrom, J.N., 2004b, Analytical screening of abandoned waste rock piles. Report on Contract No. DACW45-02-P-0212 to US Army Corps of Engineers by the Minnesota Department of Natural Resources. 91 p. plus appendices.

Lapakko, K. and Antonson, D. A., 2012, Duluth Complex Rock Dissolution and Mitigation Techniques: A Summary of 35 years of DNR Research. Minnesota Department of Natural Resources, St. Paul, MN, USA.

Lapakko, K. and Olson, M. 2015, Scaling Laboratory Sulfate Release Rates to Operational Waste Rock Piles. Minnesota Department of Natural Resources, USA (p. 246). Paper and presentation at 10th ICARD (International Conference on Acid Rock Drainage). Santiago, Chile.

Langman, J.B., Blowes, D.W., Veeramani, H., Wilson, D., Smith, L., Sego, D.C., Paktunc, D., 2015, The Mineral and Aqueous Phase Evolution of Sulfur and Nickel with Weathering of Pyrrhotite in a Low Sulfide, Granitic Waste Rock. Chemical Geology vol. 401. pp. 169-179.

Lasaga, A. C. and Kirkpatrick, R. J., 1981, Kinetics of geochemical processes. 3 Vol. 8. Reviews in Mineralogy.

Lin, Z., 1996, Leachate chemistry and precipitates mineralogy of Rudolfsgruvan mine waste rock dump in central Sweden. Water Science and Technology, 33(6), 163-171.

Listerud, W.H., and Meineke, D.G., 1977, Mineral resources of a portion of the Duluth Complex and adjacent rocks in St. Louis and Lake Counties, northeastern Minnesota: Hibbing, Minn., Minnesota Department of Natural Resources, Division of Minerals Report 93, 74p.

Maest, A.S., Kuipers, J.R., Travers, C.L., Atkins, D.A., 2005, Predicting Water Quality at Hardrock Mines: Methods and Models, Uncertainties, and State-of-the-Art: <http://www.earthworksaction.org/files/publications/PredictionsReportFinal.pdf> accessed 18 Sept. 2014

Miller, J.D., Jr., and Nicholson, S.E., 2013, Geology and mineral deposits of the 1.1 Ga Midcontinent rift in the Lake Superior Region—an overview, in Miller, J., ed., Field Guide to the copper-nickel-platinum group element deposits of the Lake Superior Region, Duluth, MN: Precambrian Research Center Guidebook 2013-01, p. 1–50.

Miller, J.D., Jr., Green, J.C., Severson, M.J., Chandler, V.W., Hauck, S.A., Peterson, D.M., and Wahl, T.E., 2002, Geology and mineral potential of the Duluth Complex and related rocks of northeastern Minnesota: Minnesota Geological Survey Report of Investigations 58, 207p.

Miller J. D., Jr., and Severson, M. J., 2005, Bedrock geology of the Babbitt quadrangle, St. Louis County, Minnesota: Minnesota Geological Survey Miscellaneous Map M-159, scale, 1:24,000.

Minnesota Environmental Quality Board, 1979, Regional copper-nickel study, Executive summary, volume 1. MN State Planning Agency, St. Paul, MN. 118 p.

Naldrett, A. J., 1999, World-class Ni-Cu-PGE deposits: key factors in their genesis. Mineralium deposita, 34(3), 227-240.

Naldrett, A. J., 2004, Magmatic sulfide deposits: geology, geochemistry and exploration. Springer Science & Business Media.

Nicholas, S.W., Haus, K.L., Hochella, M.F., 2007, Aquatic environmental nanoparticles. Journal of Environmental Monitoring. Vol. 9-12. pp. 1306-1316.

Nicholas, S.L., Wirth, K.R., Engstrom, J.N., Lapakko, K.A., 2007, Investigations of sulfide mineral leached in the presence of alkaline solids. Poster at International Lake Superior Geology Institute.

Nicholson R.V., Rinker M.J., Williams G., Napier W., 1999, Assessment of water quality associated with underwater disposal of tailings and waste rock from the Voisey's Bay Project, Labrador, Canada, Proceedings of the Sudbury'99: Mining and the Environment Conference, September 12-15. Sudbury, Ontario, pp 127–136

Nordstrom, D.K., Alpers, C.N., 1999, Geochemistry of acid mine waters. *In:* Plumlee, G.S., Logsdon, M.J. (Eds.), The Environmental Chemistry of Mineral Deposits. Part A: Processes, Techniques, and Health Issues. Rev. Econ. Geol. 6A, 133–160

Nordstrom, D.K., 2011, Mine waters: Acidic to circumneutral. Elements 7, 393-398.

Peterson, D.M., 2010, The Nokomis Cu-Ni-PGE Deposit, Minnesota. Prospectors and Developers Association of Canada. Annual Meeting, Powerpoint presentation.

Petrunic, B. M., Al, T. A., Weaver, L., & Hall, D., 2009, Identification and characterization of secondary minerals formed in tungsten mine tailings using transmission electron microscopy. Applied Geochemistry, 24(12), 2222-2233.

Plante B, Benzaazoua M, Bussière B, Biesinger M.C, Pratt AR., 2010, Study of Ni sorption onto Tio mine waste rock surfaces. Applied Geochemistry vol. 25 pp.1830–1844

Plante B, Benzaazoua M, Bussière B., 2011a, Kinetic testing and sorption studies by modified weathering cells to characterize the potential to generate contaminated neutral drainage. Mine Water Environment 30:22–37

Plante B, Benzaazoua M, Bussière B., 2011b, Predicting geochemical behaviour of waste rock with low acid generating potential using laboratory kinetic tests. Mine Water Environment 30:2–21

Plante B, Bussière B, Benzaazoua M., 2014, Lab to field scale effects on contaminated neutral drainage prediction from the Tio mine waste rocks. Journal of Geochemical Exploration 137:37–47

Plante, B., Benzaazoua, M., Bussière, B., Chopard, A., Bouzahzah, H.,, 2015, Use of EDTA in modified kinetic testing for contaminated drainage prediction from waste rocks: case of the Lac Tio mine. Environmental Science and Pollution Research, 22(10), 7882-7896.

Plumlee, G.S., Smith, K.S., Montour, M.R., Ficklin, W.S., Mosier, E., 1999, Geologic controls on the composition of natural waters and mine waters diverse mineral deposit types. *In*: Plumlee, G.S., Logsdon, M.J. (Eds.), Environmental Geochemistry of Mineral Deposits: Case Studies and Research Topics, Reviews in Economic Geology. vol. 6B, pp. 373–432

Price, W.A., 2009, Prediction Manual for Drainage Chemistry from Sulphidic Geologic Materials: Mine Environment Neutral Drainage (MEND) Report 1.20.1, 579 p.

Pugh, C.E., Hossner, L.R., Dixon, J.B., 1984, Oxidation rate of iron sulfides as affected by surface area, morphology, oxygen concentration, and autotrophic bacteria. Soil. Sci. 137, 309–314.

Queffurus, M. and Barnes, S., 2014, Selenium and sulfur concentrations in country rocks from the Duluth Complex, Minnesota, USA: Implications for the formation of the Cu-Ni-PGE sulfides. Economic Geology, v. 109, pp. 785–794

Ressler, T., 1998, WinXAS: A program for x-ray absorption spectroscopy data analysis under MS-Windows. Journal of Synchrotron Radiation v5, 118-122.

Rinker, M. J., Nicholson, R. V., Venhuis, M. A., Swarbrick, B., 2003, Implications of Non-Acid Metal Leaching on Mine Rock Management at a Nickel Mine in Permafrost Terrain: 1–Mine Rock Evaluation. In Sudbury 2003 Mining and the Environment Conference (Vol. 1).

Ripley, E.M., and Alawi, J.A., 1986, Sulfide mineralogy and chemical evolution of the Babbitt Cu–Ni deposit, Duluth Complex, Minnesota: Canadian Mineralogist, vol. 24, pp. 347–368.

Ripley, E. M., Butler, B. K., Taib, N. I., Lee, I., 1993, Hydrothermal alteration in the Babbitt Cu-Ni deposit, Duluth Complex; mineralogy and hydrogen isotope systematics. Economic Geology, 88(3), 679-696.

Ripley, E.M., Taib, N.I., Li, C., Moore, C.H., 2007, Chemical and mineralogical heterogeneity in the basal zone of the Partridge River Intrusion: Implications for the origin of Cu–Ni mineralization in the Duluth Complex, Midcontinent rift system: Contributions to Mineralogy and Petrology, v. 154, p. 35–54.

Robb L. J., 2005, Introduction to Ore-Forming Processes. Blackwell Publishing. 373 pp.

Schott, J., Pokrovsky, O. S., Oelkers, E. H., 2009, The link between mineral dissolution/precipitation kinetics and solution chemistry. Reviews in mineralogy and geochemistry, 70(1), 207-258.

Suárez, S., Nieto, F., Velasco, F., Martín, F. J., 2011, Serpentine and chlorite as effective Ni-Cu sinks during weathering of the Aguablanca sulphide deposit (SW Spain). TEM evidence for metal-retention mechanisms in sheet silicates. European Journal of Mineralogy, 23(2), 179-196.

Severson, M.J., 2014-2015, Personal communication.

Severson, M.J. and Hauck, S.A., 2008, Finish Logging of Duluth Complex Drill Core (And a Reinterpretation of the Geology at the Mesaba (Babbitt) Deposit), University of Minnesota Duluth¸ Natural Resources Research Institute, Technical Report NRRI/TR-2008/17, 68 p. + 94 plates.

Smith, L.J.D., Bailey, B.L., Blowes, D.W., Jambor, J.L., Smith, L., Sego, D.C., 2013, The Diavik waste rock project: Initial geochemical response from a low sulfide waste rock pile. Applied Geochemistry vol.36. pp. 210-221.

Steiner, Alex, 2014, Genesis of sulfide mineralization within the footwall granite of the Maturi Cu-Ni-PGE deposit of the South Kawishiwi intrusion, Duluth Complex, Minnesota. Unpublished M.S Thesis. University of Minnesota- Duluth. 211 p.

SRK Consulting Engineers and Scientists, 2007, RS53/RS42 - Waste Rock Characteristics and Waste Water Quality Modeling - Waste Rock and Lean Ore. NorthMet Project - DRAFT.

Teck American, 2010, Mesaba Cu-Ni Project. Field trip: Ni-Cu-(PGE) mineralization in mafic intrusions of the Lake Superior region. 11th International Platinum Symposium. Laurentian University, Sudbury, Canada. Power point presentation.

Thompson A. C. and Vaughan D. (Eds). X-ray Data Booklet. LBNL Pub 490 Rev 2.

Valente, T. M. and Gomes, C. L., 2009, Occurrence, properties and pollution potential of environmental minerals in acid mine drainage. Science of the total environment, 407(3), 1135-1152.

Webb S.M., 2011, The microanalysis toolkit: X-ray fluorescence image processing software. AIP Conference Proceedings, 1365, pp196-199.

Webb S.M., 2005, Sixpack: a graphical user interfaces for XAS analysis using IFEFFIT. Physica Scripta T115, pp 1011-1014.

# 7 Appendix A to F

Appendix A
Bulk chemistry by aqua regia digest and sulfur speciation/ABA

| **Sample ID** | **Ag** | **Al** | **B** | **Ba** | **Ca** | **Cr** | **Cu** | **Fe** | **K** | **Li** | **Mg** |
|---|---|---|---|---|---|---|---|---|---|---|---|
| | **ppm** | **%** | **ppm** | **ppm** | **%** | **ppm** | **ppm** | **%** | **%** | **ppm** | **%** |
| Method Code | ICM14B | ICM14B | ICM14B | ICM14B | ICM14B | ICM14B | ICM14B | ICM14B | ICM14B | ICM14B | ICM14B |
| LOD | 0.01 | 0.01 | 10 | 5 | 0.01 | 1 | 0.5 | 0.01 | 0.01 | 1 | 0.01 |
| M-SM 001 A | 1.6 | 2.62 | <10 | 93 | 1.24 | 108 | 2310 | 5.89 | 0.28 | 8 | 1.67 |
| M-SM 001 B | 1.28 | 2.66 | <10 | 93 | 1.27 | 96 | 2230 | 5.89 | 0.29 | 9 | 1.83 |
| M-SM 001 C | 1.07 | 2.73 | <10 | 96 | 1.31 | 103 | 2390 | 6.09 | 0.28 | 8 | 1.87 |
| M-SM 002 A | 0.72 | 2.16 | <10 | 84 | 1.2 | 109 | 1670 | 7.03 | 0.25 | 8 | 2.73 |
| M-SM 002 B | 0.41 | 2.19 | <10 | 85 | 1.2 | 118 | 1750 | 7.03 | 0.27 | 9 | 2.77 |
| M-SM 002 C | 0.78 | 2.18 | <10 | 87 | 1.19 | 122 | 1970 | 7.17 | 0.27 | 9 | 2.83 |
| M-SM 004a | 1.61 | 2.54 | <10 | 101 | 1.16 | 186 | 4830 | 7.27 | 0.26 | 13 | 2.13 |
| M-SM 004b A | 2.65 | 2.13 | <10 | 97 | 1.08 | 135 | 5470 | 7.99 | 0.27 | 9 | 2.76 |
| M-SM 004b B | 2.31 | 2.27 | <10 | 96 | 1.09 | 130 | 5140 | 8.06 | 0.27 | 10 | 2.73 |
| M-SM 004b C | 2.29 | 2.23 | <10 | 98 | 1.08 | 131 | 5310 | 8.06 | 0.27 | 10 | 2.72 |
| M-SM 005 A | 1.71 | 1.94 | <10 | 81 | 1.13 | 163 | 4530 | 7.56 | 0.23 | 7 | 2.85 |
| M-SM 005 B | 1.98 | 1.97 | <10 | 81 | 1.14 | 167 | 4970 | 7.34 | 0.24 | 7 | 2.73 |
| M-SM 005 C | 2 | 1.8 | <10 | 79 | 1.05 | 146 | 4890 | 7.21 | 0.22 | 6 | 2.58 |
| M-SM 006b A | 1.17 | 1.7 | <10 | 78 | 0.91 | 117 | 3260 | 8.77 | 0.22 | 9 | 3.01 |
| M-SM 006b B | 1.26 | 1.82 | <10 | 78 | 0.95 | 117 | 3290 | 8.94 | 0.22 | 10 | 3.08 |
| M-SM 006b C | 1.07 | 1.77 | <10 | 75 | 0.96 | 159 | 3040 | 8.22 | 0.22 | 9 | 3.3 |
| **Duplicate** | | | | | | | | | | | |
| M-SM 006b B | 1.29 | 1.87 | <10 | 81 | 0.99 | 117 | 3300 | 8.98 | 0.22 | 10 | 3.13 |
| **QC** | | | | | | | | | | | |
| CH4 | 1.86 | 1.73 | 20 | 291 | 0.56 | 109 | 2020 | 4.39 | 1.34 | 13 | 1.14 |
| Certified Values | 2.13 | 1.85 | #N/A | 293 | 0.61 | 103.8 | 2000 | 4.79 | 1.43 | 12.6 | 1.18 |
| Tolerance (%) | 10.9 | 11.35 | #N/A | 14.3 | 14.1 | 12.4 | 10.1 | 10.52 | 11.74 | 29.84 | 12.3 |

| Sample ID | Mn ppm | Na % | Ni ppm | P ppm | S % | Sr ppm | Ti % | V ppm | Zn ppm | Zr ppm | As ppm |
|---|---|---|---|---|---|---|---|---|---|---|---|
| Method Code | ICM14B | ICM14B | ICM14B | ICM14B | ICM14B | ICM14B | ICM14B | ICM14B | ICM14B | ICM14B | ICM14B |
| LOD | 2 | 0.01 | 0.5 | 50 | 0.01 | 0.5 | 0.01 | 1 | 1 | 0.5 | 1 |
| M-SM 001 A | 412 | 0.36 | 361 | 1020 | 0.08 | 57.6 | 0.17 | 47 | 56 | 5.5 | 5 |
| M-SM 001 B | 449 | 0.37 | 363 | 980 | 0.08 | 59.4 | 0.17 | 46 | 60 | 5.2 | 3 |
| M-SM 001 C | 450 | 0.38 | 404 | 1010 | 0.09 | 61 | 0.17 | 48 | 61 | 5.4 | 3 |
| M-SM 002 A | 620 | 0.34 | 292 | 1070 | 0.15 | 48.7 | 0.18 | 55 | 72 | 5 | 4 |
| M-SM 002 B | 632 | 0.34 | 290 | 1120 | 0.16 | 49.3 | 0.18 | 57 | 71 | 4.8 | 4 |
| M-SM 002 C | 641 | 0.35 | 301 | 1090 | 0.2 | 48.7 | 0.18 | 55 | 74 | 5 | 5 |
| M-SM 004a | 815 | 0.32 | 870 | 970 | 0.55 | 50.1 | 0.16 | 56 | 72 | 6.1 | 5 |
| M-SM 004b A | 683 | 0.29 | 663 | 930 | 0.79 | 45.4 | 0.17 | 53 | 87 | 5.4 | 5 |
| M-SM 004b B | 708 | 0.3 | 708 | 950 | 0.71 | 46.5 | 0.17 | 56 | 87 | 5.7 | 5 |
| M-SM 004b C | 715 | 0.29 | 700 | 1020 | 0.73 | 45.6 | 0.17 | 55 | 85 | 5.6 | 5 |
| M-SM 005 A | 693 | 0.32 | 529 | 830 | 0.81 | 48.4 | 0.2 | 77 | 88 | 5.7 | 3 |
| M-SM 005 B | 655 | 0.31 | 533 | 890 | 0.87 | 48.9 | 0.2 | 79 | 81 | 5.5 | 3 |
| M-SM 005 C | 624 | 0.3 | 770 | 860 | 0.97 | 44.8 | 0.18 | 70 | 80 | 5.1 | 4 |
| M-SM 006b A | 634 | 0.22 | 472 | 1190 | 0.58 | 36.4 | 0.15 | 59 | 74 | 6.2 | 5 |
| M-SM 006b B | 670 | 0.23 | 439 | 1110 | 0.58 | 39.7 | 0.15 | 60 | 73 | 5.8 | 5 |
| M-SM 006b C | 707 | 0.22 | 425 | 980 | 0.56 | 40.1 | 0.14 | 56 | 78 | 5.6 | 4 |
| **Duplicate** | | | | | | | | | | | |
| M-SM 006b B | 678 | 0.24 | 453 | 1050 | 0.56 | 41 | 0.15 | 61 | 72 | 6.1 | 5 |
| **QC** | | | | | | | | | | | |
| CH4 | 324 | 0.05 | 48.6 | 630 | 0.7 | 8.6 | 0.2 | 78 | 201 | 11.4 | 8 |
| Certified Values | 324 | 0.06 | 49.57 | 719 | 0.73 | 9.38 | 0.21 | 79.27 | 189.4 | 9 | 8.14 |
| Tolerance (%) | 11.5 | 50.3 | 12.52 | 27.4 | 13.4 | 23.3 | 23.3 | 13.2 | 11.3 | 17.7 | 13.1 |

| Sample ID | Be ppm | Bi ppm | Cd ppm | Ce ppm | Co ppm | Cs ppm | Ga ppm | Ge ppm | Hf ppm | Hg ppm | In ppm |
|---|---|---|---|---|---|---|---|---|---|---|---|
| Method Code | ICM14B | ICM14B | ICM14B | ICM14B | ICM14B | ICM14B | ICM14B | ICM14B | ICM14B | ICM14B | ICM14B |
| LOD | 0.1 | 0.02 | 0.01 | 0.05 | 0.1 | 0.05 | 0.1 | 0.1 | 0.05 | 0.01 | 0.02 |
| M-SM 001 A | 0.2 | 0.31 | 0.12 | 23 | 36.9 | 0.96 | 6.4 | 0.1 | 0.1 | 0.01 | 0.08 |
| M-SM 001 B | 0.2 | 0.37 | 0.13 | 22.3 | 38.9 | 0.95 | 6.3 | 0.1 | 0.09 | <0.01 | 0.06 |
| M-SM 001 C | 0.2 | 0.43 | 0.13 | 22.2 | 41.1 | 0.93 | 6.3 | 0.1 | 0.1 | <0.01 | 0.07 |
| M-SM 002 A | 0.2 | 0.66 | 0.18 | 26 | 44 | 0.85 | 5.4 | 0.1 | 0.09 | <0.01 | 0.06 |
| M-SM 002 B | 0.2 | 0.51 | 0.2 | 25.3 | 44.5 | 0.86 | 5.6 | 0.2 | 0.08 | <0.01 | 0.06 |
| M-SM 002 C | 0.2 | 0.88 | 0.23 | 25.9 | 46.8 | 0.89 | 5.6 | 0.2 | 0.1 | <0.01 | 0.07 |
| M-SM 004a | 0.3 | 0.51 | 0.61 | 25.1 | 82.8 | 1.22 | 6.6 | 0.2 | 0.1 | 0.01 | 0.06 |
| M-SM 004b A | 0.2 | 0.55 | 0.6 | 22.1 | 64.9 | 0.98 | 5.6 | 0.2 | 0.09 | <0.01 | 0.09 |
| M-SM 004b B | 0.2 | 0.65 | 0.55 | 22.4 | 66.2 | 1.03 | 5.7 | 0.2 | 0.09 | <0.01 | 0.08 |
| M-SM 004b C | 0.2 | 0.56 | 0.54 | 23.8 | 65.9 | 1.07 | 5.7 | 0.2 | 0.11 | <0.01 | 0.08 |
| M-SM 005 A | 0.1 | 0.46 | 0.54 | 19.4 | 58.8 | 0.7 | 5 | 0.2 | 0.1 | <0.01 | 0.07 |
| M-SM 005 B | 0.1 | 0.47 | 0.57 | 19.4 | 56.4 | 0.72 | 5 | 0.1 | 0.1 | <0.01 | 0.07 |
| M-SM 005 C | 0.2 | 0.52 | 0.6 | 19.9 | 66.1 | 0.71 | 4.9 | 0.2 | 0.1 | <0.01 | 0.07 |
| M-SM 006b A | 0.2 | 0.31 | 0.29 | 22.4 | 57.2 | 1.31 | 5.3 | 0.2 | 0.12 | <0.01 | 0.06 |
| M-SM 006b B | 0.2 | 0.43 | 0.3 | 21.4 | 56.6 | 1.32 | 5.6 | 0.2 | 0.11 | <0.01 | 0.06 |
| M-SM 006b C | 0.1 | 0.32 | 0.3 | 20.6 | 58.8 | 1.25 | 5.3 | 0.2 | 0.16 | 0.04 | 0.06 |
| **Duplicate** | | | | | | | | | | | |
| M-SM 006b B | 0.2 | 0.34 | 0.3 | 21.1 | 56.7 | 1.23 | 5.6 | 0.2 | 0.12 | <0.01 | 0.06 |
| **QC** | | | | | | | | | | | |
| CH4 | <0.1 | 0.42 | 1.08 | 28 | 24.1 | 2.64 | 9.3 | 0.3 | 0.25 | 0.03 | 0.11 |
| Certified Values | 0.11 | 0.51 | 1.17 | 28.18 | 22.8 | 2.6 | 8.72 | 0.21 | 0.29 | #N/A | 0.1 |
| Tolerance (%) | 241.3 | 19.7 | 12.1 | 10.4 | 11.1 | 14.8 | 12.9 | 127.4 | 52.8 | #N/A | 62.1 |

| Sample ID | La ppm | Lu ppm | Mo ppm | Nb ppm | Pb ppm | Rb ppm | Sb ppm | Sc ppm | Se ppm | Sn ppm | Ta ppm |
|---|---|---|---|---|---|---|---|---|---|---|---|
| Method Code | ICM14B | ICM14B | ICM14B | ICM14B | ICM14B | ICM14B | ICM14B | ICM14B | ICM14B | ICM14B | ICM14B |
| LOD | 0.1 | 0.01 | 0.05 | 0.05 | 0.2 | 0.2 | 0.05 | 0.1 | 1 | 0.3 | 0.05 |
| M-SM 001 A | 10.3 | 0.11 | 2.8 | 0.75 | 6.6 | 15.1 | 0.11 | 2.6 | 2 | 0.9 | <0.05 |
| M-SM 001 B | 9.8 | 0.11 | 2.48 | 0.69 | 5.5 | 15 | 0.1 | 2.5 | 1 | 0.8 | <0.05 |
| M-SM 001 C | 9.9 | 0.1 | 2.68 | 0.71 | 5.7 | 14.8 | 0.1 | 2.6 | 1 | 0.8 | <0.05 |
| M-SM 002 A | 11.8 | 0.12 | 2.77 | 0.59 | 6 | 13.2 | 0.12 | 2.7 | <1 | 0.8 | <0.05 |
| M-SM 002 B | 11.6 | 0.12 | 2.89 | 0.6 | 5.4 | 13.9 | 0.11 | 2.8 | <1 | 0.7 | <0.05 |
| M-SM 002 C | 12.2 | 0.13 | 3.15 | 0.65 | 6.8 | 14 | 0.15 | 2.9 | 1 | 0.8 | <0.05 |
| M-SM 004a | 11.3 | 0.1 | 4.3 | 0.9 | 6.4 | 16.5 | 0.13 | 3.2 | 2 | 1.1 | <0.05 |
| M-SM 004b A | 9.8 | 0.12 | 2.58 | 0.43 | 8 | 14.7 | 0.13 | 2.9 | 2 | 1 | <0.05 |
| M-SM 004b B | 10.1 | 0.12 | 2.53 | 0.41 | 8 | 14.2 | 0.13 | 2.9 | 2 | 1 | <0.05 |
| M-SM 004b C | 10.8 | 0.12 | 2.59 | 0.45 | 8.5 | 14.6 | 0.13 | 2.9 | 2 | 1 | <0.05 |
| M-SM 005 A | 8.4 | 0.12 | 2.88 | 0.52 | 6.5 | 12 | 0.09 | 2.7 | 2 | 0.7 | <0.05 |
| M-SM 005 B | 8.3 | 0.12 | 3.06 | 0.5 | 7 | 12.5 | 0.08 | 2.6 | 2 | 0.8 | <0.05 |
| M-SM 005 C | 8.6 | 0.12 | 2.69 | 0.5 | 7.3 | 11.4 | 0.09 | 2.6 | 2 | 0.8 | <0.05 |
| M-SM 006b A | 10.2 | 0.13 | 3.12 | 0.76 | 5.8 | 14.1 | 0.1 | 3.3 | 2 | 0.8 | <0.05 |
| M-SM 006b B | 9.6 | 0.12 | 3.04 | 0.74 | 5.6 | 14 | 0.13 | 3.3 | 2 | 0.8 | <0.05 |
| M-SM 006b C | 9.1 | 0.15 | 3.71 | 0.93 | 4.8 | 12.7 | 0.12 | 3.4 | 2 | 0.7 | 0.08 |
| **Duplicate** | | | | | | | | | | | |
| M-SM 006b B | 9.5 | 0.13 | 2.91 | 0.73 | 5.7 | 13.8 | 0.12 | 3.3 | 2 | 0.8 | <0.05 |
| **QC** | | | | | | | | | | | |
| CH4 | 14.6 | 0.06 | 2.94 | 0.57 | 8.9 | 60.9 | 0.31 | 8.1 | 2 | 0.6 | <0.05 |
| Certified Values | 14 | #N/A | 3.05 | 0.19 | 8.24 | 67 | 0.34 | 7.99 | 1.57 | 0.6 | 0.3 |
| Tolerance (%) | 11.8 | #N/A | 14.1 | 75 | 16.1 | 10.7 | 47.3 | 13.1 | 169.6 | 134.5 | 51.7 |

| Sample ID | Ta ppm | Tb ppm | Te ppm | Th ppm | Tl ppm | U ppm | W ppm | Y ppm | Yb ppm |
|---|---|---|---|---|---|---|---|---|---|
| Method Code | ICM14B | ICM14B | ICM14B | ICM14B | ICM14B | ICM14B | ICM14B | ICM14B | ICM14B |
| LOD | 0.05 | 0.02 | 0.05 | 0.1 | 0.02 | 0.05 | 0.1 | 0.05 | 0.1 |
| M-SM 001 A | <0.05 | 0.39 | 0.11 | 2.2 | 0.15 | 0.61 | <0.1 | 9.75 | 0.7 |
| M-SM 001 B | <0.05 | 0.37 | 0.08 | 2 | 0.14 | 0.52 | <0.1 | 9.38 | 0.7 |
| M-SM 001 C | <0.05 | 0.38 | 0.09 | 1.9 | 0.14 | 0.55 | <0.1 | 9.55 | 0.7 |
| M-SM 002 A | <0.05 | 0.41 | 0.07 | 1.9 | 0.11 | 0.44 | <0.1 | 10.2 | 0.7 |
| M-SM 002 B | <0.05 | 0.4 | 0.06 | 1.8 | 0.1 | 0.41 | <0.1 | 10.6 | 0.7 |
| M-SM 002 C | <0.05 | 0.43 | 0.13 | 1.9 | 0.12 | 0.44 | <0.1 | 10.7 | 0.8 |
| M-SM 004a | <0.05 | 0.39 | 0.13 | 2.1 | 0.18 | 0.65 | <0.1 | 9.3 | 0.7 |
| M-SM 004b A | <0.05 | 0.37 | 0.16 | 1.7 | 0.18 | 0.47 | <0.1 | 9.3 | 0.7 |
| M-SM 004b B | <0.05 | 0.37 | 0.13 | 1.7 | 0.17 | 0.48 | <0.1 | 9.41 | 0.7 |
| M-SM 004b C | <0.05 | 0.39 | 0.12 | 1.7 | 0.19 | 0.48 | <0.1 | 9.54 | 0.8 |
| M-SM 005 A | <0.05 | 0.35 | 0.1 | 1.4 | 0.13 | 0.41 | <0.1 | 9.11 | 0.7 |
| M-SM 005 B | <0.05 | 0.35 | 0.09 | 1.5 | 0.13 | 0.43 | <0.1 | 8.84 | 0.7 |
| M-SM 005 C | <0.05 | 0.36 | 0.1 | 1.4 | 0.13 | 0.39 | <0.1 | 9.12 | 0.7 |
| M-SM 006b A | <0.05 | 0.42 | 0.08 | 1.8 | 0.21 | 0.91 | <0.1 | 10.3 | 0.8 |
| M-SM 006b B | <0.05 | 0.38 | 0.07 | 1.8 | 0.21 | 0.86 | <0.1 | 9.88 | 0.8 |
| M-SM 006b C | 0.08 | 0.41 | 0.08 | 1.6 | 0.2 | 0.83 | 0.1 | 9.57 | 0.8 |
| **Duplicate** | | | | | | | | | |
| M-SM 006b B | <0.05 | 0.38 | 0.09 | 1.8 | 0.21 | 0.82 | <0.1 | 9.51 | 0.8 |
| **QC** | | | | | | | | | |
| CH4 | <0.05 | 0.29 | 0.4 | 2 | 0.39 | 0.27 | 2.3 | 5.94 | 0.4 |
| Certified Values | 0.3 | 0.27 | 0.42 | 2.2 | 0.4 | 0.29 | 2.15 | 5.66 | #N/A |
| Tolerance (%) | 51.7 | 28.4 | 39.6 | 21.2 | 22.6 | 52.9 | 21.6 | 12.2 | #N/A |

**CLIENT** : **SRK Consulting**
**PROJECT** : **Mesaba**
**SRK Project #** : **1UT016.002**
**SGS Project #** : **1278**
**Test** : **Modified Acid-Base Accounting**
**Date** : **November 25, 2013**

| Sample ID | Rinse pH SU | Rinse EC µS/cm | Paste pH SU | Paste EC µS/cm | TIC % | CaCO3 NP | C(T) % | S(T) % | S(SO4) % | S(SO4) % | NP | Fizz Test |
|---|---|---|---|---|---|---|---|---|---|---|---|---|
| Method Code | Sobek | Sobek | Sobek | Sobek | CSB02V | Calc. | CSA06V | CSA06V | HCl Leach | Na2CO3 Leach | Modified | Sobek |
| LOD | 0.20 | 1 | 0.20 | 1 | 0.01 | #N/A | 0.01 | 0.01 | 0.01 | 0.01 | 0.5 | #N/A |
| M-SM 001 A | 4.85 | 112.6 | 5.75 | 253 | <0.01 | <0.8 | 0.11 | 0.09 | 0.03 | 0.04 | 5.6 | None |
| M-SM 001 B | 4.86 | 71.5 | 5.88 | 267 | <0.01 | <0.8 | 0.11 | 0.09 | 0.03 | 0.04 | 6.3 | None |
| M-SM 001 C | 4.87 | 87.6 | 5.82 | 308 | <0.01 | <0.8 | 0.11 | 0.1 | 0.03 | 0.04 | 4.2 | None |
| M-SM 002 A | 4.86 | 84.1 | 5.72 | 355 | <0.01 | <0.8 | 0.08 | 0.15 | 0.03 | 0.04 | 9.7 | None |
| M-SM 002 B | 4.82 | 87.3 | 5.75 | 350 | <0.01 | <0.8 | 0.08 | 0.17 | 0.03 | 0.04 | 12.0 | None |
| M-SM 002 C | 4.79 | 97.0 | 5.71 | 367 | <0.01 | <0.8 | 0.09 | 0.2 | 0.03 | 0.05 | 11.0 | None |
| M-SM 004a | 4.09 | 8222 | 4.61 | 4850 | <0.01 | <0.8 | 0.48 | 0.54 | 0.31 | 0.34 | 3.2 | None |
| M-SM 004b A | 4.43 | 315 | 5.18 | 648 | <0.01 | <0.8 | 0.06 | 0.8 | 0.09 | 0.1 | 8.3 | None |
| M-SM 004b B | 4.37 | 226 | 5.22 | 606 | <0.01 | <0.8 | 0.08 | 0.7 | 0.07 | 0.09 | 7.8 | None |
| M-SM 004b C | 4.33 | 223 | 5.13 | 623 | <0.01 | <0.8 | 0.09 | 0.73 | 0.09 | 0.1 | 7.6 | None |
| M-SM 005 A | 4.29 | 211 | 6.12 | 611 | <0.01 | <0.8 | 0.03 | 0.81 | 0.04 | 0.08 | 12.1 | None |
| M-SM 005 B | 4.33 | 213 | 5.97 | 667 | <0.01 | <0.8 | 0.03 | 0.91 | 0.05 | 0.1 | 11.4 | None |
| M-SM 005 C | 4.34 | 238 | 5.97 | 620 | <0.01 | <0.8 | 0.04 | 1.04 | 0.05 | 0.1 | 11.7 | None |
| M-SM 006b A | 3.93 | 250 | 4.93 | 634 | <0.01 | <0.8 | 0.16 | 0.59 | 0.14 | 0.17 | 12.5 | None |
| M-SM 006b B | 3.92 | 228 | 4.95 | 640 | <0.01 | <0.8 | 0.16 | 0.58 | 0.14 | 0.17 | 12.5 | None |
| M-SM 006b C | 3.90 | 203 | 5.38 | 762 | <0.01 | <0.8 | 0.11 | 0.57 | 0.09 | 0.13 | 12.1 | None |
| **Duplicates** | | | | | | | | | | | | |
| M-SM 001 A | 4.88 | 93.9 | 5.79 | 256 | | | | | | | 5.8 | None |
| M-SM 002 C | | | | | | | | | | 0.05 | | |
| M-SM 006b B | | | | | | | | | | 0.18 | | |
| M-SM 006b C | | | 5.26 | 786 | | | | | | | 12.6 | None |
| **QC** | | | | | | | | | | | | |
| GTS-2A | | | | | | | 1.98 | 0.34 | | | | |
| PD-1 | | | | | | | | | 4.19 | | | |
| RTS-3A | | | | | | | | | | 1.44 | | |
| SY-4 | | | | | 0.91 | | | | | | | |
| NBM-1 Reference | | | | | | | | | | | 38.4 | Slight |
| Expected Values | | | | | 0.95 | | 2.01 | 0.35 | 4.27 | 1.34 | 42.0 | Slight |
| Tolerance +/- | | | | | 0.06 | | 0.15 | 0.03 | 0.3 | 0.1 | 4.0 | |

**Note:**

NP = Neutralization potential in tonnes CaCO3 equivalent per 1000 tonnes of material.

Carbonate NP is calculated from CO2 originating from carbonate minerals and is expressed in kg CaCO3/tonne.

# Appendix B
# Powder X-Ray Diffraction Scans

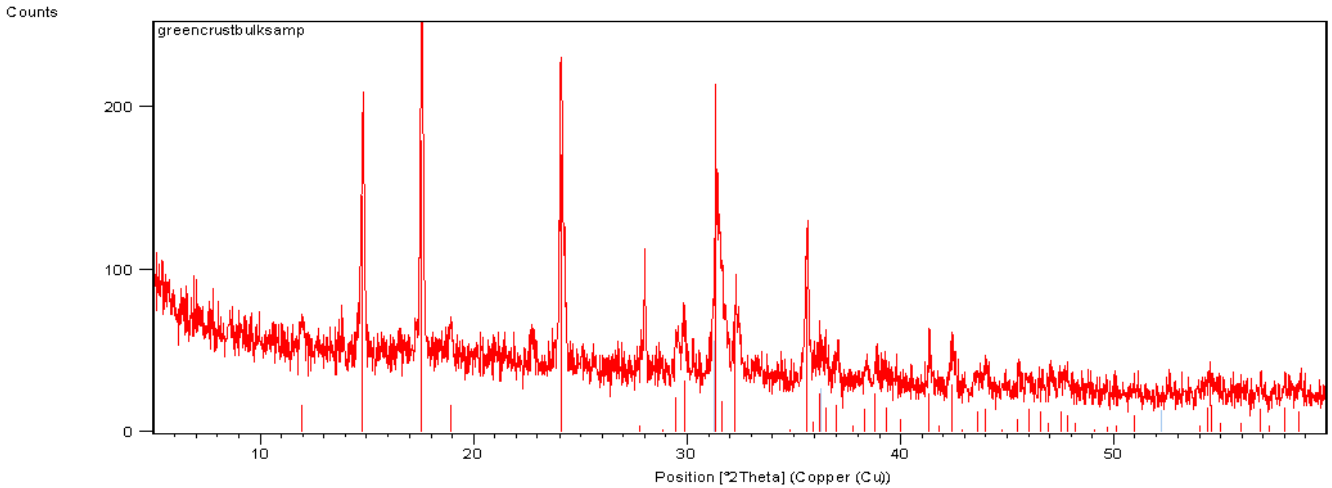
Counts
greencrustbulksamp
200
100
0
10
20
30
40
50
Position [°2Theta] (Copper (Cu))

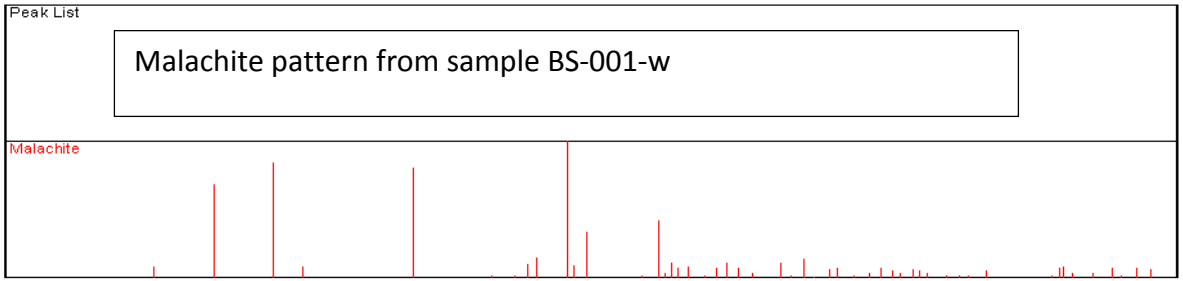
Peak List
Malachite pattern from sample BS-001-w
Malachite

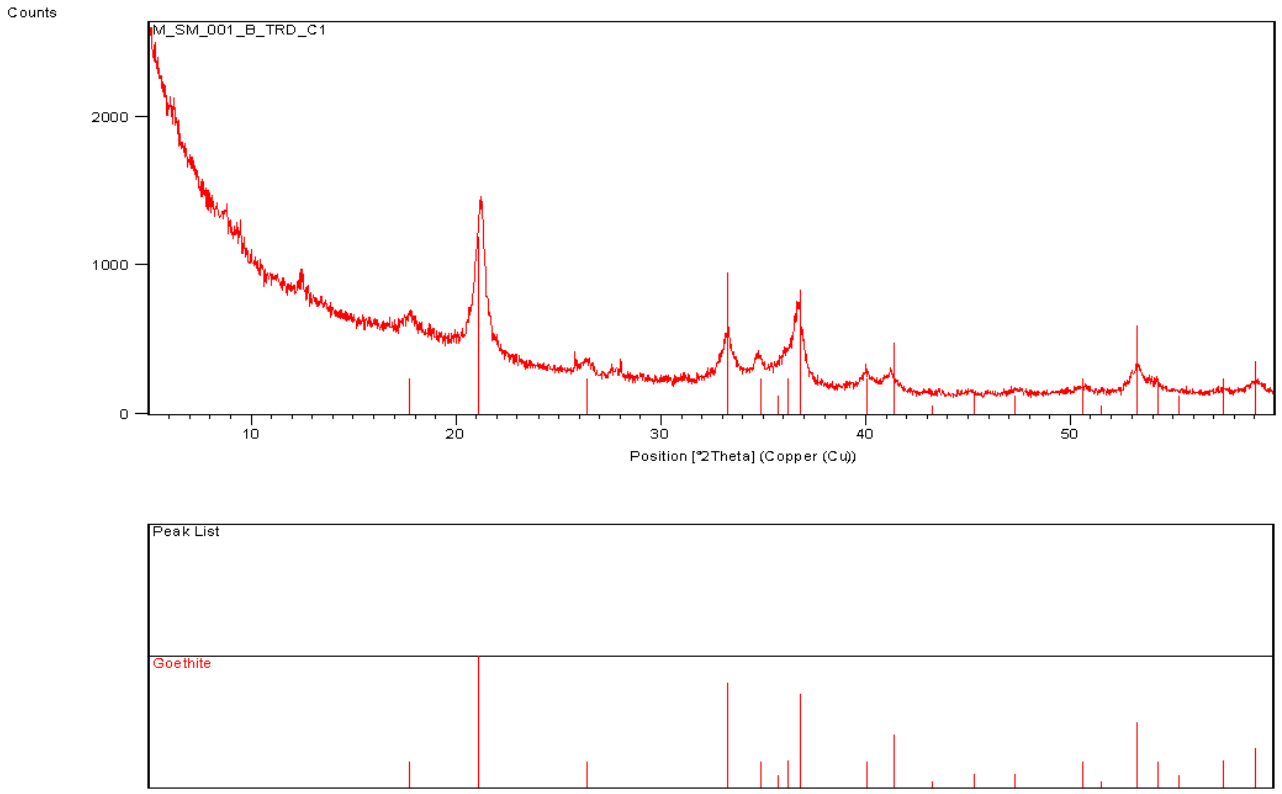
Counts
M_SM_001_B_TRD_C1
2000
1000
0
10
20
30
40
50
Position [°2Theta] (Copper (Cu))
Peak List
Goethite

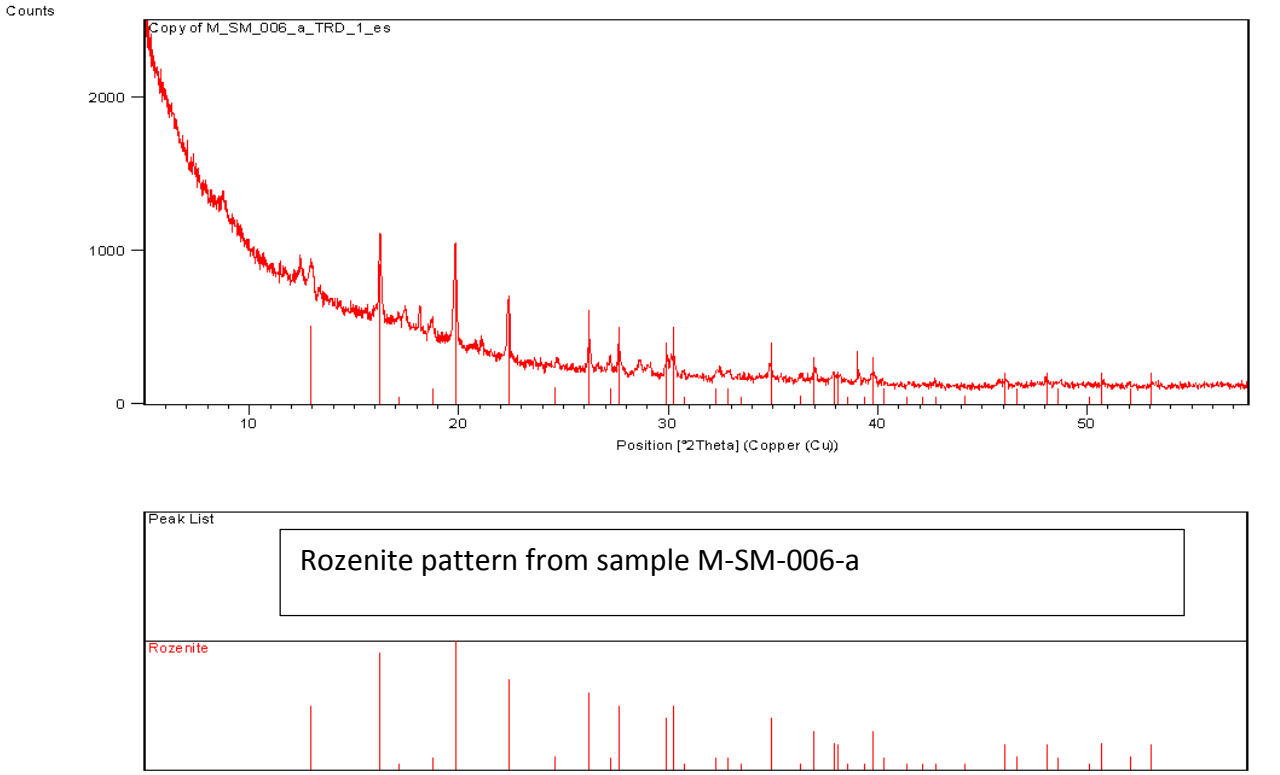
Counts
Copy of M_SM_006_a_TRD_1_es
2000
1000
0
10
20
30
40
50
Position [°2Theta] (Copper (Cu))
Peak List
Rozenite pattern from sample M-SM-006-a
Rozenite

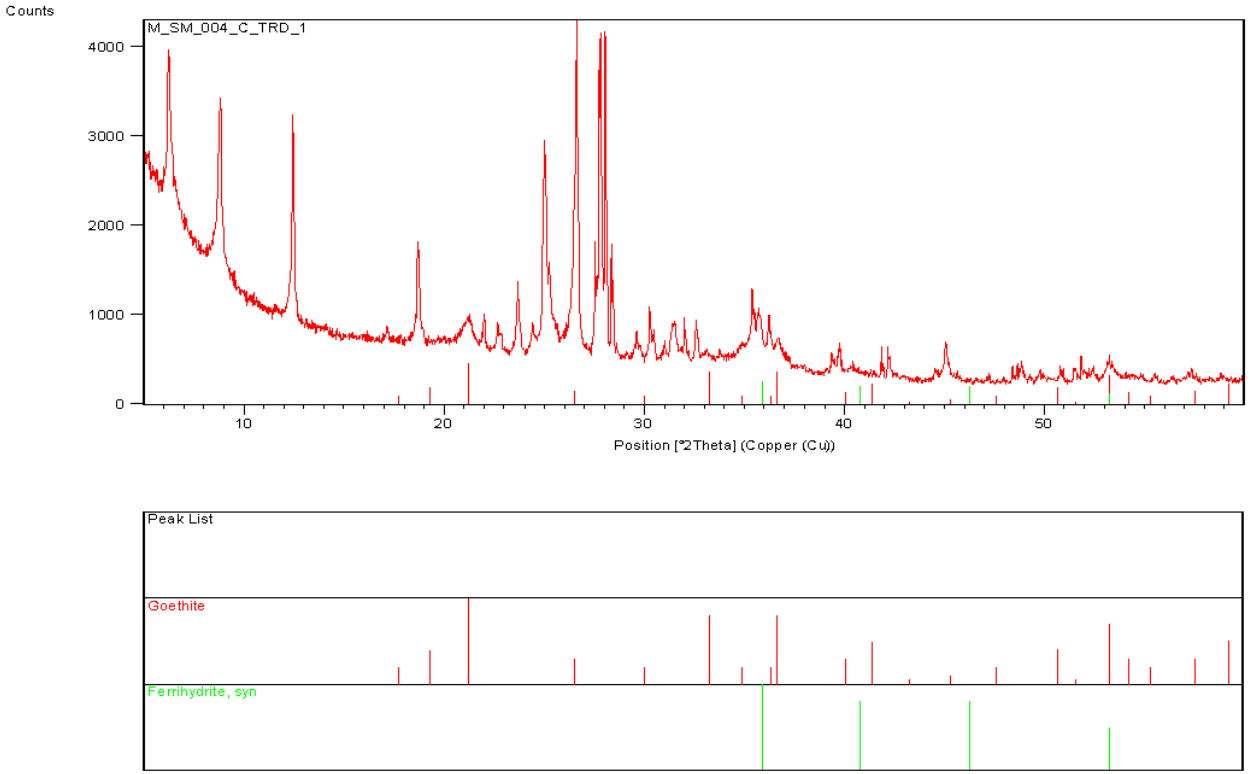
Counts
M_SM_004_C_TRD_1
4000
3000
2000
1000
0
10
20
30
40
50
Position [°2Theta] (Copper (Cu))
Peak List
Goethite
Ferrihydrite, syn

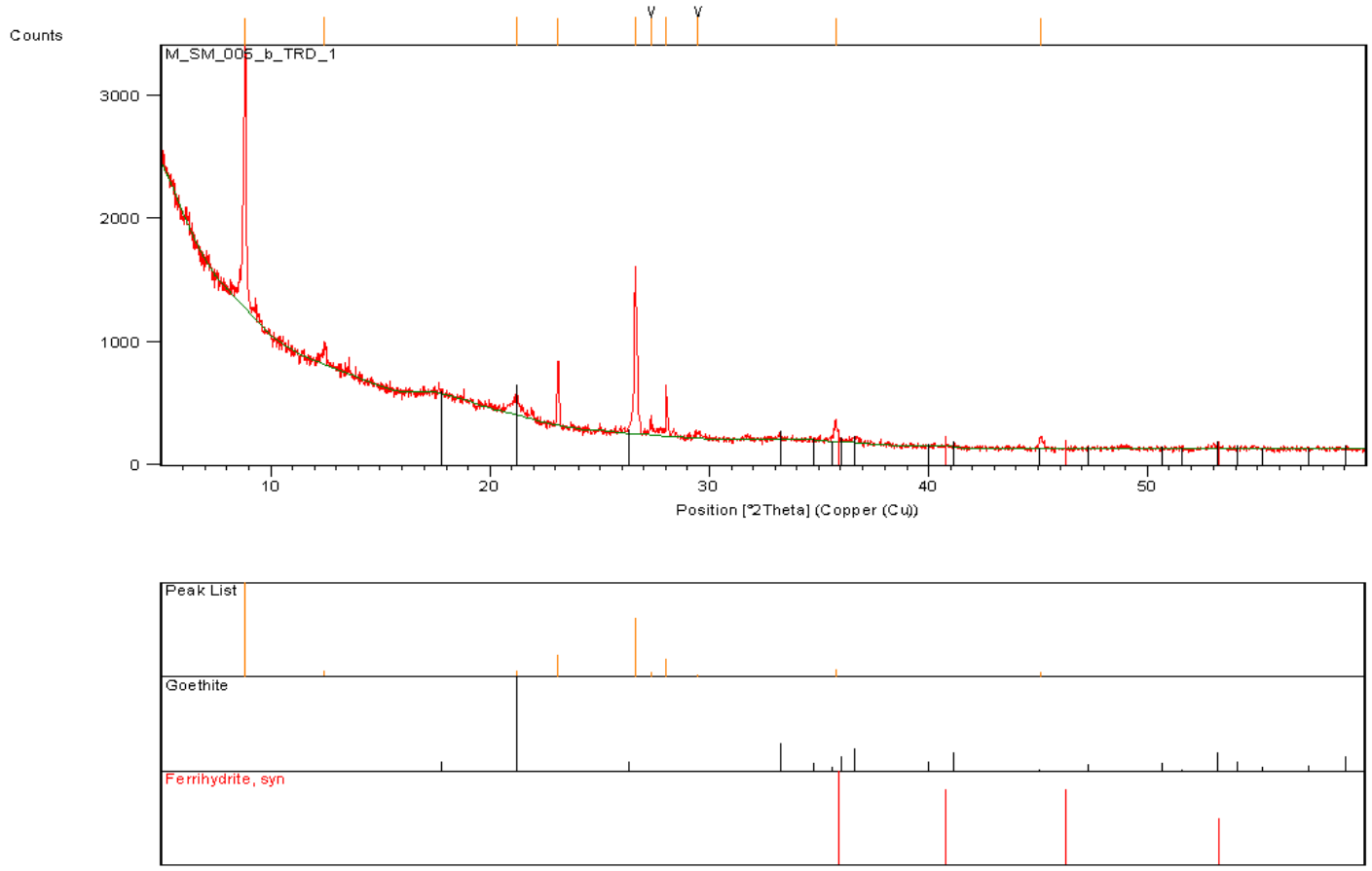
Counts
M_SM_005_b_TRD_1
3000
2000
1000
0
10
20
30
40
50
Position [°2Theta] (Copper (Cu))
Peak List
Goethite
Ferrihydrite, syn

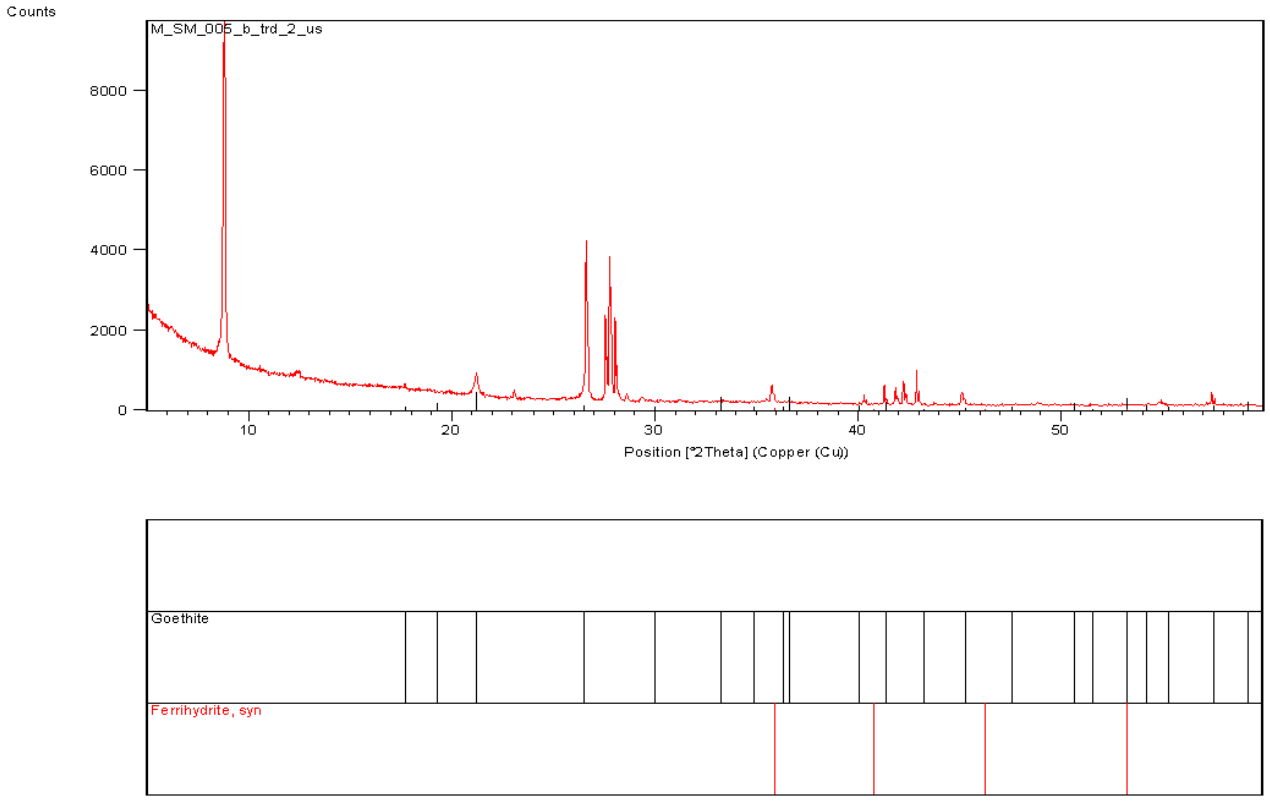
Counts
M_SM_005_b_trd_2_us
8000
6000
4000
2000
0
10
20
30
40
50
Position [°2Theta] (Copper (Cu))
Goethite
Ferrihydrite, syn

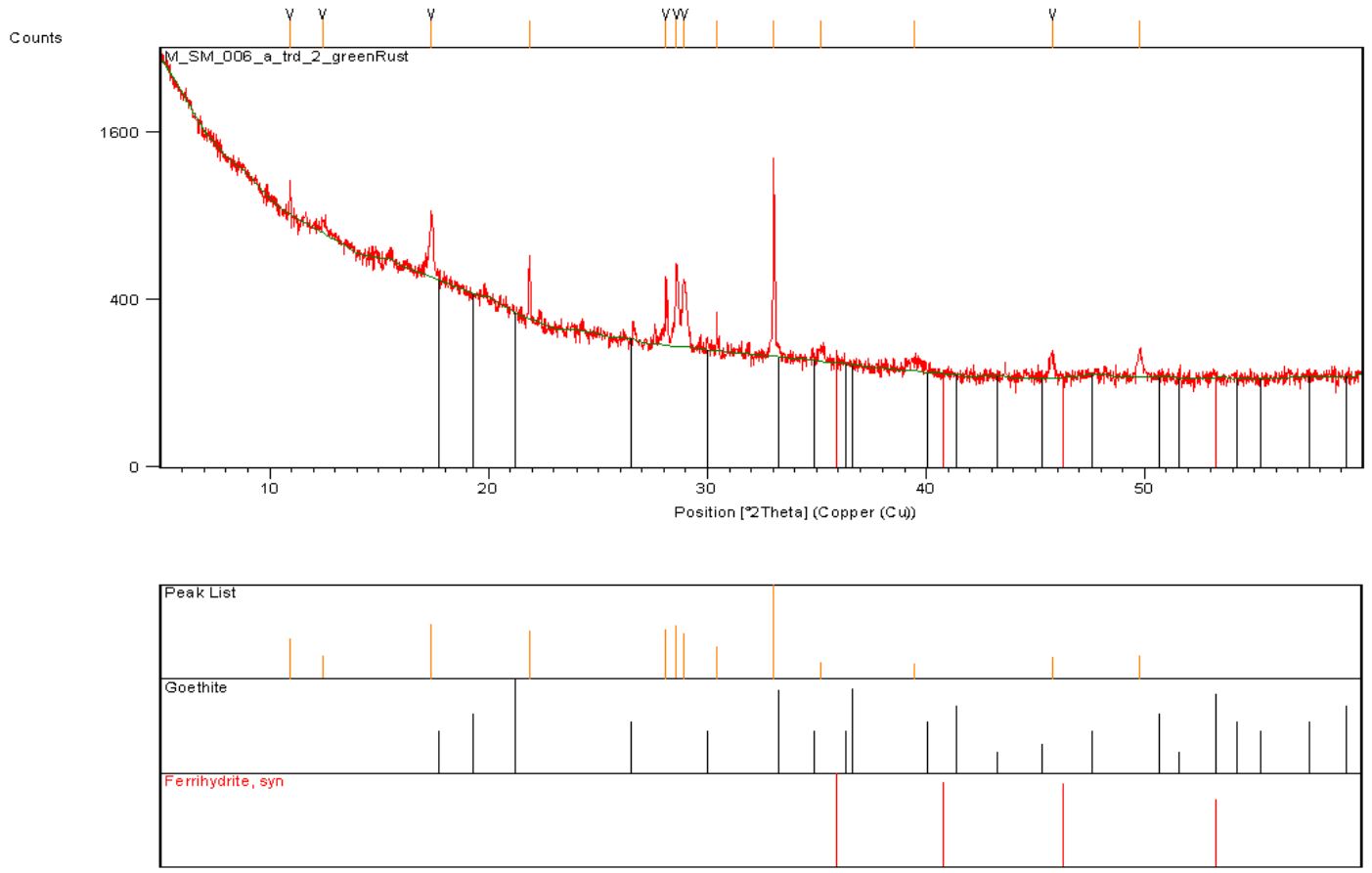
Counts
M_SM_006_a_trd_2_greenRust
1600
400
0
10
20
30
40
50
Position [°2Theta] (Copper (Cu))
Peak List
Goethite
Ferrihydrite, syn

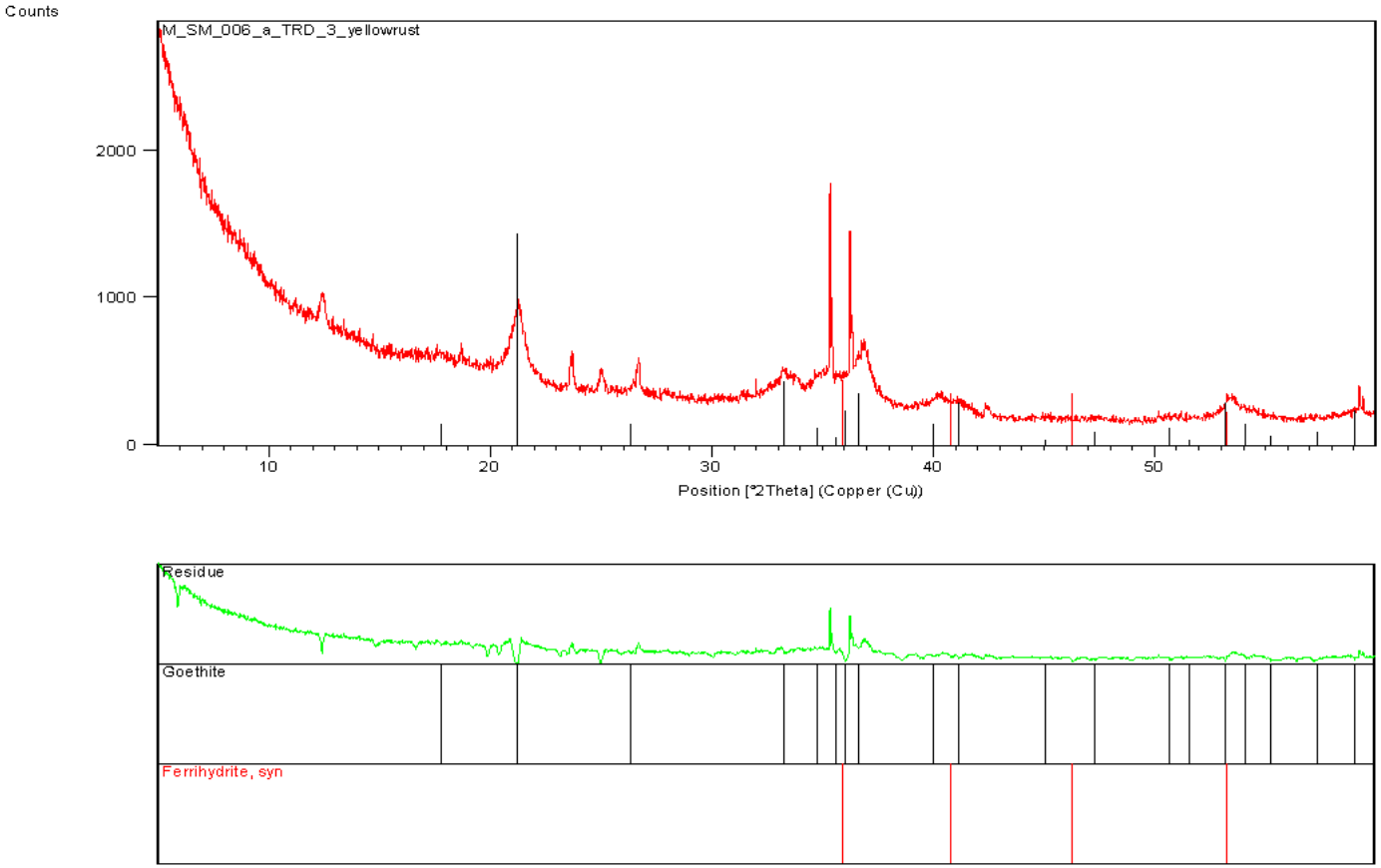
Counts
M_SM_006_a_TRD_3_yellowrust
2000
1000
0
10
20
30
40
50
Position [°2Theta] (Copper (Cu))
Residue
Goethite
Ferrihydrite, syn

Appendix B
Transmitted Light Petrography Notes

17mm

## IGNEOUS ROCK PETROGRAPHIC DESCRIPTION

Petrographer Paul Fix Date 5-2-2015

Sample ID m-SM-001-b Location UTM N- UTM E-

Geologic/Tectonic Setting Mesaba - Swamp Outcrop - Sept 2013

Hand Sample Description Outer surface contains lichen and black coatings suggesting long time exposure. Broken surfaces show extensive FeOx staining.

**TEXTURES** Sulfide replacement pits.

Crystallinity Ø

Grain Size (general) medium

Avg Plagioclase width- 1 mm

Bulk Rock Textures (relative grain shapes)

Poikilitic olivine
ophitic
Euhedral plagioclase

Oriented Textures Non-foliated
taxitic

Intergrowth Textures Ø

Overgrowth Textures Biotite on FeOx Some Symplectite

Exsolution Textures inv. Pigeonite

**Photomicrograph/Sketch**

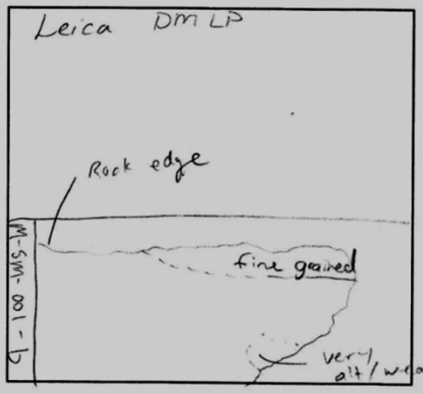


Banding Textures Ø

Cavity Textures Ø

**MINERALOGY**

| Phase | Plag | Cpx | Ol | Opx | Bt | FeOx |
|---|---|---|---|---|---|---|
| Mode | 60 | 15 | 10 | 10 | ~3 | ~3 |
| Habit | tabular | ophitic | Sub-poik | Sub-oph | int-anh | int-anh |

Alteration Ol → iddingsite near sample outer surface
Some Chlorite ~2%

Other Comments Seriate, esp plag. Abundant cracks w/ secondary FeOx fill. Plag → Clay near outer edge?

Summary Rock Name Medium grained, non-foliated, ophitic/sub-poikilitic olivine gabbronorite with minor oxide and biotite.

Cumulate Code m ~~i~~ifb

*Developed by J. Miller, May, 2013*

## IGNEOUS ROCK PETROGRAPHIC DESCRIPTION

Petrographer Paul Fix Date 5-2-2015

Sample ID m-sm-001-b-sum Location UTM N- UTM E-

Geologic/Tectonic Setting Mesaba - Swamp outcrop - Sept. 2013

Hand Sample Description lichen covered, extensive surface weathering, sulfide replacement pits and well developed FeOx coatings.

**TEXTURES**

Crystallinity ∅

Grain Size (general) medium

Avg Plagioclase width- 1 mm

Bulk Rock Textures (relative grain shapes)

sub-poik Ol

ophitic Augite / inv. pig

tabular eu. pl.

Oriented Textures non-foliated

Intergrowth Textures ∅

Overgrowth Textures Bt. on FeOx

Opx on Olivine

Exsolution Textures FeOx on Pl

**Photomicrograph/Sketch**

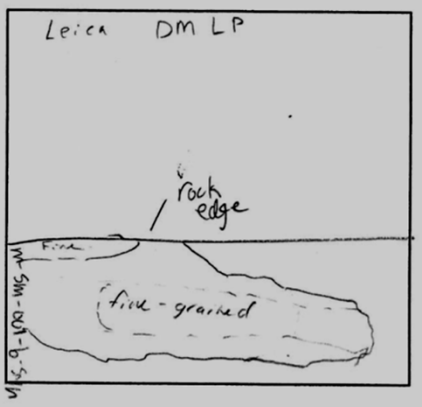


Banding Textures >1 cm band → fine grained pl rich troctolite

Cavity Textures ∅

**MINERALOGY**

| Phase | Pl | Ol | Opx | Cpx | FeOx | Bt |
|---|---|---|---|---|---|---|
| Mode | 60 | 10 | 10 | 10 | ~3 | ~3 |
| Habit | tab. | Poik | oph | oph | int-anh | int-ann |

Alteration Url.? Saus? Ol → iddingsite

Some chlorite.

Other Comments Zoned pl. Partially altered Ol near edge. Surface weathering, abundant cracking + secondary FeOx

Summary Rock Name Medium grained, non-foliated, ophitic / sub-poikilitic olivine gabbronorite with minor oxide + biotite.

Cumulate Code m,POCIfb

*Developed by J. Miller, May, 2013*

SEM Notes → contains apatite

## IGNEOUS ROCK PETROGRAPHIC DESCRIPTION

Petrographer Paul Fix Date 5-2-, 2015

Sample ID M-Sm-004-C Location UTM N- UTM E-

Geologic/Tectonic Setting Mesaba - Railroad OC - Sept 2013

Hand Sample Description Pervaisivly weathered, Secondary FeOx coatings on most of exposed surfaces as well as inside upon breaking w/ hammer. No green coating observed. Some sand some soil on surface

**TEXTURES**

Crystallinity holo

Grain Size (general) medium

Avg Plagioclase width- 1 mm

Bulk Rock Textures (relative grain shapes)

"Bulk" Band
- Euhedral olivine
- tabular plag ophitic Px
- Poikilitic olivine

Oriented Textures non-foliated

Intergrowth Textures ∅

Overgrowth Textures biotite on FeOx

Exsolution Textures ∅

**Photomicrograph/Sketch**

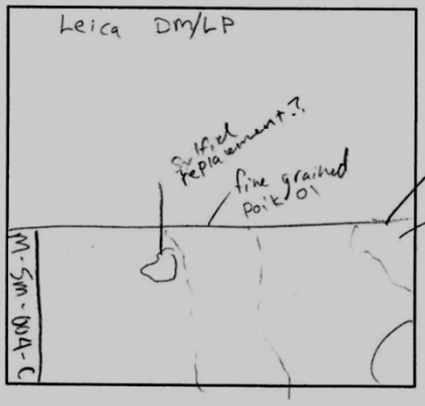


Banding Textures fine grained poik. Ol. band ↑

Cavity Textures Sulfide replacement

**MINERALOGY**

| Phase | Plag | Ol | Opx | Cpx | bt | FeOx |
|---|---|---|---|---|---|---|
| Mode | 60 | 15 | 10 | 7 | 3 | 3 |
| Habit | tabular | var | sub.oph. | oph | int. | int. |

Alteration minor chlorite minor Salts.

Other Comments Sulfide rich - less FeOx than 001 samples ?

Summary Rock Name Varitextured - medium grained, intergranular intergranular to ophitic olivine gabbro Norite w/ minor biotite and chlorite

Cumulate Code Poikfb

*Developed by J. Miller, May, 2013*

## IGNEOUS ROCK PETROGRAPHIC DESCRIPTION

Petrographer Paul Fix Date 5-2-2015

Sample ID M-SM-005-b Location UTM N- UTM E-

Geologic/Tectonic Setting Mesaba – Railcut – Sept. 2013

Hand Sample Description Sample appears "fresh." Some FeOx coatings occur on exposed surface, but weathering does not appear to be pervasive upon breaking. mineralized, coarse grained.

**TEXTURES**

Crystallinity Ø

Grain Size (general) med - coarse

Avg Plagioclase width- 4 mm

Bulk Rock Textures (relative grain shapes)

Euhedral → Poikilitic Ol

Oriented Textures non-foliated

Intergrowth Textures Ø

Overgrowth Textures Biotite on FeOx

Exsolution Textures Ø

**Photomicrograph/Sketch**

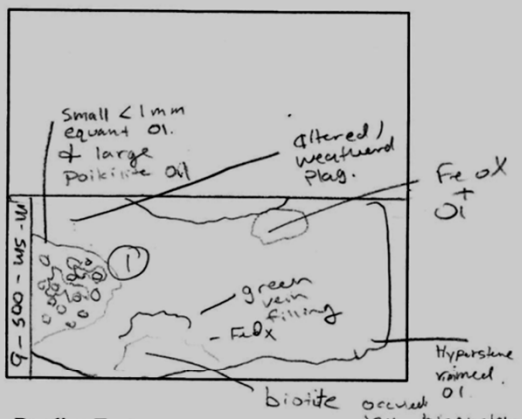


Banding Textures

(1) Localized area of small equant ol. crystals

Cavity Textures Ø

**MINERALOGY**

| Phase | Plag. | Ol | Cpx | Opx | Bt | Ox |
|---|---|---|---|---|---|---|
| Mode | 55 | 20 | 10 | 7 | ~3 | ~3 |
| Habit | tab. | Eu- Poik | int-anh | int-anh | int-anh | |

Alteration Fairly unaltered sample.

Other Comments Less FeOx staining in fractures. Large "thin section sized" Poik Ol.

Summary Rock Name Varitextured, med-coarse grained, non-foliated Olivine poikilitic augite troctolite with oxide and biotite

Cumulate Code mC P0Ĉ1^f b

*Developed by J. Miller, May, 2013*

Reflected Light

**IGNEOUS ROCK PETROGRAPHIC DESCRIPTION**

Petrographer Paul Fix Date 5-8-2014

Sample ID m-sm-005-syn Location UTM N- UTM E-

Geologic/Tectonic Setting

Hand Sample Description See transmitted light sheet.

**TEXTURES**

Crystallinity ø

Grain Size (general) Coarse grained Sulfide

Avg Sulfide width- 0.5 mm

Textures (relative grain shapes)

Oriented Textures ø

Intergrowth Textures ø

Overgrowth Textures ø

Exsolution Textures Pn - Po

Cpy - Cub

Banding Textures ø

Cavity Textures ø

**Photomicrograph/Sketch**

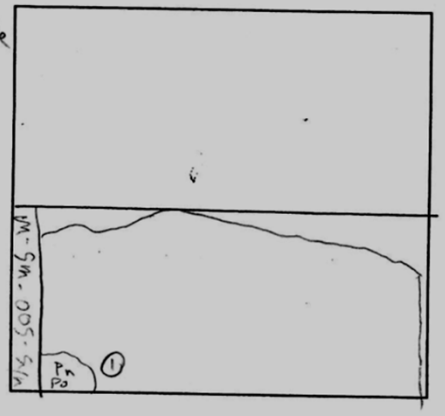


**MINERALOGY**

| Phase | Cub | Cpy | Po | Pn | | |
|---|---|---|---|---|---|---|
| Mode | 40 | 30 | 15 | 15 | | |
| Habit | var | var | var | intergrown w/ Po "symplectic" | | |

Alteration Slight

Other Comments Highly mineralized, less primary FeOx than 004. not weathered.

Appears to have more Pn than other samples

Some interstitial "long rivers"

(1) Some fracture filling of FeOx around Cpy and Cub. Primary?

m-sm-005-b-syn - PP-5x
"Bx"-5x

## IGNEOUS ROCK PETROGRAPHIC DESCRIPTION

Petrographer Paul Fix Date 5-2-2015

Sample ID m-sm-006-a Location UTM N- UTM E-

Geologic/Tectonic Setting Mesaba - Railcut - Sept 2013

Hand Sample Description Fairly extensive sulfide weathering. Broad range of FeOx coating color from light orange to very dark brown. "sulfide replacement" pits.

**TEXTURES**

Crystallinity ∅

Grain Size (general) medi

Avg Plagioclase width- 1 mm

Bulk Rock Textures (relative grain shapes)

Sub-Poik Ol

Sub-ophitic Cpx + Opx

Oriented Textures non-foliated

Intergrowth Textures Fe inclusions in plag

Overgrowth Textures Biotite on FeOx

Exsolution Textures FeOx in Pl

**Photomicrograph/Sketch**

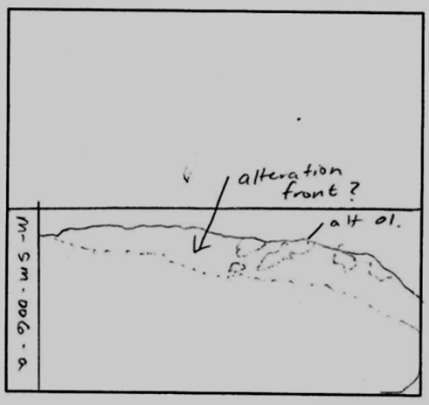


Banding Textures ∅

Cavity Textures ∅

**MINERALOGY**

| Phase | Plag | Ol | Cpx | Opx | FeOx+Sul | Bt |
|---|---|---|---|---|---|---|
| Mode | 60 | 20 | 10 | 5 | ~3 | 3 |
| Habit | tab. | Subpoik | sub oph | sub oph | int | int |

Alteration Pl → Sau. Some FeOx-in fractures Ol - iddingsite Chlorite + minor amphibole?

Other Comments ∅ Abundand inclusions in plag including bt, FeOx

Summary Rock Name medium grained non-foliated, sub poikilitic, sub-ophitic, olivin gabb troctolite with biotite and FeOx

Cumulate Code mPtCifb

*Developed by J. Miller, May, 2013*

* BS samples show evidence of hydrothermal alteration

**IGNEOUS ROCK PETROGRAPHIC DESCRIPTION**

Petrographer Paul Fix Date 5-2-2015

Sample ID bs-001-w Location UTM N- UTM E-

Geologic/Tectonic Setting Mesaba - Bulk sample site - July 2014

Hand Sample Description Extensively weathered / fractured sample. Weathered prior to bulk sample collection? Primary FeOx rich, mineralized. Sample has malachite coatings.

**TEXTURES**

Crystallinity ø

Grain Size (general) Med - coarse

Avg Plagioclase width- 5 mm

Bulk Rock Textures (relative grain shapes)

subhedral Ol.

oph 2 pyroxenes

Oriented Textures non-foliated

Intergrowth Textures a lot of FeOx

Overgrowth Textures Pyx on Ol

Exsolution Textures abundant FeOx / sulf

**Photomicrograph/Sketch**

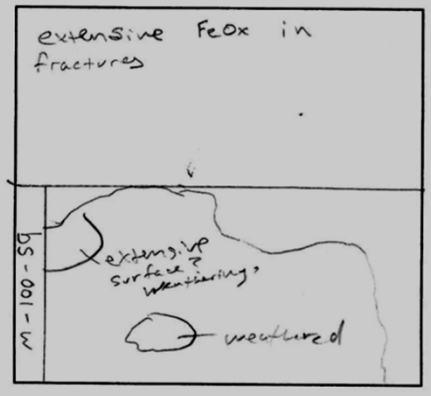


Banding Textures ø

Cavity Textures ø

**MINERALOGY**

| Phase | Pl. | Ol | Cpx | OPX | FeOx | Bt |
|---|---|---|---|---|---|---|
| Mode | 50 | 20 | 10 | 10 | 5 | 5 |
| Habit | tab | subhedral | int-anh. | int-anh | | |

Alteration Pl → Sauss. Ol – idding. Fairly extensive alteration

Other Comments Is the alteration primary or "surface"?

Summary Rock Name Medium to coarse grained, sub-ophitic, non-foliated olivine gabbronorite + iron oxide

Cumulate Code mP0ĉ^fb

*Developed by J. Miller, May, 2013*

## IGNEOUS ROCK PETROGRAPHIC DESCRIPTION

Petrographer Paul Fix Date 5-3-2015

Sample ID bS-002-W Location UTM N- UTM E-

Geologic/Tectonic Setting Mesabo - bS site - July 2014

Hand Sample Description "non-weathered" Sample from the "BS" site. non-weathered Sulfide exposed in field suggests very little weathering. med-coarse grained. Mineralized. Check Sheet

**TEXTURES**

Crystallinity ø

Grain Size (general) med.

Avg Plagioclase width- 2 mm

Bulk Rock Textures (relative grain shapes)
euh. - sub Ol.

Oriented Textures non-foliated

Intergrowth Textures ø

Overgrowth Textures Biotite on FeOx. Amp. on Ol.

Exsolution Textures oxide → Pl

**Photomicrograph/Sketch** silicate composition

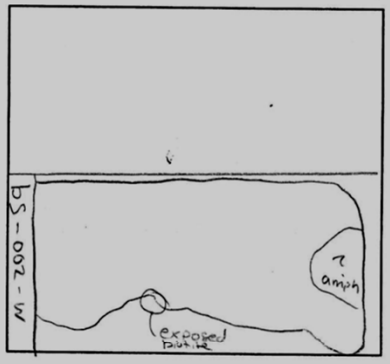


Banding Textures

Cavity Textures

**MINERALOGY**

| Phase | Pl | Ol | Cpx/opx | FeOx | Bt | ? Amphibole |
|---|---|---|---|---|---|---|
| Mode | 55 | 25 | 5/5 | 5 | 3 | 3 |
| Habit | tab. | ex-suber. | 5.6-0 | int | int | int |

Alteration Primary chl, sericite, amphibole,

Other Comments more chlorite, amphibole, and biotite than other samples Plag. appears "raggy." mostly oxide, less sulfide? ALTERED

Summary Rock Name Medium grained, non-foliated, mafic rock like with biotite, amphibole, and FeOx

Cumulate Code mPOxifbHb

*Developed by J. Miller, May, 2013*

## IGNEOUS ROCK PETROGRAPHIC DESCRIPTION

Petrographer Paul Fix Date 5-3-2015

Sample ID bs-003-w Location UTM N- UTM E-

Geologic/Tectonic Setting Mesaba - BS site - July 2014

Hand Sample Description Sample appears "bleached", perhaps extensively weathered but w/o much sulfide influence. Fractured. Large clots of ophitic Pyx. + oxide. Coarse grained.

**TEXTURES**

Crystallinity ø

Grain Size (general) med

Avg Plagioclase width- 2 mm

Bulk Rock Textures (relative grain shapes)

Ophitic Cpx

Sub-poik. Ol

Oriented Textures non foliated

Intergrowth Textures Some Symplectite

Overgrowth Textures ø

Exsolution Textures ø

Banding Textures ø

Cavity Textures ø

**Photomicrograph/Sketch**

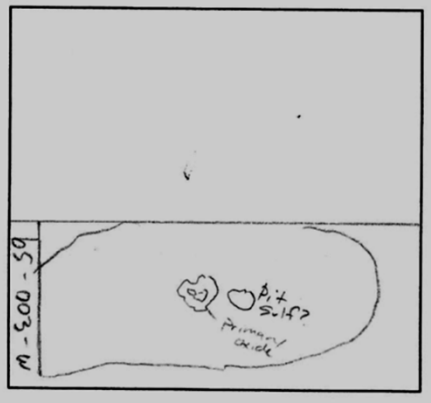


**MINERALOGY**

| Phase | Pl | Cpx | Ol | Fe Ox | Bt | |
|---|---|---|---|---|---|---|
| Mode | 60 | 20 | 10 | 5 | 3 | |
| Habit | tab. | ophitic | sub-poik | int | int | |

Alteration Fractures w/ Fe Ox fill Ol - iddingsite

Some Saussurite (weak - mod)

Other Comments

Summary Rock Name Medium grained, non foliated, sub-poikilitic olivine gabbro.

Cumulate Code mPC$\bar{O}$1$\hat{}$fb

*Developed by J. Miller, May, 2013*

## IGNEOUS ROCK PETROGRAPHIC DESCRIPTION

Petrographer Paul Fix Date 5-3-2015

Sample ID bs-004-w Location UTM N- UTM E-

Geologic/Tectonic Setting Mesaba - bs site - July 2014

Hand Sample Description "Non-weathered" Certainly only exposed on surface since BS collection. Mineralized. Med-grained, troctolitic, Some fractures. FeOx generally absent

**TEXTURES**

Crystallinity ø

Grain Size (general) med - coarse

Avg Plagioclase width- 4 mm

Bulk Rock Textures (relative grain shapes)

Sub poik ol

Oriented Textures non-foliated

Intergrowth Textures ø

Overgrowth Textures ø

Exsolution Textures FeOx in Pl

**Photomicrograph/Sketch**

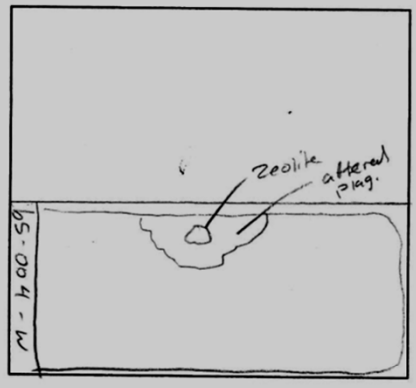


Banding Textures ø

Cavity Textures ø

**MINERALOGY**

| Phase | Pl | Ol | CPX/hyp | bt | hb | FeOx |
|---|---|---|---|---|---|---|
| Mode | 60 | 20 | 10/5 | 5 | 5 | 5 |
| Habit | | | | | | |

Alteration Ol - iddingsite Pl - Saus. Extensive ALTERATION

Other Comments Contains zealite, hornblende chloride

Summary Rock Name Medium to Coarse grained non-foliated poikilitic augite troctolite with minor hornblende.

Cumulate Code mc/ad f hb

*Developed by J. Miller, May, 2013*

Appendix C
Reflected Light Petrography Notes

Reflected Light

**IGNEOUS ROCK PETROGRAPHIC DESCRIPTION**

Petrographer Paul Fix Date 5-5-2015

Sample ID m-sm-001-b Location UTM N- UTM E-

Geologic/Tectonic Setting

Hand Sample Description See transmitted light sheet

**TEXTURES**

Crystallinity

Grain Size (general)

Avg sulfide width- ~200μm mm

Textures (relative grain shapes)
replacement

Oriented Textures Ø

Intergrowth Textures Ø

Overgrowth Textures Ø

Exsolution Textures

**Photomicrograph/Sketch**

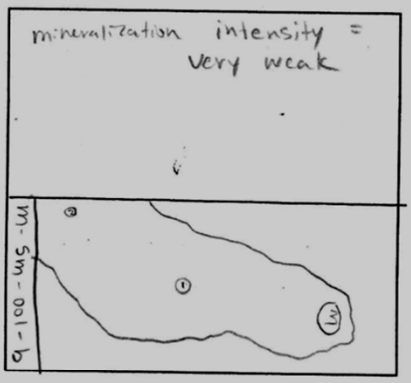


Banding Textures Ø

Cavity Textures

**MINERALOGY**

hard to see - low abundance fine grained

| Phase | Cub | | Cpy | Po | | | |
|---|---|---|---|---|---|---|---|
| Mode | 50 | ≈ | 40 | 10 | | | |
| Habit | | | | | | | |

Alteration weathered, sample appears to have low sulfide abundance, but has it been weathered or started

Other Comments Very low sulfide abundance, Abundant FeOx fractures. Fine grained occluded? sulfides ccp?

① 200μm CCP replaced ~50% by FeOx. NO exsolution observed.
② 25μm ccp ~75% by FeOx [m-sm-001-b-pp-5x]
③ 100μm ccp in large replacement by FeOx

Reflected Light

**IGNEOUS ROCK PETROGRAPHIC DESCRIPTION**

Petrographer Paul Fix Date 5-8-2014

Sample ID rn-sm-001-b-syn Location UTM N- UTM E-

Geologic/Tectonic Setting

Hand Sample Description See transmitted light sheet

**TEXTURES**

Crystallinity ø

Grain Size (general) ø

Avg sulfide width-~200μmmm

Textures (relative grain shapes)

replacement

Oriented Textures ø

Intergrowth Textures ø

Overgrowth Textures ø

Exsolution Textures ø

**Photomicrograph/Sketch**

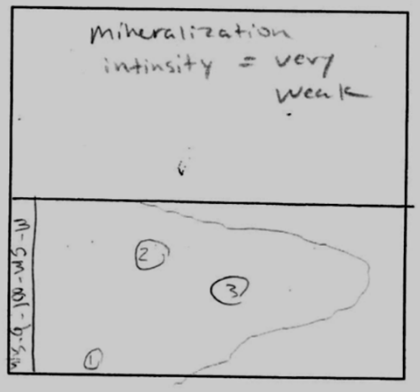


Banding Textures ø

Cavity Textures ø

**MINERALOGY**

| | | | | | | | |
|---|---|---|---|---|---|---|---|
| Phase | Cpy ≈ | Cvb > | Po | | | | |
| Mode | | | | | | | |
| Habit | | | | | | | |

(hard to determine)

Alteration extensively weathered, secondary oxide filling abundant fractures, minor sulfide

Other Comments very low sulfide abundance.

① large secondary FeOx filling near primary oxide phase small remnant sulfide.

② Small secondary FeOx zone. rn-sm-001-b-syn-1-pp

③ Small Cpy oxidation rim plus feOx vein fill

rn-sm-001-b-syn-2 "pp Dx"

Reflected Light

**IGNEOUS ROCK PETROGRAPHIC DESCRIPTION**

Petrographer Paul Fix Date

Sample ID m-sm-004-c Location UTM N- UTM E-

Geologic/Tectonic Setting

Hand Sample Description See transmitted light sheet.

**TEXTURES**

Crystallinity

Grain Size (general) Variable

Avg width- 500 μmm

Textures (relative grain shapes)

Sulfide in veins / grain-boundries. int.

"Symplectite like"

Oriented Textures

Intergrowth Textures

Overgrowth Textures

Exsolution Textures Cub → cpy

**Photomicrograph/Sketch**

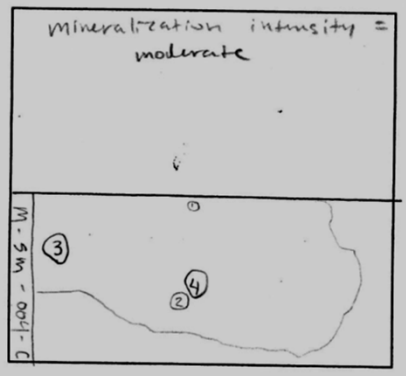


Banding Textures

Cavity Textures

**MINERALOGY** @ 100% S

| Phase | Cub | cpy | Po | | | |
|---|---|---|---|---|---|---|
| est. Mode | 80% | 15% | 5% | | | |
| Habit | | | | | | |

Alteration

Other Comments Po weathered out. Seems to be mostly Cub.

Vein sulfide, interstitial. Moderate mineralization

(1) Complex exsolution shows Po, Cpy, Cub, + minor Chalcocite? (blue pp) isotropic covellite?

(2) Symplectite like [m-sm-004-c-1-pp-5x-3

(3) Intense sulfide weathering [m-sm-004-c-2-pp-5x // // Px

Cub > cpy?

(4) Weathered sulfide Po > Cub? [m-sm-004-c-3-pp-10x // Px

Reflected Light

**IGNEOUS ROCK PETROGRAPHIC DESCRIPTION**

Petrographer Paul Fix Date 5-5-2015

Sample ID m-sm-005-b Location UTM N- UTM E-

Geologic/Tectonic Setting

Hand Sample Description See transmitted light sheet.

**TEXTURES**

Crystallinity

Grain Size (general) Fairly Coarse Sulfides

Avg width- <1 mm

Textures (relative grain shapes)

pFeOx & Sulfids, interstitial

Oriented Textures

Intergrowth Textures

Overgrowth Textures

Exsolution Textures Cpy → Cub

Pn → Po

**Photomicrograph/Sketch**

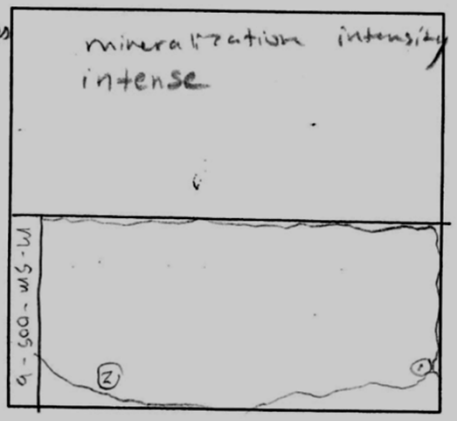


Banding Textures

Cavity Textures

**MINERALOGY**

| Phase | 40 | 30 | 25 | 5 | | |
|---|---|---|---|---|---|---|
| Mode | Cub | ccp | Po | Pn | | |
| Habit | | | | | | |

Alteration minimal, primary FeOx

Other Comments a lot of primary FeOx in close relation to sulfides, mod-strong mineralization sample does not "weathered" all sulfides are "in tact" Check primary oxide pitting w/ SEM

(1) FeOx, Cpy, Po, Cub/Pn phase relationships (typical) m-sm-005-b-pp-5x

(2) weathered or polish pits in sulfide. m-sm-005 b-2-pp 5x

Reflected Light

**IGNEOUS ROCK PETROGRAPHIC DESCRIPTION**

Petrographer Paul Fix Date 5-8-2014

Sample ID m-sm-005-syn Location UTM N- UTM E-

Geologic/Tectonic Setting

Hand Sample Description See transmitted light sheet

**TEXTURES**

Crystallinity ø

Grain Size (general) Coarse grained Sulfide

Avg Sulfide width- 0.5 mm

Textures (relative grain shapes)

Oriented Textures ø

Intergrowth Textures ø

Overgrowth Textures ø

Exsolution Textures Pn - Po

Cpy - Cub

Banding Textures ø

Cavity Textures ø

**Photomicrograph/Sketch**

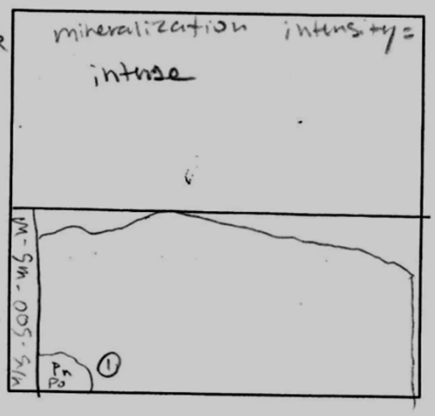


**MINERALOGY**

| Phase | Cub | Cpy | Po | Pn | | |
|---|---|---|---|---|---|---|
| Mode | 40 | 30 | 15 | 10 | | |
| Habit | var | var | var | intergrown w/ Po "symplectic" | | |

Alteration Slight

Other Comments Intensely mineralized, less primary feox than 004. Does not appear weathered

Some interstitial long "veins"

Appears to have more Pn than other samples

(1) Some fracture filling of feox around cpy and cub. Primary?

m-sm-005-b-syn - pp-5x "Ax"-5x

Reflected Light

**IGNEOUS ROCK PETROGRAPHIC DESCRIPTION**

Petrographer Paul Fix Date 5-5-2015

Sample ID m-sm-006-a Location UTM N - UTM E -

Geologic/Tectonic Setting

Hand Sample Description See transmitted light sheet

**TEXTURES**

Crystallinity Smaller sulfide grains

Grain Size (general)

Avg width- <1 mm

Textures (relative grain shapes)

Oriented Textures ø

Intergrowth Textures ø

Overgrowth Textures ø

Exsolution Textures

Banding Textures ø

Cavity Textures ø

**Photomicrograph/Sketch**

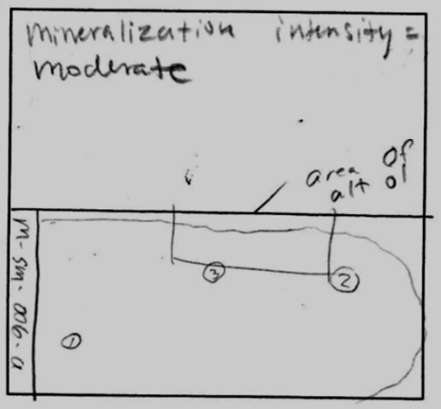


**MINERALOGY**

| Phase | Cpy | Cub | Po | | | |
|---|---|---|---|---|---|---|
| Mode | 60 | 20 | 20 | | | |
| Habit | small incl/int | inc/int | ? | | | |

← seems to be more Cpy rich

Alteration altered Ol, probably magmatic

Other Comments Not extensively weathered?

Moderate mineralization, magmatic alteration

① talnakatite? + Cpy

② weathered sulfide m-sm-006-a-2-pp-5x

③ "Fresh" sulfide in close proximity to iddingsite altered Olivine m-sm-006-a-3-pp-5x / m-sm-006-a-3-px-5x

Reflected Light

**IGNEOUS ROCK PETROGRAPHIC DESCRIPTION**

Petrographer Paul Fix Date 5-6-2015

Sample ID bs-001-w Location UTM N- UTM E-

Geologic/Tectonic Setting

Hand Sample Description See transmitted light sheet

**TEXTURES**

Crystallinity ø

Grain Size (general) var

Avg width- 1-2 mm

Textures (relative grain shapes)

Oriented Textures ø

Intergrowth Textures ø

Overgrowth Textures ø

Exsolution Textures Cub → Cpy

**Photomicrograph/Sketch**

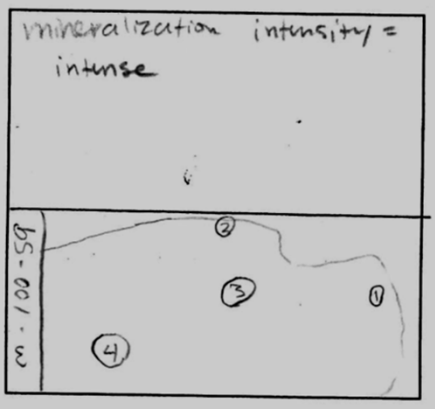


Banding Textures ø

Cavity Textures x

**MINERALOGY**

| Phase | Cub | Cpy | Po | Pn | Cov | |
|---|---|---|---|---|---|---|
| Mode | 60 | 25 | 10 | 5 | 1-2 | |
| Habit | var | var | | trace | trace/Secondary | |

Alteration extensive, FeOx, Boxwork

Other Comments highly mineralized sample showing extensive weathering. Covellite may suggest subsurface weathering. Covellite in boxwork structure.

① 900 μm boxwork Cu-sulfide w/ covellite rim? pp blue xp Bright red-orange Po near by

② Partially reacted sulfide showing cub > cpy oxidation

③ oxidized sulfide at fracture interface

④ Covellite and FeOxide

bs-001-w-1-pp-Sx "Px"

bs-001-w-2-pp-Sx-Px

July 2nd

Reflected Light

**IGNEOUS ROCK PETROGRAPHIC DESCRIPTION**

Petrographer Paul Fix Date 5-12-2015

Sample ID bS-002-w Location UTM N- UTM E-

Geologic/Tectonic Setting

Hand Sample Description See transmitted light sheet

**TEXTURES**

Crystallinity ø

Grain Size (general) fine grained sulfide

Avg width- <25μm mm

Textures (relative grain shapes)

Oriented Textures ø

Intergrowth Textures ø

Overgrowth Textures ø

Exsolution Textures

**Photomicrograph/Sketch**

mineralization intensity = weak

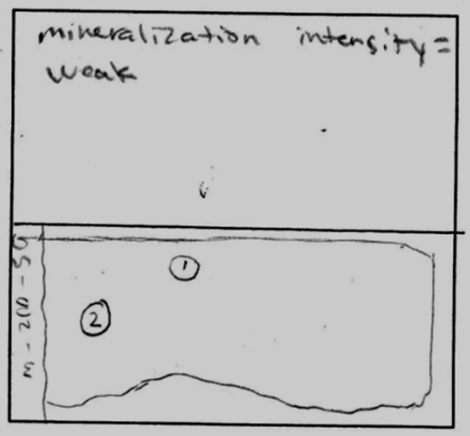


Banding Textures ø

Cavity Textures ø

**MINERALOGY**

| Phase | Cpy | Cub | Po | | | |
|---|---|---|---|---|---|---|
| Mode | | | | | | |
| Habit | | | some | | | |

hard to determine

Alteration some dueteric alteration, not much surface weathering / FeOx filling

Other Comments Low Sulfide sample, most sulfides are micron-scale as inclusions in Plag, associated w/ FeOx biotite, and potentially remobilized by dueteric fluids

(1) fracture w/ Cub / Po and associated biotite

(2) Dueteric alteration w/ sulfide Po

(1) bS-002-w-p-5x "Px"

(2) bS-002-w-2-pp-5x "Px"

Reflected Light

**IGNEOUS ROCK PETROGRAPHIC DESCRIPTION**

Petrographer Paul Fix Date 5-8-,2015

Sample ID bs-003-w Location UTM N- UTM E-

Geologic/Tectonic Setting

Hand Sample Description See transmitted light sheet.

**TEXTURES**

Crystallinity 100%

Grain Size (general) 0

Avg width-0.001 mm

Textures (relative grain shapes)

fine grained Sulfide

Oriented Textures 0

Intergrowth Textures 0

Overgrowth Textures 0

Exsolution Textures cub - cpy

Banding Textures 0

Cavity Textures 0

**Photomicrograph/Sketch**

mineralization intensity = very weak

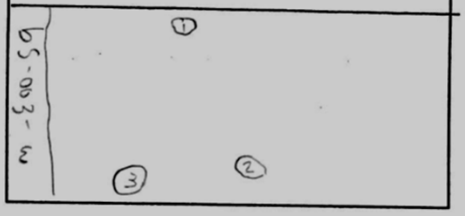


**MINERALOGY**

| Phase | Po | > | Cub | = | CPy | | | |
|---|---|---|---|---|---|---|---|---|
| Mode | 60 | | 20 | | 20 | | | |
| Habit | | | | | | | | |
| Alteration | Diabasic alteration | | | | | | | |

Other Comments Extensive iron oxidation. Very low Sulfide abundance. Remobilization of S, or Surface weathering? Minor - very low Sulfide mineralization

(1) complete sulfide replacement - to FeOx? m-sm-003-w-1-pp-5x

(2) " m-sm-003-2-pp-5x

m-sm-003-2-PX-5x"

(3) reacted / oxidized CPY "m-sm-003-3-pp-5x"

Reflected Light

**IGNEOUS ROCK PETROGRAPHIC DESCRIPTION**

Petrographer Paul Fix Date 5-8-2015

Sample ID bs-004-w Location UTM N- UTM E-

Geologic/Tectonic Setting

Hand Sample Description See transmitted light sheet

**TEXTURES**

Crystallinity x

Grain Size (general)

Avg width-0.001 mm

Textures (relative grain shapes)

Oriented Textures x

Intergrowth Textures x

Overgrowth Textures x

Exsolution Textures

**Photomicrograph/Sketch**

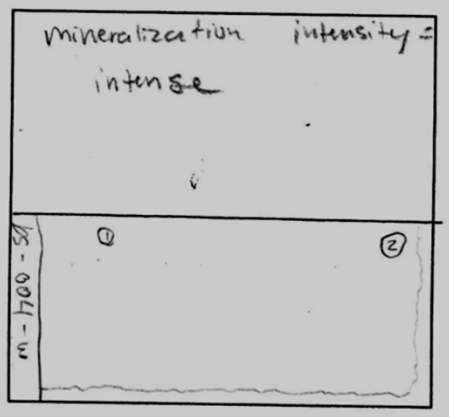


Banding Textures

Cavity Textures

**MINERALOGY**

| Phase | cub | > | Po | > | Cpy | | | |
|---|---|---|---|---|---|---|---|---|
| Mode | 60 | | 20 | | 20 | | | |
| Habit | | | | | | | | |

Alteration Sulfide remobilization by diuric processes

Other Comments Sample may be altered hydrothermally. Sulfur remobilization? Generally finer grained sulfides. Highly mineralized.

① String sulfides hosted in alteration phase? Almost complete sulfide oxidation? m-sm-004-w-1-pp-5x

② reacted cpy and cub. m-sm-004-w-2-pp-5x

Appendix E

Summary of SEM-EDS semi-quantitative compositional data for banded coatings and SEM images/EDS data for synchrotron areas of interest

| Sample-Site | Spectrum | Al | Si | P | S | Ca | Fe | Cu | O |
|---|---|---|---|---|---|---|---|---|---|
| m-sm-001-syn-S7 2 | Spectrum 1 | 1.23 | 15.1 | | 0.4 | | 45.91 | 4.25 | 33.11 |
| m-sm-001-syn-S7 2 | Spectrum 2 | | 7.76 | | 0.7 | | 53.96 | 9.77 | 27.81 |
| m-sm-001-syn-S7 2 | Spectrum 3 | | 9.44 | | 0.5 | | 53.35 | 7.93 | 28.78 |
| m-sm-001-syn-S7 3 | Spectrum 4 | 0.96 | 13.74 | 0.43 | 0.34 | 0.29 | 47.68 | 4.15 | 32.4 |
| m-sm-001-syn-S7 4 | Spectrum 5 | | 8.19 | | 0.81 | | 52.58 | 10.2 | 28.19 |
| m-sm-001-syn-S7 5 | Spectrum 6 | 1.36 | 11.62 | | 0.28 | 0.29 | 52.94 | 2.69 | 30.83 |
| m-sm-001-syn-S7 6 | Spectrum 7 | 2.39 | 5.82 | 0.41 | 0.85 | | 58.91 | 3.35 | 28.27 |
| m-sm-001-syn-S7 7 | Spectrum 8 | 1.88 | 10.82 | 0.55 | 0.5 | 0.29 | 51.51 | 3.3 | 31.15 |
| m-sm-001-syn-S7 8 | Spectrum 9 | | 10.83 | | 0.6 | | 50.73 | 8.04 | 29.8 |
| m-sm-001-syn-S4 2 | Spectrum 1 | 1.51 | 12.47 | | 0.77 | | 50.68 | 2.67 | 31.9 |
| m-sm-001-syn-S4 3 | Spectrum 2 | 2.04 | 10.84 | | 1.34 | 0.33 | 51.17 | 2.67 | 31.62 |
| m-sm-001-syn-S4 4 | Spectrum 3 | 1.74 | 13.82 | | 0.54 | | 48.86 | 2.35 | 32.69 |
| m-sm-001-syn-S4 5 | Spectrum 4 | 1.54 | 13.92 | | 0.5 | | 49.01 | 2.41 | 32.62 |
| m-sm-001-syn-S4 6 | Spectrum 5 | 1.97 | 11.11 | | 1.41 | 0.3 | 50.11 | 3.28 | 31.82 |
| m-sm-001-syn-S4 7 | Spectrum 6 | 1.63 | 12.66 | | 0.57 | | 50.19 | 3.08 | 31.87 |
| m-sm-001-syn-S4 8 | Spectrum 7 | 4.32 | 14.92 | | 0.53 | 0.48 | 41.87 | 3.25 | 34.64 |
| m-sm-001-syn-S11 | Spectrum 1 | 3.51 | 16.25 | 0.45 | 1.15 | 0.47 | 40.21 | 1.84 | 36.11 |
| m-sm-001-syn-S11 | Spectrum 2 | 3 | 16.45 | 0.44 | 0.93 | 0.42 | 40.84 | 2.12 | 35.78 |
| m-sm-001-syn-S11 | Spectrum 1 | 0.96 | 4.22 | | 0.67 | | 63.07 | 3.85 | 26.31 |
| m-sm-001-syn-S12 | Spectrum 2 | 2.7 | 15.89 | 0.42 | 0.24 | 0.34 | 42.83 | 1.58 | 34.86 |
| m-sm-001-syn-S13 | Spectrum 3 | 4.78 | 15.85 | 0.32 | 1.17 | 0.4 | 35.56 | 3.66 | 36.62 |
| m-sm-001-syn-S14 | Spectrum 4 | 2.1 | 6.41 | 0.57 | 0.58 | | 58.84 | 3.09 | 28.41 |
| m-sm-001-b_syn S 1 3 | Spectrum 1 | 2.64 | 6.97 | 0.39 | 0.61 | 0.27 | 52.63 | 1.66 | 34.84 |
| m-sm-001-b_syn S 1 4 | Spectrum 2 | 4.06 | 8.91 | 0.57 | 0.67 | 0.31 | 47.3 | 1.8 | 36.39 |
| m-sm-001-b_syn S 1 5 | Spectrum 3 | 5.37 | 10.63 | 0.59 | 0.76 | 1.09 | 41.24 | 1.46 | 37.92 |
| m-sm-001-b_synS2 3 | Spectrum 1 | 1.3 | 9.28 | | 1.65 | | 49.89 | 1.79 | 36.09 |
| m-sm-001-b_synS3 2 | Spectrum 2 | 3.07 | 15.97 | | 0.63 | 0.31 | 39.01 | 1.8 | 39.21 |
| m-sm-001-b_synS3 3 | Spectrum 3 | 3.22 | 16.09 | | 0.57 | 0.46 | 38.11 | 2.37 | 39.2 |
| m-sm-001-b_synS4 3 | Spectrum 1 | 1.34 | 9.79 | | | | 50.87 | 3.03 | 34.97 |
| m-sm-001-b_synS4 4 | Spectrum 2 | 1.47 | 11.51 | | 0.73 | | 47.53 | 2.24 | 36.51 |
| m-sm-001-b_synS4 5 | Spectrum 5 | 1.56 | 11.36 | | 0.37 | | 48.19 | 2.34 | 36.18 |
| m-sm-001-b_synS4 6 | Spectrum 6 | 1.49 | 12.07 | | 0.4 | | 47.7 | 1.73 | 36.61 |
| m-sm-001-b_synS4 7 | Spectrum 7 | 1.95 | 11.15 | | 0.59 | 0.3 | 46.93 | 2.77 | 36.3 |
| m-sm-001-b_synS4 8 | Spectrum 8 | 2.93 | 12.19 | | 0.62 | 0.29 | 44.26 | 2.52 | 37.19 |
| m-sm-001-b_synS8 3 | Spectrum 1 | 0.29 | 2.49 | | 0.9 | | 62.98 | 1.44 | 31.88 |
| m-sm-001-b_synS8 4 | Spectrum 2 | 0.66 | 4.43 | | 0.53 | | 60.09 | 1.64 | 32.65 |
| m-sm-001-b_synS8 5 | Spectrum 3 | 1.21 | 7.82 | | 0.89 | | 53.31 | 2.03 | 34.74 |
| m-sm-001-b_synS8 6 | Spectrum 4 | 0.36 | 3.19 | | 0.53 | | 62.99 | 0.88 | 32.04 |
| m-sm-001-b_synS10 3 | Spectrum 1 | 0.95 | 12.31 | | 0.52 | | 46.81 | 2.7 | 36.5 |
| m-sm-001-b_synS10 4 | Spectrum 2 | 1.16 | 9.57 | | 0.59 | | 50.85 | 2.51 | 35.31 |
| m-sm-001-b_synS10 5 | Spectrum 3 | 1.19 | 13.02 | | 0.5 | 0.23 | 46.39 | 1.61 | 37.06 |

| Sample-Site | Spectrum | Al | Si | P | S | Ca | Fe | Cu | O |
|---|---|---|---|---|---|---|---|---|---|
| m-sm-001-bS1 2 | Spectrum 1 | 1.15 | 9.97 | | 0.42 | | 50.75 | 2.31 | 35.4 |
| m-sm-001-bS1 3 | Spectrum 2 | 1.06 | 10.98 | | 0.45 | | 49.91 | 1.62 | 35.98 |
| m-sm-001-bS1 4 | Spectrum 3 | 3.19 | 16.19 | 0.45 | 0.31 | 0.31 | 35.19 | 4.23 | 39.03 |
| m-sm-001-bS1 5 | Spectrum 1 | 1.11 | 3.49 | | 0.57 | | 60.72 | 1.76 | 32.35 |
| m-sm-001-bS1 6 | Spectrum 2 | 1.12 | 8.07 | | 0.69 | | 52.7 | 2.84 | 34.58 |
| m-sm-001-bSi2 2 | Spectrum 2 | 2.47 | 5.57 | | 1.82 | | 47.78 | 8.43 | 33.92 |
| m-sm-001-bSite: 3 3 | Spectrum 1 | 1.37 | 5.87 | 0.57 | 3.04 | | 51.44 | 1.91 | 35.79 |
| m-sm-001-bS3 3 | Spectrum 2 | 1.47 | 6.32 | 0.62 | 2.95 | | 51.12 | 1.47 | 36.06 |
| m-sm-001-bS4 2 | Spectrum 4 | 1.37 | 8.97 | 0.56 | 0.65 | | 51.39 | 1.48 | 35.58 |
| m-sm-001-bS5 3 | Spectrum 1 | 0.86 | 3.76 | | 0.68 | | 59.42 | 2.34 | 32.49 |
| m-sm-001-bS8 3 | Spectrum 1 | 2.18 | 11.15 | | 1.2 | 0.2 | 45.44 | 1.95 | 37.07 |
| m-sm-001-bS8 4 | Spectrum 2 | 1.47 | 6.19 | 0.37 | 1.07 | | 54.33 | 2.25 | 34.34 |
| m-sm-001-bS8 5 | Spectrum 3 | 0.76 | 4.97 | | 0.6 | | 58.43 | 2.31 | 32.93 |
| m-sm-001-bS8 6 | Spectrum 4 | 1.56 | 12.01 | | 0.6 | 0.2 | 46.86 | 2.06 | 36.7 |
| m-sm-001-bS9 | Spectrum 1 | 8.87 | 10.92 | 0.62 | 0.33 | | 39.02 | 1.5 | 38.76 |
| m-sm-001-bS9 | Spectrum 3 | 0.73 | 1.52 | | 10.44 | | 43.07 | 1.42 | 37.89 |
| bs-001-wS9-2 | Spectrum 1 | 1.12 | 9.08 | 0.61 | 0.62 | | 49.12 | 4.22 | 35.23 |
| bs-001-wS9-3 | Spectrum 2 | | 11.5 | | | | 47.6 | 5.86 | 35.04 |
| bs-001-wS9-4 | Spectrum 3 | | 8.56 | | 1.24 | | 45.69 | 10.6 | 33.91 |
| bs-001-wS9-5 | Spectrum 4 | | 11.76 | 1.19 | | | 47.35 | 3.54 | 36.17 |
| bs-001-wS9-6 | Spectrum 5 | 0.31 | 10.97 | 2.43 | | | 45.08 | 4.74 | 36.47 |
| bs-001-wS10 2 | Spectrum 1 | 2.33 | 7.78 | | 2.37 | | 48.98 | 2.41 | 36.13 |
| bs-001-wS10 3 | Spectrum 2 | 2.59 | 7.02 | | 3.1 | | 49.28 | 1.5 | 36.5 |
| bs-001-wS10 4 | Spectrum 3 | 1.24 | 4.99 | | 0.76 | | 56.89 | 2.99 | 33.13 |
| bs-001-wS10 5 | Spectrum 4 | 2.03 | 6.27 | | 2.75 | | 51.87 | 1.38 | 35.7 |
| m-sm-004-S11-2 | Spectrum 3 | 13.16 | 17.29 | | 1.79 | | 22.84 | 0.83 | 44.1 |
| m-sm-004-S11-3 | Spectrum 4 | 3.87 | 11.36 | | 1.2 | 0.24 | 44.55 | 1.1 | 37.69 |
| m-sm-004-S11-4 | Spectrum 5 | 5.22 | 9.24 | 0.49 | 2.64 | | 42.21 | 1.5 | 38.45 |

Site: m-sm-001-syn-S7 2

Processing option : Oxygen by stoichiometry (Normalised)

| Spectrum | In stats. | Al | Si | P | S | Ca | Fe | Cu | O | Total |
|---|---|---|---|---|---|---|---|---|---|---|
| Spectrum 1 | Yes | 1.23 | 15.10 | | 0.40 | | 45.91 | 4.25 | 33.11 | 100.00 |
| Spectrum 2 | Yes | | 7.76 | | 0.70 | | 53.96 | 9.77 | 27.81 | 100.00 |
| Spectrum 3 | Yes | | 9.44 | | 0.50 | | 53.35 | 7.93 | 28.78 | 100.00 |
| Spectrum 4 | Yes | 0.96 | 13.74 | 0.43 | 0.34 | 0.29 | 47.68 | 4.15 | 32.40 | 100.00 |
| Spectrum 5 | Yes | | 8.19 | | 0.81 | | 52.58 | 10.23 | 28.19 | 100.00 |
| Spectrum 6 | Yes | 1.36 | 11.62 | | 0.28 | 0.29 | 52.94 | 2.69 | 30.83 | 100.00 |
| Spectrum 7 | Yes | 2.39 | 5.82 | 0.41 | 0.85 | | 58.91 | 3.35 | 28.27 | 100.00 |
| Spectrum 8 | Yes | 1.88 | 10.82 | 0.55 | 0.50 | 0.29 | 51.51 | 3.30 | 31.15 | 100.00 |
| Spectrum 9 | Yes | | 10.83 | | 0.60 | | 50.73 | 8.04 | 29.80 | 100.00 |
| Max. | | 2.39 | 15.10 | 0.55 | 0.85 | 0.29 | 58.91 | 10.23 | 33.11 | |
| Min. | | 0.96 | 5.82 | 0.41 | 0.28 | 0.29 | 45.91 | 2.69 | 27.81 | |

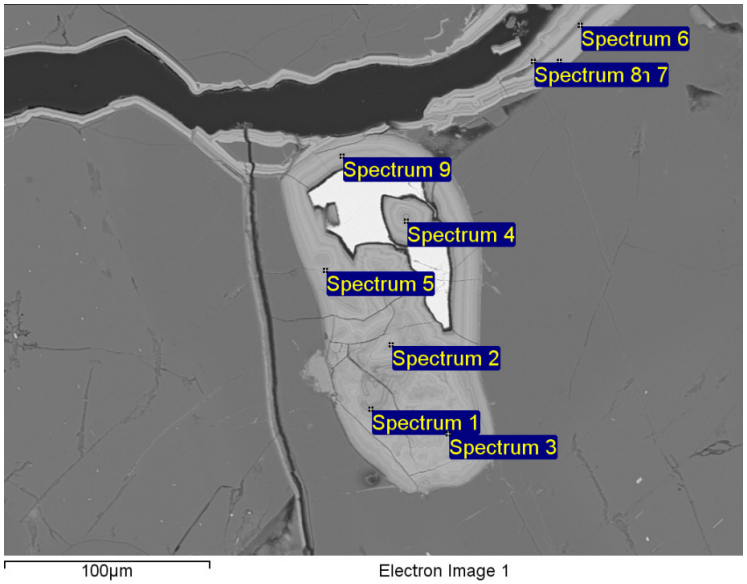

Site: m-sm-001-syn-S7 2

Processing option : Oxygen by stoichiometry (Normalised)

| Spectrum | In stats. | Na | Al | Si | K | Ca | O | Total |
|---|---|---|---|---|---|---|---|---|
| Spectrum 1 | Yes | 5.46 | 14.11 | 26.99 | 0.37 | 5.59 | 47.50 | 100.00 |
| Spectrum 2 | Yes | 5.55 | 13.68 | 27.61 | 0.34 | 5.13 | 47.68 | 100.00 |
| Spectrum 3 | Yes | 5.84 | 13.87 | 27.26 | | 5.43 | 47.59 | 100.00 |
| Max. | | 5.84 | 14.11 | 27.61 | 0.37 | 5.59 | 47.68 | |
| Min. | | 5.46 | 13.68 | 26.99 | 0.34 | 5.13 | 47.50 | |

All results in weight%

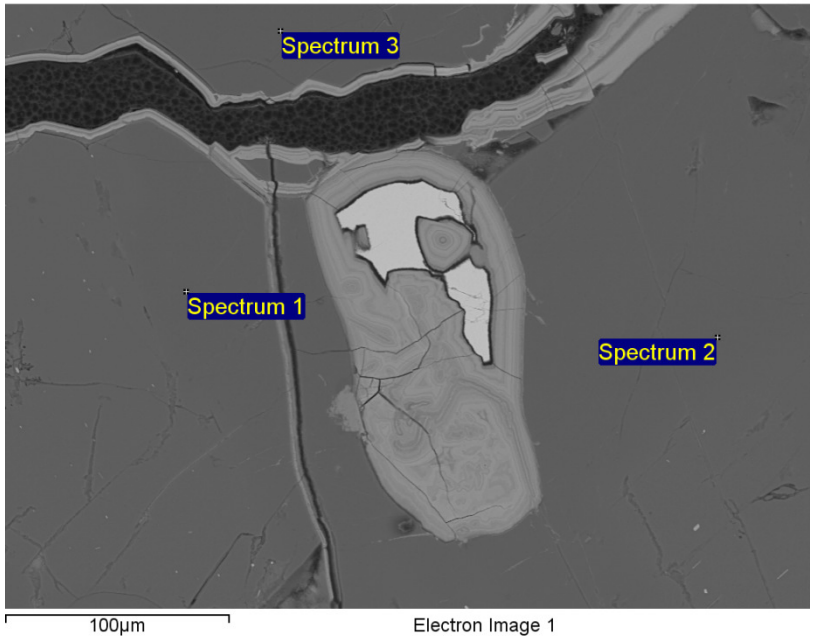

Site: m-sm-001-syn-S7 2

Processing option : Oxygen by stoichiometry (Normalised)

| Spectrum | In stats. | Na | Al | Si | K | Ca |
|---|---|---|---|---|---|---|
| Spectrum 1 | Yes | 5.43 | 14.04 | 27.09 | 0.24 | 5.65 |
| Spectrum 2 | Yes | 5.81 | 13.69 | 27.46 | 0.26 | 5.17 |
| Spectrum 3 | Yes | 5.72 | 13.86 | 27.21 | 0.28 | 5.40 |
| Mean | | 5.65 | 13.86 | 27.26 | 0.26 | 5.41 |
| Std. deviation | | 0.20 | 0.18 | 0.19 | 0.02 | 0.24 |
| Max. | | 5.81 | 14.04 | 27.46 | 0.28 | 5.65 |

Site: m-sm-001-syn-S7 3

Processing option : All elements analysed (Normalised)

| Spectrum | In stats. | S | Fe | Cu | Total |
|---|---|---|---|---|---|
| Spectrum 1 | Yes | 33.62 | 27.80 | 38.58 | 100.00 |
| Spectrum 2 | Yes | 33.59 | 27.70 | 38.71 | 100.00 |
| Spectrum 3 | Yes | 33.12 | 27.58 | 39.30 | 100.00 |
| Mean | | 33.44 | 27.69 | 38.86 | 100.00 |
| Std. deviation | | 0.28 | 0.11 | 0.38 | |
| Max. | | 33.62 | 27.80 | 39.30 | |
| Min. | | 33.12 | 27.58 | 38.58 | |

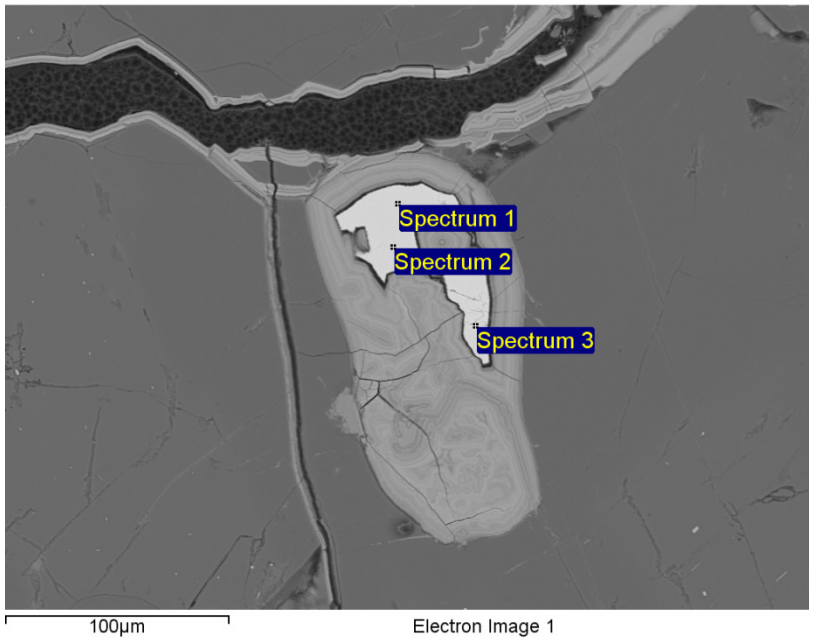

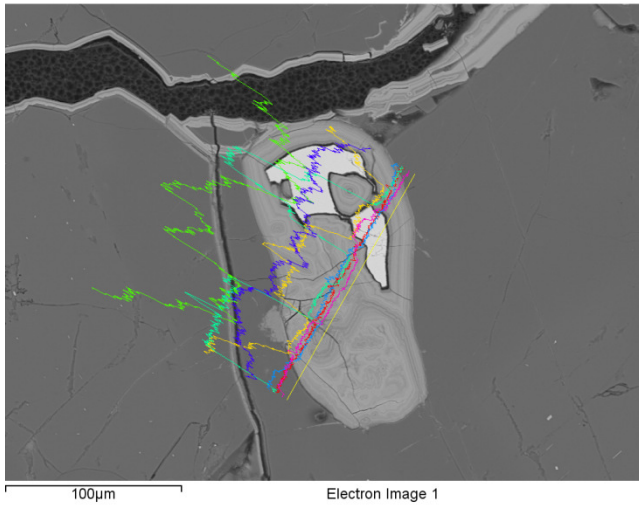
100µm
Electron Image 1

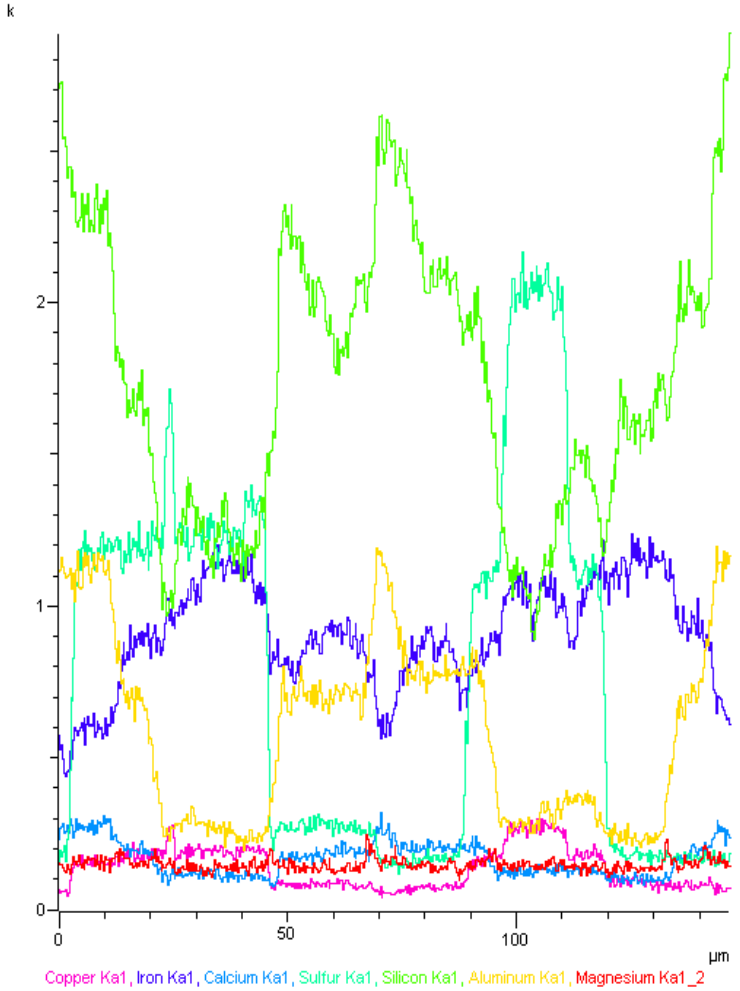
k
2
1
0
0
50
100
µm
Copper Ka1, Iron Ka1, Calcium Ka1, Sulfur Ka1, Silicon Ka1, Aluminum Ka1, Magnesium Ka1_2

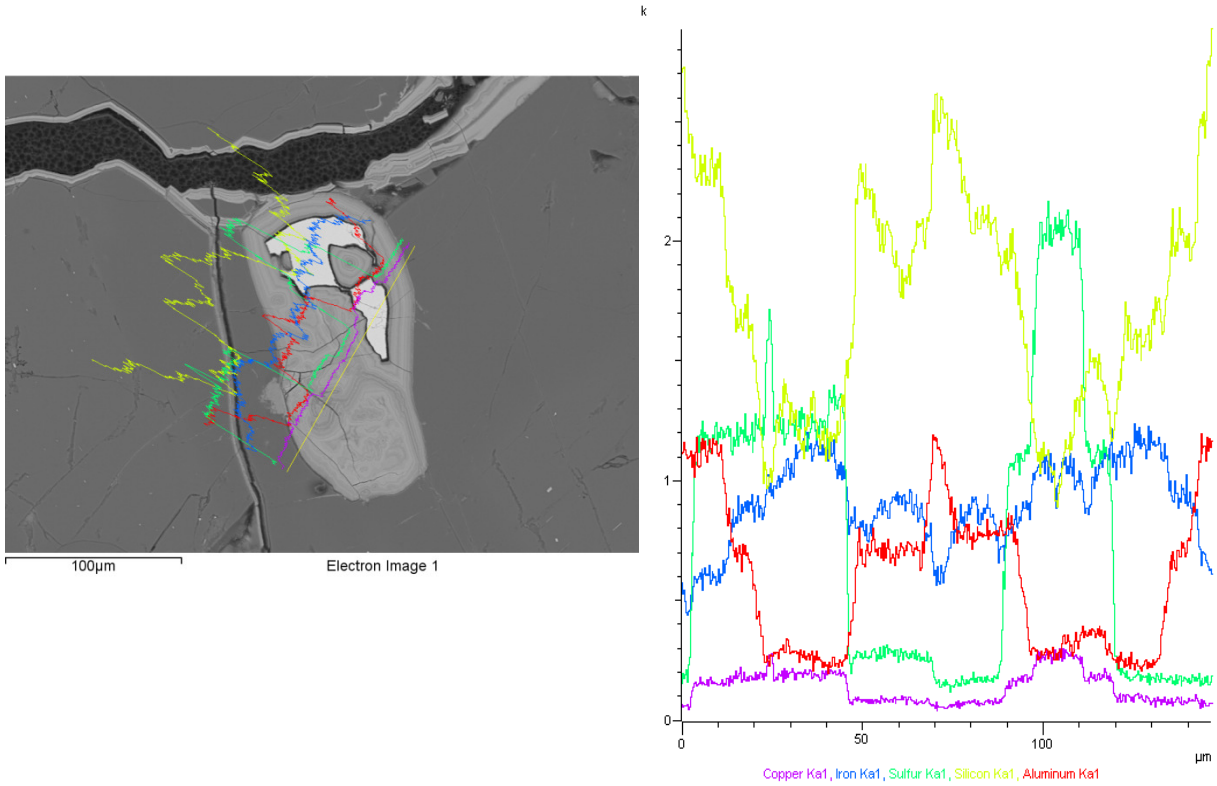
100µm
Electron Image 1
k
2
1
0
0
50
100
µm
Copper Ka1, Iron Ka1, Sulfur Ka1, Silicon Ka1, Aluminum Ka1

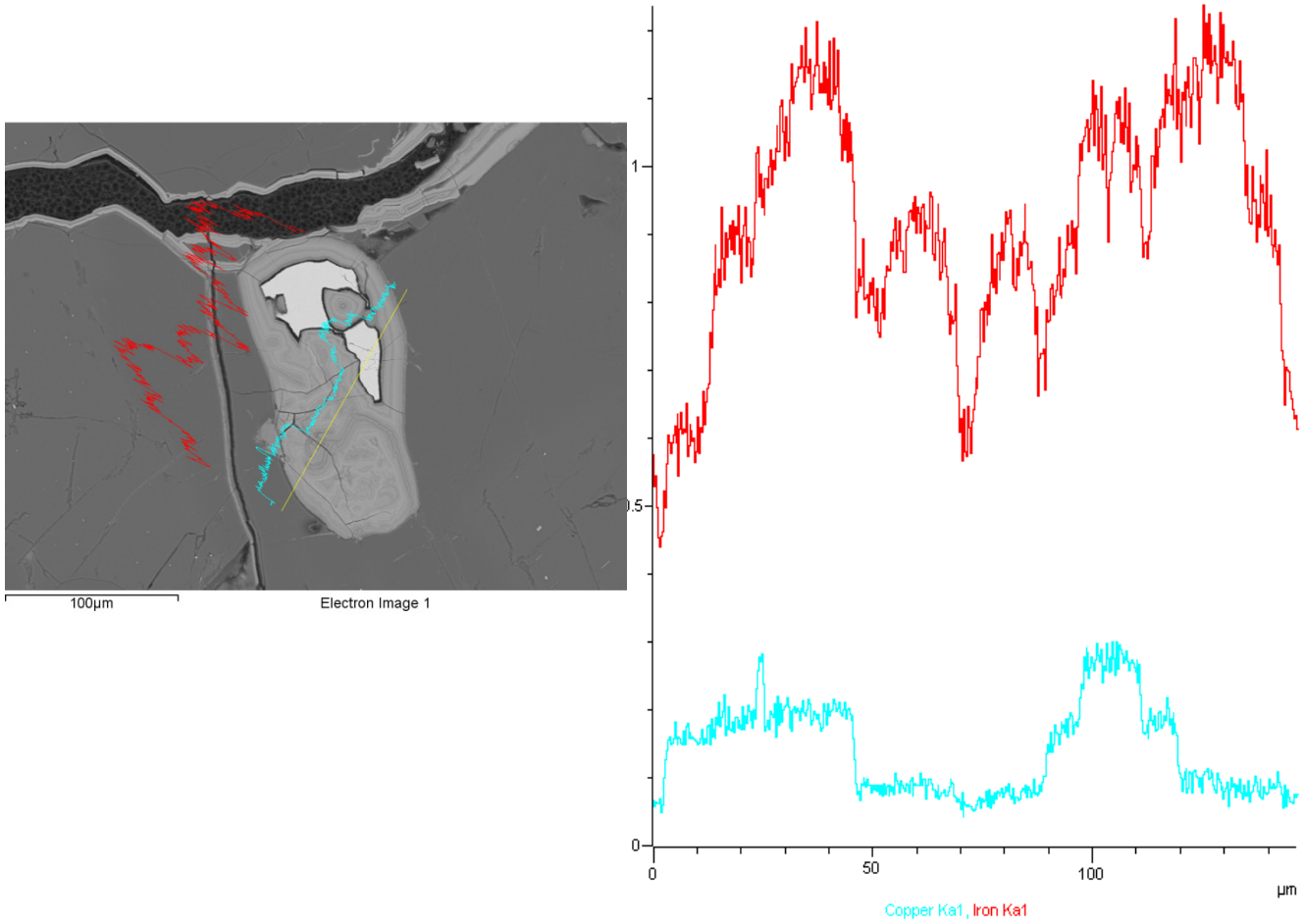
100µm
Electron Image 1
1
.5
0
0
50
100
µm
Copper Ka1 , Iron Ka1

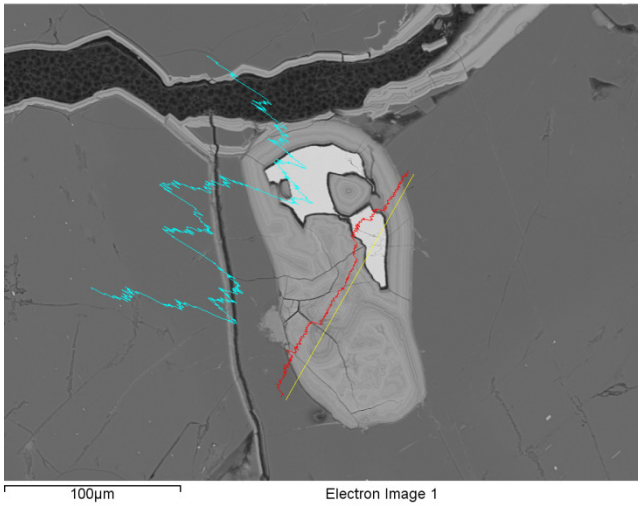
100µm
Electron Image 1

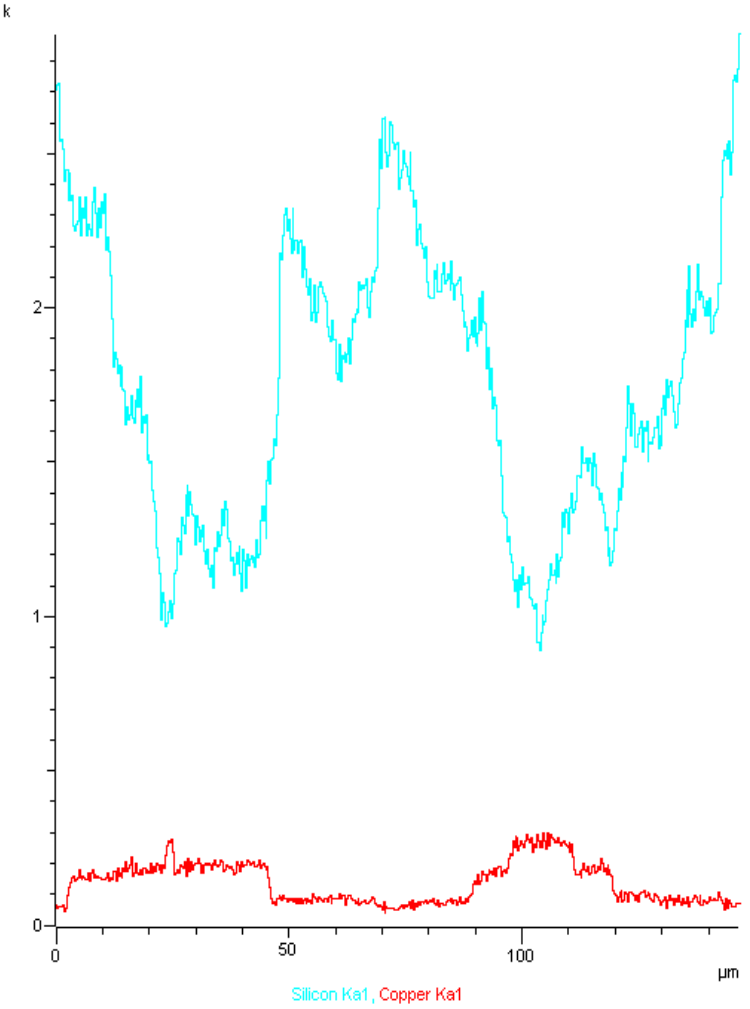
k
2
1
0
0
50
100
µm
Silicon Ka1, Copper Ka1

Electron Image 1

O Ka1

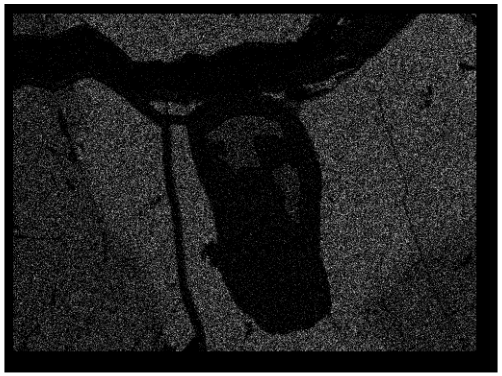

Na Ka1_2

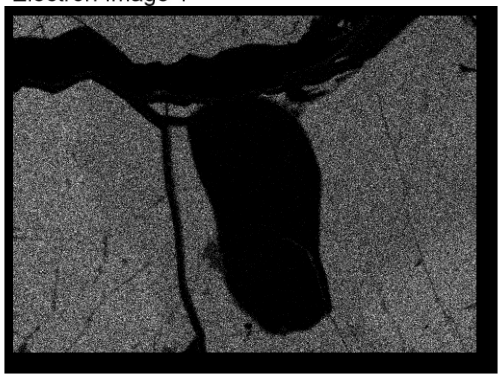

Al Ka1

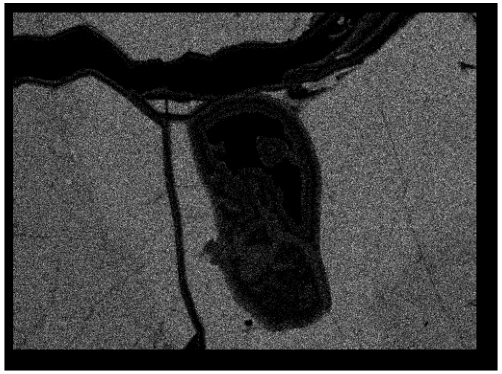

Si Ka1

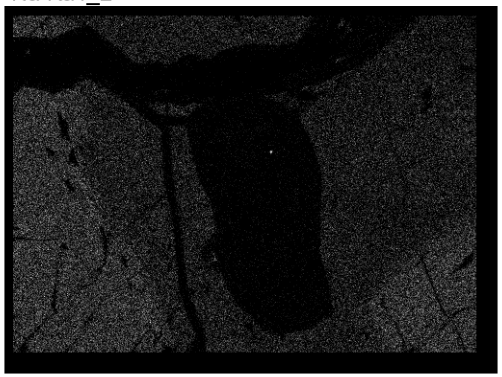

Ca Ka1

Fe Ka1

Cu Ka1

Site: m-sm-001-syn-S11

Processing option : Oxygen by stoichiometry (Normalised)

| Spectrum | In stats. | Mg | Ti | Mn | Fe | O | Total |
|---|---|---|---|---|---|---|---|
| Spectrum 1 | Yes | 0.64 | 31.96 | 0.40 | 35.07 | 31.93 | 100.00 |
| Spectrum 2 | Yes | 0.67 | 32.24 | | 35.07 | 32.02 | 100.00 |
| Spectrum 3 | Yes | 0.63 | 31.96 | 0.39 | 35.09 | 31.93 | 100.00 |
| Spectrum 4 | Yes | 0.68 | 31.75 | 0.39 | 35.30 | 31.88 | 100.00 |
| Spectrum 5 | Yes | 0.70 | 31.74 | 0.40 | 35.27 | 31.89 | 100.00 |
| Spectrum 6 | Yes | 0.72 | 31.75 | 0.41 | 35.23 | 31.89 | 100.00 |
| Spectrum 7 | Yes | 0.71 | 31.89 | 0.43 | 35.04 | 31.93 | 100.00 |
| Max. | | 0.72 | 32.24 | 0.43 | 35.30 | 32.02 | |
| Min. | | 0.63 | 31.74 | 0.39 | 35.04 | 31.88 | |

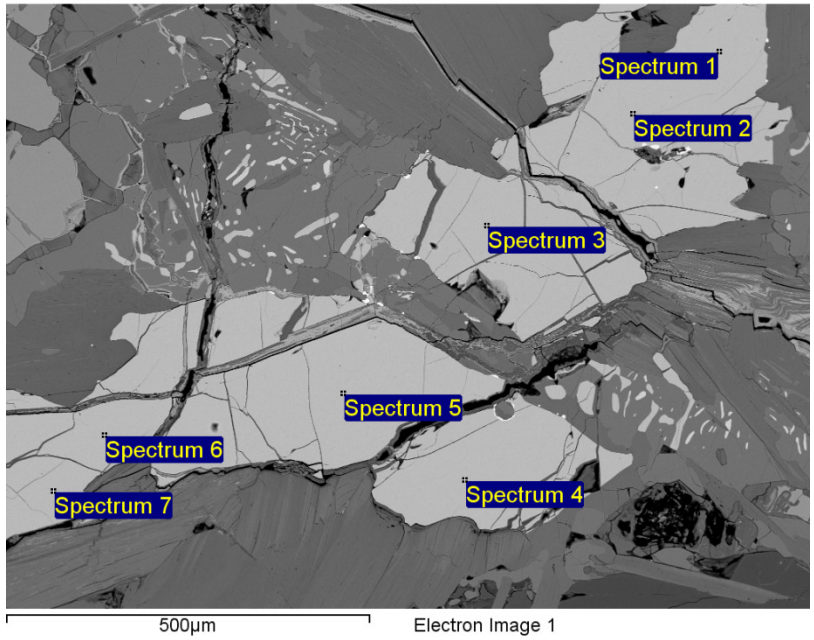

Site: m-sm-001-syn-S11 2

Processing option : Oxygen by stoichiometry (Normalised)

| Spectrum | In stats. | Mg | Al | Si | Cl | K | Ti | Cr | Fe | O | Total |
|---|---|---|---|---|---|---|---|---|---|---|---|
| Spectrum 1 | Yes | 9.38 | 7.98 | 17.63 | | 7.75 | 3.16 | 0.33 | 12.88 | 40.89 | 100.00 |
| Spectrum 2 | Yes | 9.96 | 7.88 | 17.70 | | 8.08 | 2.86 | 0.40 | 12.15 | 40.96 | 100.00 |
| Spectrum 3 | Yes | 9.59 | 7.93 | 17.46 | 0.24 | 7.82 | 3.12 | 0.44 | 12.63 | 40.76 | 100.00 |
| Spectrum 4 | Yes | 10.40 | 8.14 | 17.49 | 0.27 | 8.03 | 2.58 | 0.44 | 11.71 | 40.94 | 100.00 |
| Spectrum 5 | Yes | 10.26 | 7.98 | 17.56 | 0.21 | 7.99 | 2.62 | 0.39 | 12.12 | 40.88 | 100.00 |
| Max. | | 10.40 | 8.14 | 17.70 | 0.27 | 8.08 | 3.16 | 0.44 | 12.88 | 40.96 | |
| Min. | | 9.38 | 7.88 | 17.46 | 0.21 | 7.75 | 2.58 | 0.33 | 11.71 | 40.76 | |

All results in weight%

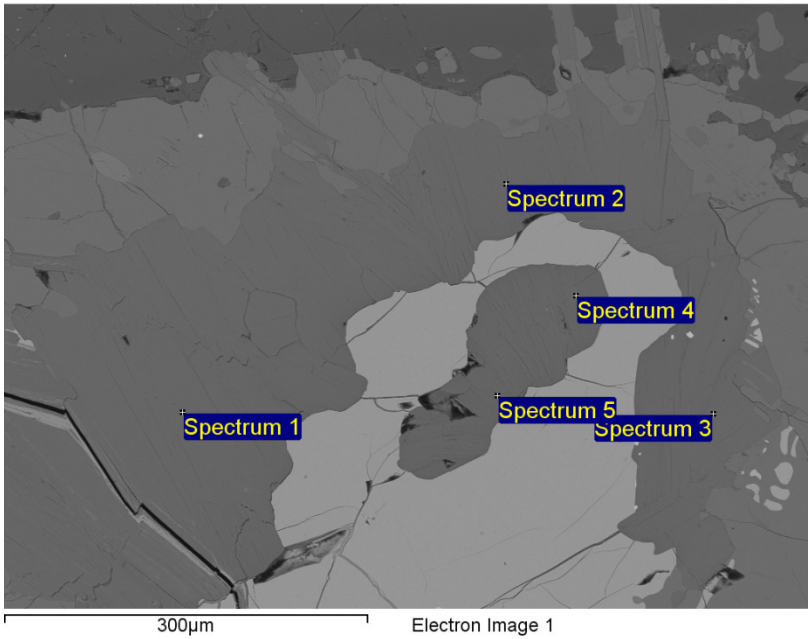

Site: m-sm-001-syn-S11 3

Processing option : Oxygen by stoichiometry (Normalised)

| Spectrum | In stats. | Mg | Si | Ca | Mn | Fe | O | Total |
|---|---|---|---|---|---|---|---|---|
| Spectrum 1 | Yes | 12.19 | 23.80 | 0.71 | 0.44 | 21.23 | 41.63 | 100.00 |
| Spectrum 2 | Yes | 12.25 | 23.73 | 0.63 | 0.36 | 21.44 | 41.59 | 100.00 |
| Spectrum 3 | Yes | 11.96 | 23.88 | 0.65 | 0.33 | 21.57 | 41.61 | 100.00 |
| Mean | | 12.13 | 23.80 | 0.66 | 0.38 | 21.41 | 41.61 | 100.00 |
| Std. deviation | | 0.16 | 0.08 | 0.04 | 0.06 | 0.17 | 0.02 | |
| Max. | | 12.25 | 23.88 | 0.71 | 0.44 | 21.57 | 41.63 | |
| Min. | | 11.96 | 23.73 | 0.63 | 0.33 | 21.23 | 41.59 | |

All results in weight%

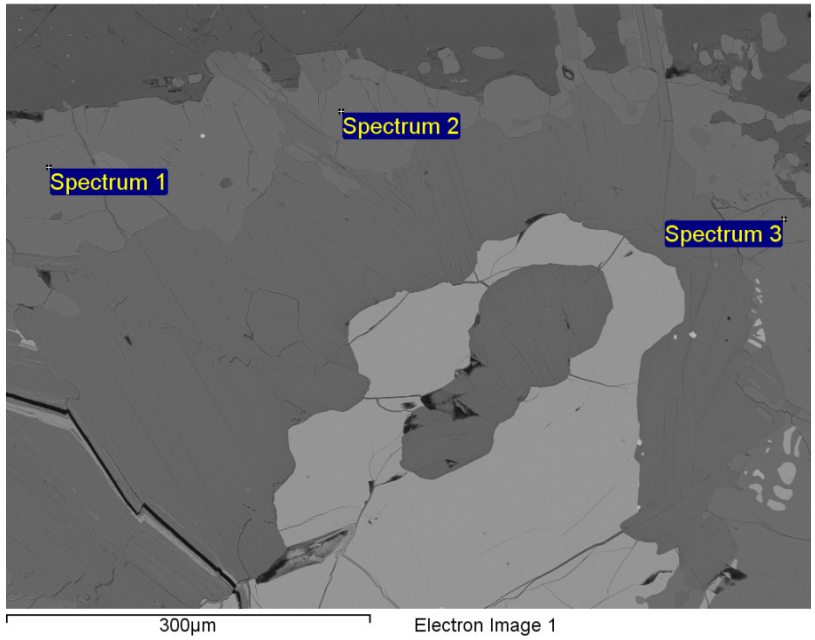

Processing option : Oxygen by stoichiometry (Normalised)

| Spectrum | In stats. | Na | Mg | Al | Si | Cl | K | Ca | Ti | Cr | Fe | Ni | Cu | O | Total |
|---|---|---|---|---|---|---|---|---|---|---|---|---|---|---|---|
| Spectrum 1 | Yes | | 10.15 | 8.27 | 17.84 | | 7.28 | | 2.79 | 0.31 | 12.06 | | | 41.31 | 100.00 |
| Spectrum 2 | Yes | | 9.45 | 7.92 | 17.46 | | 6.97 | | 2.90 | 0.33 | 13.63 | 0.60 | | 40.74 | 100.00 |
| Spectrum 3 | Yes | | 7.94 | 7.25 | 15.37 | | 4.54 | | 2.27 | | 22.94 | 0.59 | 0.57 | 38.51 | 100.00 |
| Spectrum 4 | Yes | | 7.11 | 7.13 | 15.01 | | 0.25 | | 1.85 | | 26.59 | 2.60 | 1.37 | 38.08 | 100.00 |
| Spectrum 5 | Yes | | 7.30 | 7.16 | 16.15 | | | | 1.83 | | 23.58 | 3.50 | 1.58 | 38.90 | 100.00 |
| Spectrum 6 | Yes | | 8.21 | 7.16 | 15.43 | | | | 2.12 | | 22.72 | 4.58 | 1.02 | 38.77 | 100.00 |
| Spectrum 7 | Yes | | 8.26 | 7.01 | 14.94 | | | | 2.27 | | 22.34 | 4.33 | 2.44 | 38.40 | 100.00 |
| Spectrum 8 | Yes | | 8.57 | 7.45 | 14.98 | 0.26 | 0.29 | | 1.98 | 0.28 | 23.12 | 3.62 | 0.79 | 38.65 | 100.00 |
| Spectrum 9 | Yes | | 7.91 | 7.01 | 14.42 | | | | 2.13 | 0.31 | 25.81 | 3.79 | 0.61 | 38.02 | 100.00 |
| Spectrum 10 | Yes | | 9.69 | 8.02 | 17.57 | | 7.99 | | 3.00 | 0.34 | 12.49 | | | 40.90 | 100.00 |
| Spectrum 11 | Yes | | 9.50 | 8.33 | 17.40 | | 6.91 | 0.73 | 2.95 | | 13.23 | | | 40.95 | 100.00 |
| Spectrum 12 | Yes | 0.29 | 9.85 | 7.95 | 17.49 | 0.21 | 7.94 | | 2.82 | 0.31 | 12.37 | | | 40.77 | 100.00 |

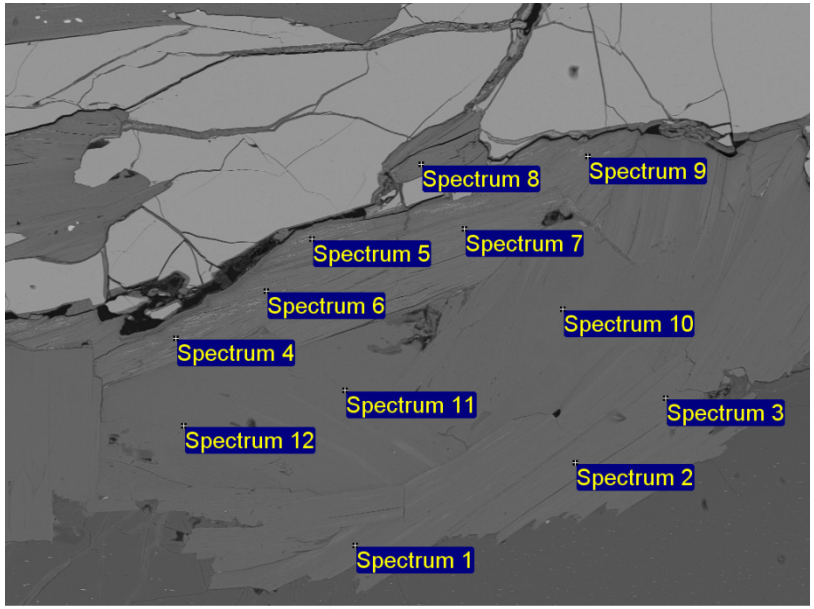

Site: m-sm-001-syn-S11fracfill

Processing option : Oxygen by stoichiometry (Normalised)

| Spectrum | In stats. | Mg | Al | Si | P | S | K | Ca | Ti | Fe | Cu | O | Total |
|---|---|---|---|---|---|---|---|---|---|---|---|---|---|
| Spectrum 1 | Yes | | 0.96 | 4.22 | | 0.67 | | | 0.91 | 63.07 | 3.85 | 26.31 | 100.00 |
| Spectrum 2 | Yes | | 2.70 | 15.89 | 0.42 | 0.24 | 0.23 | 0.34 | 0.91 | 42.83 | 1.58 | 34.86 | 100.00 |
| Spectrum 3 | Yes | 0.20 | 4.78 | 15.85 | 0.32 | 1.17 | 0.48 | 0.40 | 0.97 | 35.56 | 3.66 | 36.62 | 100.00 |
| Spectrum 4 | Yes | | 2.10 | 6.41 | 0.57 | 0.58 | | | | 58.84 | 3.09 | 28.41 | 100.00 |
| Max. | | 0.20 | 4.78 | 15.89 | 0.57 | 1.17 | 0.48 | 0.40 | 0.97 | 63.07 | 3.85 | 36.62 | |
| Min. | | 0.20 | 0.96 | 4.22 | 0.32 | 0.24 | 0.23 | 0.34 | 0.91 | 35.56 | 1.58 | 26.31 | |

All results in weight%

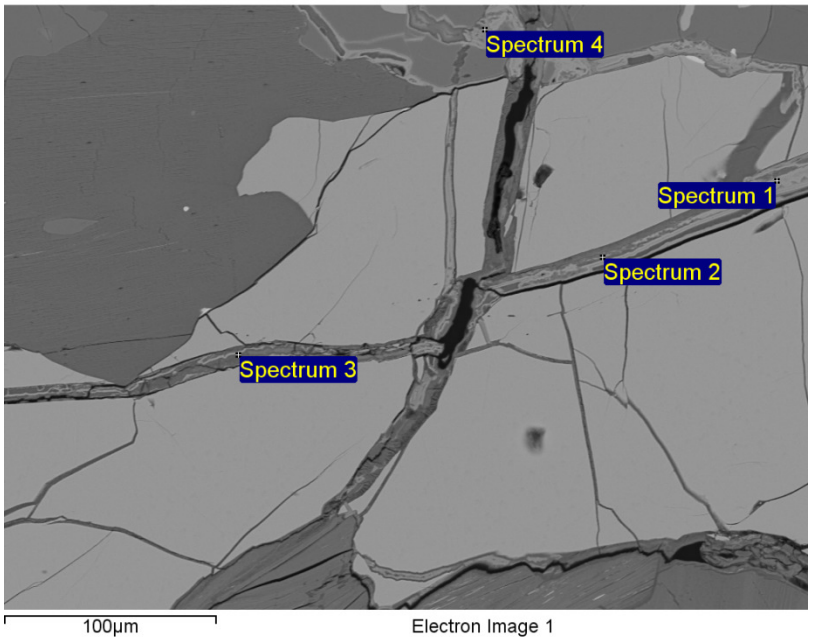

Site: m-sm-001-syn-S11_ss4

Processing option : Oxygen by stoichiometry (Normalised)

| Spectrum | In stats. | Mg | Si | Mn | Fe | O | Total |
|---|---|---|---|---|---|---|---|
| Spectrum 1 | Yes | 11.56 | 15.21 | 0.48 | 37.07 | 35.69 | 100.00 |
| Mean | | 11.56 | 15.21 | 0.48 | 37.07 | 35.69 | 100.00 |
| Std. deviation | | 0.00 | 0.00 | 0.00 | 0.00 | 0.00 | |
| Max. | | 11.56 | 15.21 | 0.48 | 37.07 | 35.69 | |
| Min. | | 11.56 | 15.21 | 0.48 | 37.07 | 35.69 | |

All results in weight%

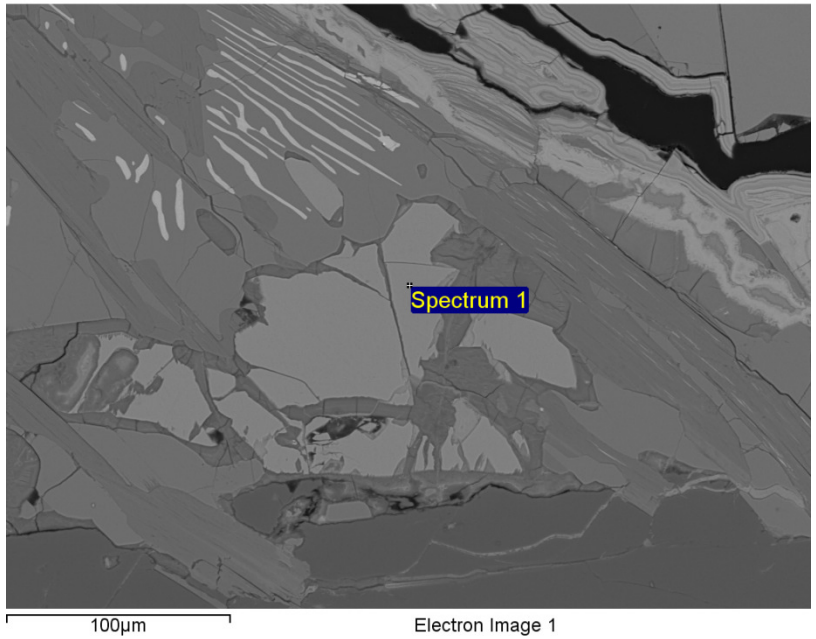

Site: m-sm-001-syn-S11_ss10

Processing option : Oxygen by stoichiometry (Normalised)

| Spectrum | In stats. | Mg | Al | Si | Ca | Fe | Cu | O | Total |
|---|---|---|---|---|---|---|---|---|---|
| Spectrum 1 | Yes | 3.20 | 2.87 | 30.66 | 0.80 | 14.50 | 3.11 | 44.85 | 100.00 |
| Mean | | 3.20 | 2.87 | 30.66 | 0.80 | 14.50 | 3.11 | 44.85 | 100.00 |
| Std. deviation | | 0.00 | 0.00 | 0.00 | 0.00 | 0.00 | 0.00 | 0.00 | |
| Max. | | 3.20 | 2.87 | 30.66 | 0.80 | 14.50 | 3.11 | 44.85 | |
| Min. | | 3.20 | 2.87 | 30.66 | 0.80 | 14.50 | 3.11 | 44.85 | |

All results in weight%

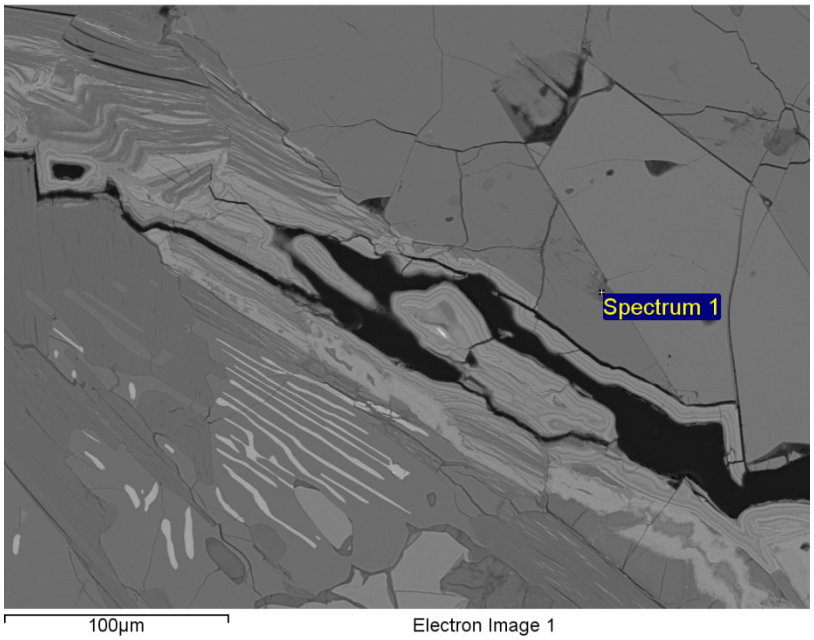

Site: m-sm-001-syn-S11_ss5zoom

Processing option : Oxygen by stoichiometry (Normalised)

| Spectrum | In stats. | Na | Al | Si | P | S | Ca | Fe | Cu | O | Total |
|---|---|---|---|---|---|---|---|---|---|---|---|
| Spectrum 1 | Yes | | 3.51 | 16.25 | 0.45 | 1.15 | 0.47 | 40.21 | 1.84 | 36.11 | 100.00 |
| Spectrum 2 | Yes | | 3.00 | 16.45 | 0.44 | 0.93 | 0.42 | 40.84 | 2.12 | 35.78 | 100.00 |
| Spectrum 3 | Yes | 0.95 | 2.73 | 7.60 | | 0.45 | 0.72 | 56.13 | 2.38 | 29.05 | 100.00 |
| Spectrum 4 | Yes | 1.37 | 4.16 | 9.04 | 0.32 | 0.42 | 1.07 | 50.69 | 1.97 | 30.96 | 100.00 |
| Spectrum 5 | Yes | 1.29 | 3.90 | 9.29 | | 0.42 | 1.21 | 51.05 | 2.08 | 30.76 | 100.00 |
| Max. | | 1.37 | 4.16 | 16.45 | 0.45 | 1.15 | 1.21 | 56.13 | 2.38 | 36.11 | |
| Min. | | 0.95 | 2.73 | 7.60 | 0.32 | 0.42 | 0.42 | 40.21 | 1.84 | 29.05 | |

All results in weight%

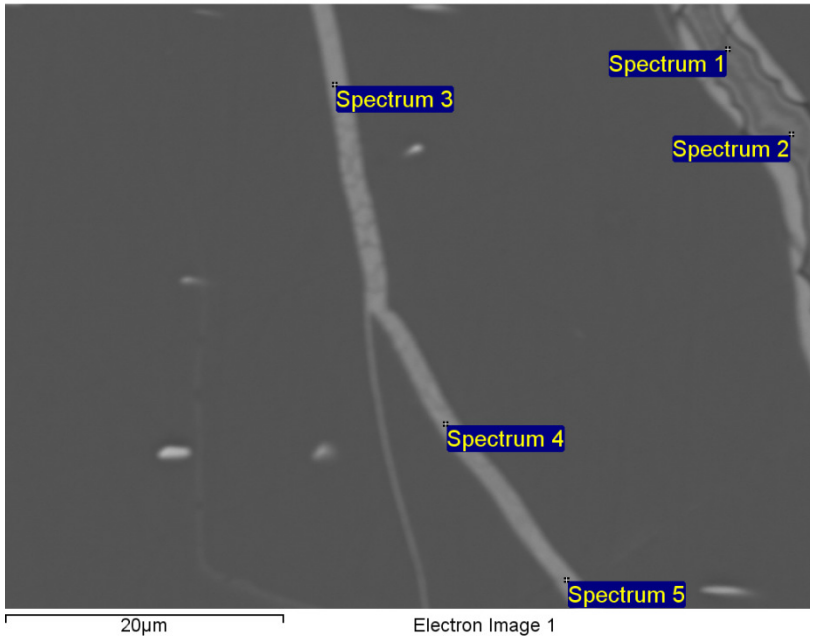

Project: remap_synch
Owner: Inca User
Site: m-sm-001-syn-S11_ss8

Processing option : Oxygen by stoichiometry (Normalised)

| Spectrum | In stats. | Mg | Al | Si | K | Ca | Fe | Cu | O | Total |
|---|---|---|---|---|---|---|---|---|---|---|
| Spectrum 1 | Yes | 0.49 | 2.20 | 26.20 | 0.21 | 0.82 | 27.31 | 1.95 | 40.82 | 100.00 |
| Mean | | 0.49 | 2.20 | 26.20 | 0.21 | 0.82 | 27.31 | 1.95 | 40.82 | 100.00 |
| Std. deviation | | 0.00 | 0.00 | 0.00 | 0.00 | 0.00 | 0.00 | 0.00 | 0.00 | |
| Max. | | 0.49 | 2.20 | 26.20 | 0.21 | 0.82 | 27.31 | 1.95 | 40.82 | |
| Min. | | 0.49 | 2.20 | 26.20 | 0.21 | 0.82 | 27.31 | 1.95 | 40.82 | |

All results in weight%

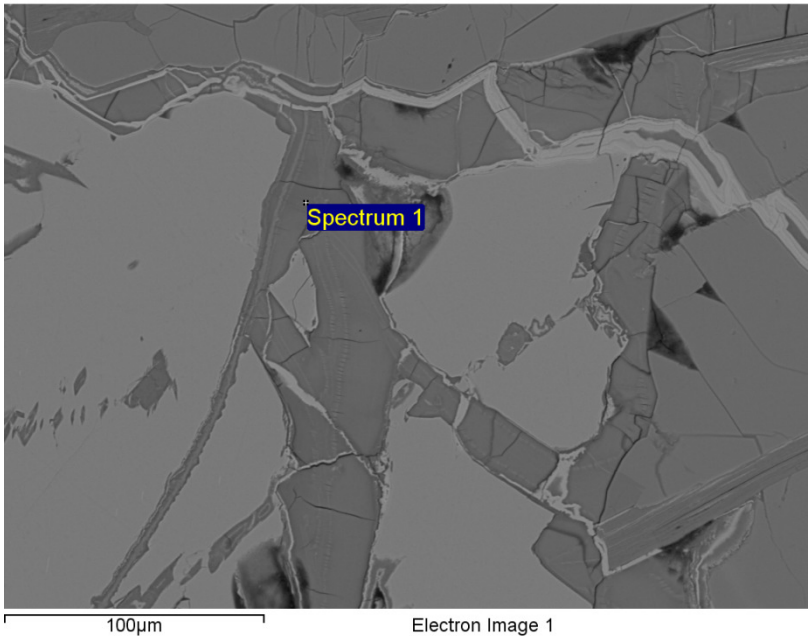

# Appendix A
# Geochemical Model Setup

**Example (malachite) setup for pure phase curves in GWB V.7**

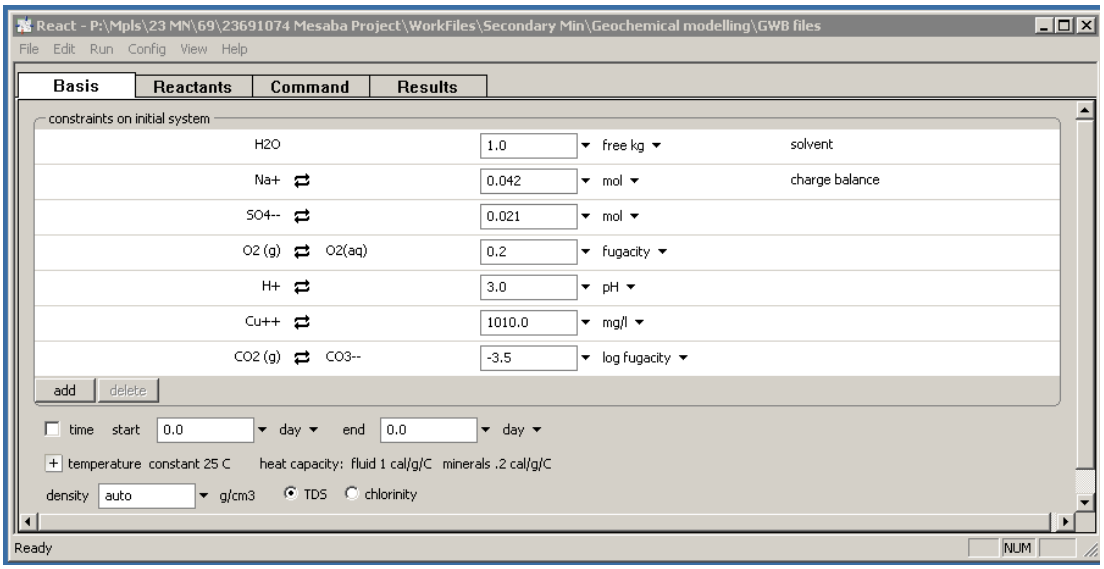


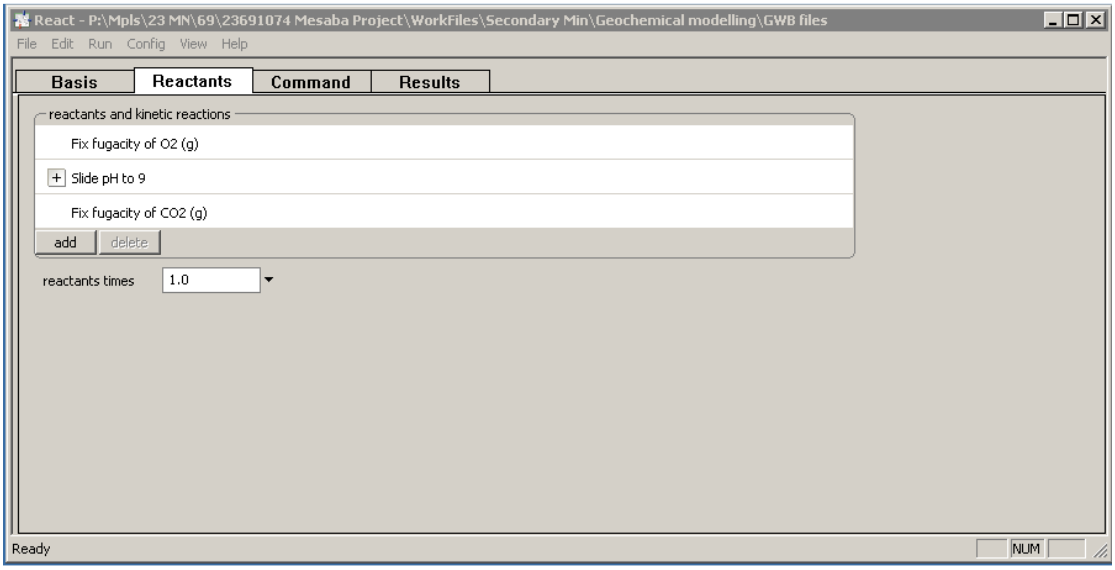

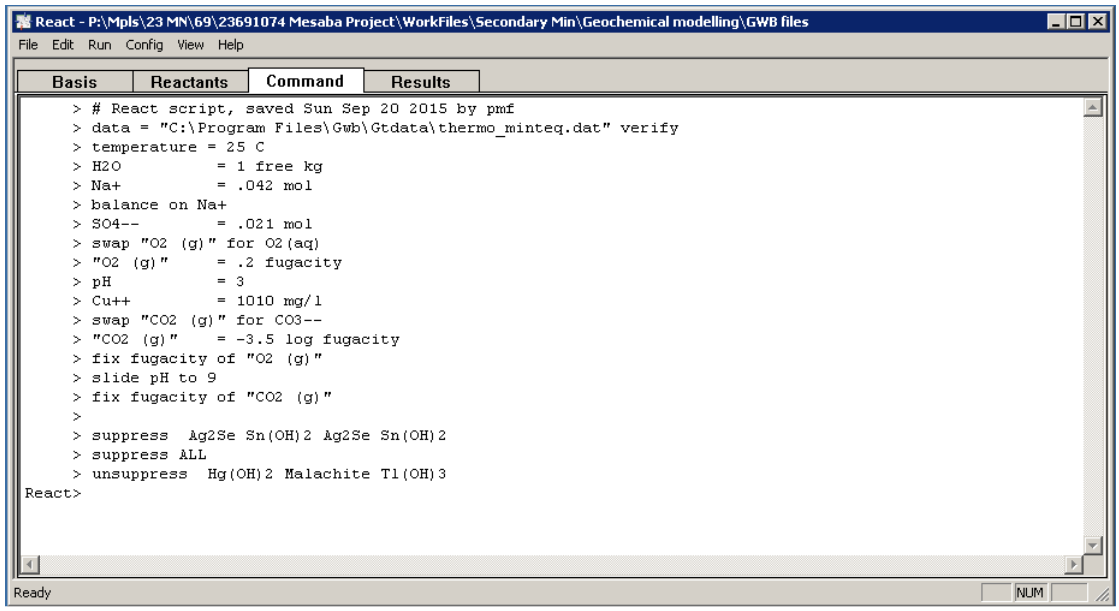
React - P:\Mpls\23 MN\69\23691074 Mesaba Project\WorkFiles\Secondary Min\Geochemical modelling\GWB files
File Edit Run Config View Help
Basis Reactants Command Results
> # React script, saved Sun Sep 20 2015 by pmf
> data = "C:\Program Files\Gwb\Gtdata\thermo_minteq.dat" verify
> temperature = 25 C
> H2O = 1 free kg
> Na+ = .042 mol
> balance on Na+
> SO4-- = .021 mol
> swap "O2 (g)" for O2(aq)
> "O2 (g)" = .2 fugacity
> pH = 3
> Cu++ = 1010 mg/l
> swap "CO2 (g)" for CO3--
> "CO2 (g)" = -3.5 log fugacity
> fix fugacity of "O2 (g)"
> slide pH to 9
> fix fugacity of "CO2 (g)"
>
> suppress Ag2Se Sn(OH)2 Ag2Se Sn(OH)2
> suppress ALL
> unsuppress Hg(OH)2 Malachite Tl(OH)3
React>
Ready
NUM

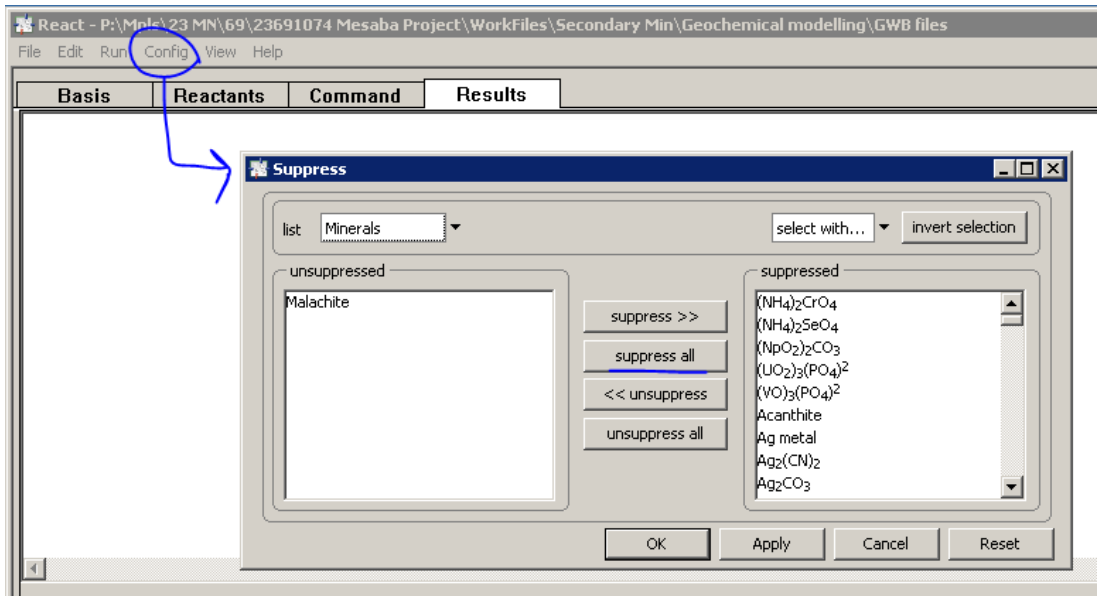
React - P:\Mpls\23 MN\69\23691074 Mesaba Project\WorkFiles\Secondary Min\Geochemical modelling\GWB files
File Edit Run Config View Help
Basis Reactants Command Results
Suppress
list Minerals
select with...
invert selection
unsuppressed
Malachite
suppress >>
suppress all
<< unsuppress
unsuppress all
suppressed
(NH4)2CrO4
(NH4)2SeO4
(NpO2)2CO3
(UO2)3(PO4)2
(VO)3(PO4)2
Acanthite
Ag metal
Ag2(CN)2
Ag2CO3
OK
Apply
Cancel
Reset

**Example setup for sorption curves in GWB V.7**

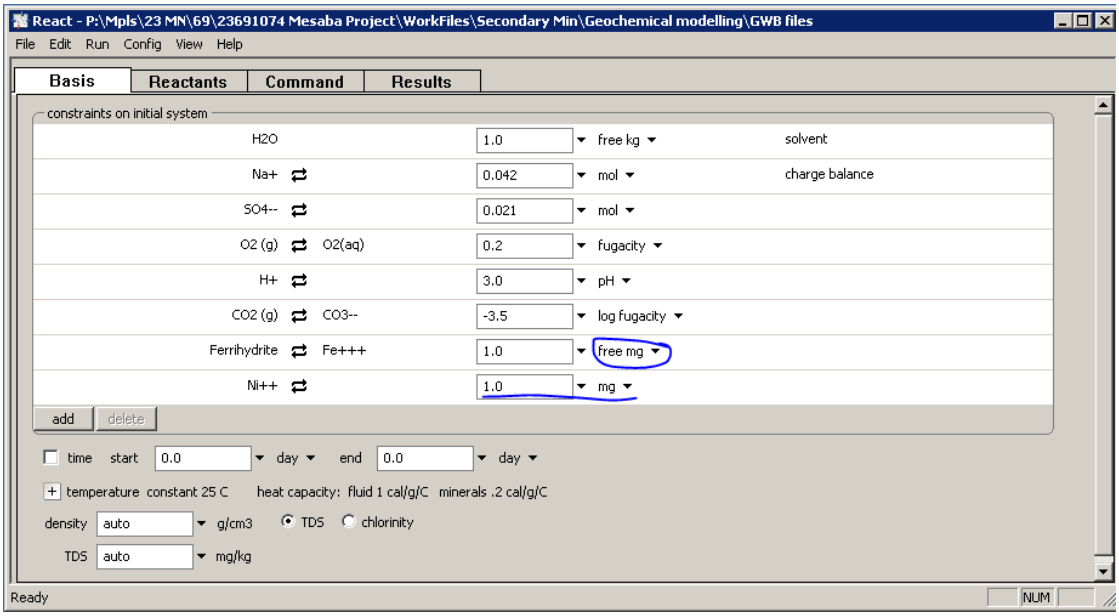


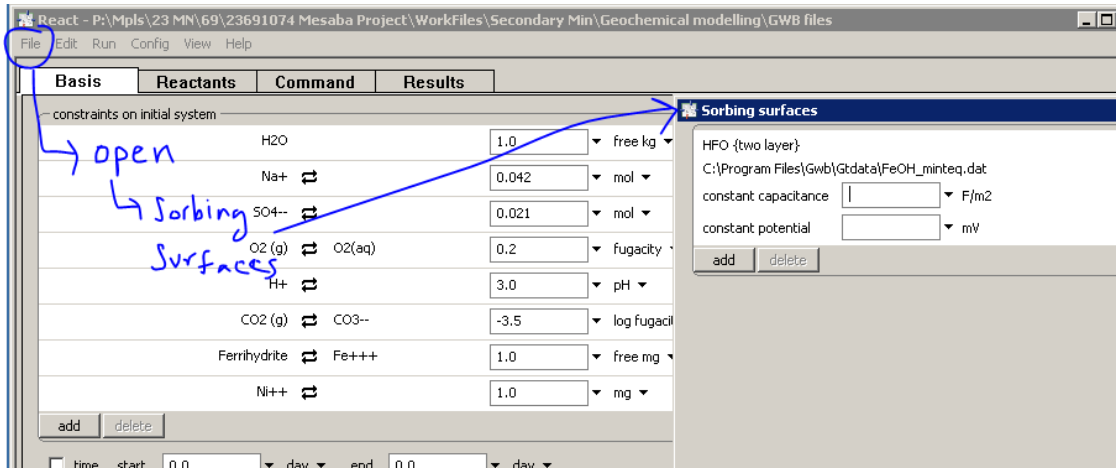


**Thermo_minteq**

***General***

```
S-Ferrihydrite(s)
     charge=  0.0      ion size=  0.0 A b=  0.0000      mole
    wt.=  106.8689 g
     4 species in reaction
       1.000 Fe+++          -3.000 H+              1.000 Ts1-Fer
       3.000 H2O
         2.5000    2.5000    2.5000    2.5000
         2.5000    2.5000    2.5000    2.5000
*    logK=      2.500000     deltaH=      0.000000 kJ
```

```
Gypsum                          type=
     formula=
     mole vol.=    0.000 cc      mole wt.=  172.1720 g
     3 species in reaction
       2.000 H2O             1.000 Ca++            1.000 SO4--
        -4.6260   -4.6177   -4.6100   -4.6016
        -4.5940   -4.5870   -4.5807   -4.5748
*    logK=     -4.610000     deltaH=      1.000000 kJ

Chalcedony                      type=
     formula=
     mole vol.=    0.000 cc      mole wt.=   60.0843 g
     2 species in reaction
       1.000 H4SiO4          -2.000 H2O
        -3.8659   -3.7010   -3.5500   -3.3847
        -3.2345   -3.0974   -2.9718   -2.8563
*    logK=     -3.550000     deltaH=     19.700000 kJ
```

***<u>Copper</u>***

```
Tenorite(c)                     type=
     formula=
     mole vol.=    0.000 cc      mole wt.=   79.5454 g
     3 species in reaction
       1.000 Cu++            -2.000 H+             1.000 H2O
         8.6806    8.1375    7.6400    7.0954
         6.6006    6.1490    5.7353    5.3548
*    logK=      7.640000     deltaH=    -64.900000 kJ

Cu(OH)2                         type=
     formula=
     mole vol.=    0.000 cc      mole wt.=   97.5606 g
     3 species in reaction
       1.000 Cu++            -2.000 H+             2.000 H2O
        10.1417    9.6972    9.2900    8.8442
         8.4392    8.0696    7.7310    7.4196
*    logK=      9.290000     deltaH=    -53.120000 kJ

Malachite                       type=
     formula=
     mole vol.=    0.000 cc      mole wt.=  221.1158 g
     4 species in reaction
       2.000 Cu++            -2.000 H+             2.000 H2O
       1.000 CO3--
        -4.7603   -5.1302   -5.4690   -5.8399
        -6.1769   -6.4844   -6.7662   -7.0253
*    logK=     -5.469000     deltaH=    -44.200000 kJ
```

```
Brochantite                          type=
     formula=
     mole vol.=    0.000 cc      mole wt.=  452.2894 g
     4 species in reaction
       4.000 Cu++           -6.000 H+              6.000 H2O
       1.000 SO4--
        18.4747   16.7772   15.2220   13.5197
        11.9730   10.5616    9.2683    8.0791
*    logK=     15.222000     deltaH=   -202.860000 kJ
```

***Nickel***

```
NiCO3                                type=
     formula=
     mole vol.=    0.000 cc      mole wt.=  118.7192 g
     2 species in reaction
       1.000 Ni++            1.000 CO3--
       -10.5332  -10.8812  -11.2000  -11.5490
       -11.8661  -12.1555  -12.4206  -12.6644
*    logK=    -11.200000     deltaH=    -41.589000 kJ

Ni(OH)2 (am)                         type=
     formula=
     mole vol.=    0.000 cc      mole wt.=   92.7246 g
     3 species in reaction
      -2.000 H+              1.000 Ni++            2.000 H2O
        14.4286   13.6256   12.8900   12.0847
        11.3531   10.6854   10.0737    9.5111
*    logK=     12.890000     deltaH=    -95.960000 kJ


Ni(OH)2 (c)                          type=
     formula=
     mole vol.=    0.000 cc      mole wt.=   92.7246 g
     3 species in reaction
      -2.000 H+              1.000 Ni++            2.000 H2O
        10.7900   10.7900   10.7900   10.7900
        10.7900   10.7900   10.7900   10.7900
*    logK=     10.790000     deltaH=      0.000000 kJ
*    deltaH not known; therefore log K is certain only for 25
deg C
```

***Cobalt***

```
Co(OH)2 (am)                    type=
     formula=
     mole vol.=    0.000 cc      mole wt.=   92.9478 g
     3 species in reaction
       1.000 Co++           -2.000 H+              2.000 H2O
        13.0940   13.0940   13.0940   13.0940
        13.0940   13.0940   13.0940   13.0940
*    logK=     13.094000     deltaH=      0.000000 kJ
*    deltaH not known; therefore log K is certain only for 25
         deg C

Co(OH)2 (c)                     type=
     formula=
     mole vol.=    0.000 cc      mole wt.=   92.9478 g
     3 species in reaction
       1.000 Co++           -2.000 H+              2.000 H2O
        12.2900   12.2900   12.2900   12.2900
        12.2900   12.2900   12.2900   12.2900
*    logK=     12.290000     deltaH=      0.000000 kJ
*    deltaH not known; therefore log K is certain only for 25
    deg C

CoCO3                           type=
     formula=
     mole vol.=    0.000 cc      mole wt.=  118.9424 g
     2 species in reaction
       1.000 Co++            1.000 CO3--
       -10.9954  -11.1022  -11.2000  -11.3071
       -11.4044  -11.4932  -11.5745  -11.6493
*    logK=    -11.200000     deltaH=    -12.761200 kJ

Co3O4                           type=
     formula=
     mole vol.=    0.000 cc      mole wt.=  240.7972 g
     4 species in reaction
       1.000 Co++            2.000 Co+++          -8.000 H+
       4.000 H2O
        -8.7719   -9.6715  -10.4956  -11.3977
       -12.2173  -12.9653  -13.6506  -14.2808
*    logK=    -10.495600     deltaH=   -107.499900 kJ
```

***Zinc***

```
Hydrozincite                    type=
     formula=
     mole vol.=    0.000 cc      mole wt.=  548.9117 g
     4 species in reaction
       5.000 Zn++           -6.000 H+              2.000 CO3--
       6.000 H2O
        12.4920   10.5131    8.7000    6.7154
         4.9122    3.2667    1.7590    0.3726
*    logK=      8.700000     deltaH=   -236.500000 kJ


Smithsonite                     type=
     formula=
     mole vol.=    0.000 cc      mole wt.=  125.3791 g
     2 species in reaction
       1.000 Zn++            1.000 CO3--
       -10.8391  -10.8709  -10.9000  -10.9319
       -10.9609  -10.9873  -11.0115  -11.0338
*    logK=    -10.900000     deltaH=     -3.800000 kJ

Zn(OH)2 (am)                    type=
     formula=
     mole vol.=    0.000 cc      mole wt.=   99.3845 g
     3 species in reaction
       1.000 Zn++           -2.000 H+              2.000 H2O
        13.8468   13.1304   12.4740   11.7555
        11.1027   10.5070    9.9612    9.4592
*    logK=     12.474000     deltaH=    -85.620000 kJ
```

***Thermo.com.V8.R6+***

```
Dioptase                        type=
     formula= CuSiO2(OH)2
     mole vol.=   48.240 cc      mole wt.=  157.6450 g
     4 species in reaction
 -2.0000 H+                  1.0000 Cu++                1.0000
    SiO2(aq)
  2.0000 H2O
         6.4141    6.0773    5.5913    5.1877
         4.9020    4.7840  500.0000  500.0000
*    gflag = 1 [reported delG0f used]
*    extrapolation algorithm: constant enthalpy approximatio
*    reference-state data source = 87woo/gar
*         delG0f =  -1207.500 kj/mol
*         delH0f =  -1358.466 kj/mol
*         S0PrTr =     86.600 j/(mol*K)
```

***Phreeqc***

```
Willemite                          type=
     formula= Zn2SiO4
     mole vol.=    0.000 cc      mole wt.=  222.8243 g
     3 species in reaction
       1.000 H4SiO4          2.000 Zn++           -4.000 H+
        17.5687   16.4004   15.3300   14.1584
        13.0939   12.1224   11.2323   10.4138
* used van't Hoff equation to compute logKs
```